ABSTRACT

MYERS, NICHOLAS J. Applications of Mathematical Modeling in Ecology and Health Care. (Under the direction of H.T. Banks and Hien Tran.)

Mathematical modeling is a valuable tool in multidisciplinary research that has found use in a variety of fields such as physics, chemistry, engineering and biology. Modeling using differential equations is common in biological applications such as modeling populations or physiological based pharmacokinetics. This research follows two distinct projects: one related to ecology and toxicology and the other in health care modeling immunosuppression. With regards to the first project, the focus is on using mathematical modeling to examine the annual cycle of bumblebee colonies. There is a global decline of pollinators for reasons that include habitat loss and pesticides. While honeybees are well studied, less is known about bumblebees and their decline. Using the species *Bombus terrestris* as an example, population dynamics of each individual class are modeled using delay differential equations since this is common with insect populations. Initially the development of the differential equation model is presented. This model includes important aspects of colonies over their annual lifestyle such as each class's metamorphosis, resource dynamics (pollen and nectar), and a switch time for the colony. Next, the model is updated significantly yielding the ability to explore the effects of common pesticides (e.g., imidacloprid) on survivability of the colony. Currently in the United States, risk assessment on all arthropods is based on acute toxicity tests (LC_{50}) on the European honeybee *Apis mellifera*. These tests fail to account for sub-lethal effects of these pesticides on the bumblebee colonies and the model shows the dangers that sub-lethal effects present to the survivability of a colony. The second project examines immunosuppression in the case of renal transplant recipients. Millions of Americans suffer from chronic kidney disease (CKD) and the individuals diagnosed as Stage 5 have almost entirely lost kidney functionality. Their only available treatment options are a lifetime of dialysis or kidney transplantation. The solid organ the host receives undergoes some degree of rejection in almost all cases since the host's immune system treats the allograft as foreign tissue. A variety of drugs are used presently to suppress the host's immune system to prevent the rejection of the allograft and preserve its functionality for the host. Immunosuppressed renal transplant patients have an increased risk of infection by pathogens, in particular human polyomavirus type 1 (also known as BK virus or BKV). BK virus presents a significant danger to renal transplant patients because an infection attacks renal tubule cells within the allograft damaging kidney function. Therefore, a balanced treatment is needed with enough immunosuppression occurring to prevent rejection of the allograft while avoiding over-suppression where the immune system cannot fight off pathogens. Currently, protocols for immunosuppressant treatments vary by treatment center and this research aims to assist physicians in finding well balanced treatment strategies. The model presented in this work accounts for the efficacy of an immunosuppression treatment and the effect it has on the dynamics of the host's immune system,

allograft and BK virus concentrations. The model includes a control theory framework to produce a receding horizon controller that represents immunosuppression efficacy over time in order to find a balance treatment. The ensemble Kalman filter is also utilized to include patient data as a feedback mechanism for the model.

Applications of Mathematical Modeling in Ecology and Health Care

by
Nicholas J. Myers

A dissertation submitted to the Graduate Faculty of
North Carolina State University
in partial fulfillment of the
requirements for the Degree of
Doctor of Philosophy

Applied Mathematics

Raleigh, North Carolina

2021

APPROVED BY:

John Banks	Alun Lloyd
Kevin Flores	Hien Tran Chair of Advisory Committee

DEDICATION

in memory of Dr. H.T. Banks

BIOGRAPHY

Nicholas Myers grew up in a small town in Wisconsin. He developed a likeness for computers and mathematics throughout grade school. Nicholas attended Ripon College where he earned a bachelor's degree in computer science. After a nine year break from academia, he returned to receive a bachelor's degree in mathematics from the University of Wisconsin - Milwaukee under the advisement of Dr. Gabriella Pinter. In 2015, Nicholas entered the Applied Mathematics Ph.D. program at North Carolina State University. He joined the Center for Research in Scientific Computation to complete his Ph.D. under the direction of Dr. H.T. Banks and Dr. Hein Tran.

TABLE OF CONTENTS

LIST OF TABLES

LIST OF FIGURES

CHAPTER

1

INTRODUCTION

Today, an essential tool in multidisciplinary research across many fields is mathematical modeling. Mathematical modeling is the practice of using mathematical methods to determine meaningful approximations of real world systems for the purpose of gaining insight and guidance to understand those systems. These mathematical models can be as simple as an equation describing a savings account with regular deposits and withdrawals. More advanced modeling is often found in physical science applications such as the movement of particles in fluids or weather forecasting. Chemistry and biology also harness the power of mathematical modeling in research.

Many biological applications have utilized mathematical modeling as a tool. Differential equations are often used in constructing these mathematical models in the biological sciences. Modeling of metabolic pathways in crops and animals is becoming common in systems biology applications. Other examples include modeling animal populations in ecology, chemical and drug absorption in physiological based pharmacokinetic (PBPK) modeling, and diseases both in populations of susceptible individuals and at an organic level to further understand disease behavior. Our research explores bumblebee population modeling in ecotoxicolgy (chapters 2 and 3) and also immuno-suppression modeling in humans (chapter 4).

The motivation behind our work on bumblebees stems from interest in the world wide decline of pollinator populations which is occurring for a variety of reasons including the use of pesticides and resource limitations. Declining pollinator populations are negatively effecting both biodiveristy and the global food supply. Bumblebees are the primary pollinators for a variety wild plants and have interactions (both direct and indirect) with hundreds of other species. As the population of

bumblebees declines in a habitat so will the abundance of the species that depend on bumblebees and complete loss of bumblebees would result in loss of many of those species as well. In agriculture, there are a number of crops that rely specifically on insect pollination (predominantly honey bees and bumblebees) where further decreases of their populations would likely result in less crop yield or higher costs due to need for more expensive mechanical pollination. Although much research has been focused on honey bees, much less is known about bumblebee populations. We examine the bumblebee species *Bombus terrestris* in this work in order to provide insight into colony dynamics.

In chapter 2, we develop a mathematical model for bumblebee colonies while focusing on the individual level of the hive, i.e., queens, workers, males, and gynes. We also include two known food sources for bumblebees, nectar and pollen which sustain a colony through an annual cycle. The mathematical model utilizes delay differential equations to represent the different groups of individuals and also the resources. Since bumblebee development involves three pre-adult stages, progression through the stages are easily captured using a system of delay differential equations. In addition, bumblebee colonies expire at the end of an annual cycle hence, the success of a colony can be attributed to the number of gynes that survive long enough to hibernate and also the number of males available to mate with gynes outside the colony to preserve genetic information.

Following the work in the previous chapter, the focus of chapter 3 is to understand pesticide effects on the reproductive output of bumblebee colonies. There is a variety of pesticides approved for use on crops which bumblebee populations can become exposed to. These pesticides can be lethal at certain doses and also have alternative effects at sub-lethal doses. We examine some of these sub-lethal effects on the viability of a *Bombus terrestris* colony. To examine sub-lethal effects of pesticides on colonies, adjustments to the model presented in chapter 2 are necessary. The larval stage of the bumblebee life cycle is most sensitive to resource dynamics within the colony, thus making the larval stage vital to include in the mathematical model. Other changes involve the introduction of oophagy and larval ejection mechanisms to provide realisic loss functions for pre-adult members of the colony. This updated mathematical model allows us to understand the sub-lethal and lethal effects of pesticides on individual classes within a colony.

In chapter 4, we address a need for better drug dosing regimens in renal transplant patients. Many of the individuals on the solid organ transplant list require a kidney transplant which is the result of severe impairment of the patient's existing kidneys. Chronic kidney disease is the most likely cause for kidney impairment where individuals at stage 5 have lost almost all kidney function and are required to undergo regular dialysis. Renal transplantation is the only other treatment option available. For transplant recipients, an immunosuppression treatment is necessary to prevent the host's immune system from attacking the allograft. A balanced suppression regimen is necessary to prevent the over-suppression of the immune system which results in the bodies inability to protect itself from pathogens.

With the lack of universally accepted treatment schemes, control theory methods for the problem

are revisited. A differential equation model for a renal transplant patient is utilized, focusing on renal tubule cells (susceptible and infected), BK virus which attacks the kidneys during infection, serum creatinine levels as a surrogate for kidney function and lastly separate immune responses to both BK virus and the allograft. A receding horizon controller is used to find optimal controllers between discrete days when patient data is available. As a feedback mechanism for introducing patient data into the model, the ensemble Kalman filter (EnKF) provides a methodology that preserves the nonlinearities of the differential equation model. The EnKF provides better approximations to the state of transplant patient than either the differential equation model or data alone.

In chapter 5, we focus on the future directions for both modeling pesticide effects on bumblebee populations and immunosuppression in kidney transplant patients. Assumptions made in developing the mathematical model of bumblebee colonies could be revisited for a more generalized version of the model such as assuming a dynamic switch time, changes to modeling larval dynamics, and developing a framework for multi-year simulations. With regards to immunosuppression modeling, specific drug types and treatment schemes are considered for making more accurate modeling predictions. Methods such as parameter estimation are discussed to make the model more personalized. A conclusion of our work is also provided.

CHAPTER

2

MODELING BUMBLEBEE POPULATION DYNAMICS WITH DELAY DIFFERENTIAL EQUATIONS

Adopted from publication: Ecological Modeling, Volume 351, March 2017 [14]

2.1 Introduction

The protection of bumblebee populations, among other pollinators, is vital to sustain global agricultural food production [110, 77], biodiversity and ecosystem functioning [71, 140]. It is now widely accepted that bumblebee diversity has dramatically declined in the past several decades [27, 33, 36]. Diminishing populations have been ascribed to habitat loss, resulting in loss of nest and flower resources, pathogens, climate change and exposure to chemical insecticides [156, 193]. The buff-tailed bumblebee *Bombus terrestris* has been the subject of much study (see for example, [63, 146, 62, 63, 7]), as it is abundant in Europe and known to be an important pollinator [109]. Much experimental and analytic effort has been devoted to mapping its biology and natural history [32, 84]. However, much less is understood about its population *dynamics* over time and the growth of bumblebee populations subjected to pressures and limitations of resources (see [51]).

Mathematical modeling based on empirical information on life history parameters can be a strong tool to project population dynamics and identify vulnerable traits and life stages, e.g., through sensitivity analysis [52, 21, 133]. With a realistic time-dependent model, it is possible to implement

and study many suggested single and combined pressures that may affect bumblebees. Empirical research has concluded that forage resources (pollen and nectar) in the landscape affect overall bumblebee abundance. Furthermore, explicit modeling of resource dynamics over time has the potential to elucidate the mechanisms underlying these patterns and explain observed discrepancies (e.g., [190, 162, 41, 194]) in which life stages (of queens, workers, males, and gynes) are supported under contrasting timing, amount, type and quality of food resources. Previous theoretical [143] and empirical [31] work has focused on the influence of particular aspects of foraging behavior and queen survival on colony growth. Special attention in particular has been given to modeling the allocation of resources among workers and sexual offspring and its implications for colony growth [143], with some evidence that optimal tradeoffs are a function of colony size as well as queen egg-laying rates [152, 30]. We take a broader approach here, developing a population model in which we can explicitly test hypotheses about how landscape use and exposure to environmental toxins affect bumblebee populations.

We are motivated by the desire to understand the various ways in which *B. terrestris* populations are dynamically affected by environmental pressures, including pesticide exposure and resource limitation [81, 85, 120]. Mathematical modeling, especially in an iterative approach [21], can be used for projecting population abundance and understanding the importance of life history traits, such as survival, reproduction and seasonal reproductive switch times under contrasting scenarios. Mathematical modeling, particularly when paired with rich empirical data, provides analytic tools that experimentation alone cannot offer [19]. In this paper, we present a delay differential equation (DDE) model to simulate the abundance of different bumblebee castes and in-nest resources over time, with dynamics including colony establishment, mortality, colony growth, reproduction, and queen hibernation. Delay equations have been used in various applications, including biology, ecology, engineering (see [9, 53, 83, 100] for examples) and even honeybee population modeling [108]. We refer the reader to [168] for an introduction to DDEs and applications, as well as [112] for DDEs in ecology.

We present our model with the underlying assumptions, including a description of the literature references which provided us either direct or indirect estimates of some model parameters. We naturally introduce the class of DDEs and provide a brief overview for the reader. We introduce a linear spline approximation method for obtaining a numerical solution to our model. Next, we provide model simulations in the absence of pressures. Lastly, we propose ways in which pressures such as resource limitation and insecticide exposure can be reflected in the model.

2.2 Model

2.2.1 Our Proposed Model

As we shall further develop below, our model is naturally a nonlinear system of delay differential equations (DDE) which describe six state variables in a collection of bumblebee colonies: in-nest nectar abundance $A(t)$, in-nest pollen abundance $B(t)$, queens $Q(t)$, workers $W(t)$, males $M(t)$ and gynes (daughter queens) $G(t)$. According to [80], only 70% of foragers return to their own colony after a foraging trip; we therefore assume that there is not-insignificant interaction between colonies and model a collection of bumblebee colonies which share a common pool of resources. While our model certainly allows for multiple year projections, we consider a time span of less than one year here. We define the first day of spring $T_S := 0$, which denotes the day on which all hibernating gynes emerge from hibernation to become queens and found new colonies. The independent variable t measures time in days.

We consider the following assumptions and basic seasonal timeline [84, 63, 134, 32]. Hibernating gynes emerge and become queens that found new colonies at $t = T_S$. These queens immediately begin foraging for and storing resources (nectar and pollen) inside the nest, as well as producing worker eggs. In the absence of information about queen foraging efficacy, we assume that the queen accumulates a negligible store of resources during this time, primarily providing for herself and the initial brood of workers. Assuming a 22-day worker incubation time (from an egg laid to the emergence of an adult worker) [84, 63], the first workers emerge at $t = T_S+22$. At this time, the workers take over resource foraging to develop a store of in-nest resources and tending to new eggs, while the queens devote all energy to production of worker eggs [84]. The authors of [84, 32] discuss in detail the somewhat mysterious process of bumblebee reproduction. There are varying theories on what factors contribute to the switch from worker to male and queen offspring production; these factors include, but are not limited to, queen condition during the season or during hibernation, queen pheromones, and worker abundance [84, 32, 97, 161, 64, 63, 119, 134]. Environmental conditions can also cause nests to have either early or late season switch times [63]. In our model, we assume at some time $t = T^*$, the queen begins to lay sexual (male and gyne) eggs while continuing to produce worker eggs [32]. At time $t = T^{**}$, the queen stops producing worker eggs and devotes all energy to sexual egg production. At time $t = T^{**} + 22$, the last new worker emerges. At times $t = T^* + 26$, and $t = T^* + 30$, respectively, the first males and gynes emerge (assuming respective 26 and 30 day incubation periods [63]).

Sexuals continue to emerge until time $t = T_W$, at which point workers, queens and males die, and gynes go into hibernation and prepare to become queens in the following year [84, 32]. The exact values of these timeline points depend greatly on geography, environment and weather. Furthermore, we believe that allowing T^* and T^{**} to be functions of the worker population will allow us, in future

work, to explore whether environmental changes and pressures such as insecticide exposure can have an indirect effect on reproductive switch times. A timeline of the bumblebee's seasonal life cycle is depicted in Figure 2.1. To demonstrate the usefulness of the DDE model, we fix timeline values T^*, T^{**}, T_S and T_W at the values estimated by [134] as given in Table 2.2 and described in section 2.2.2 below.

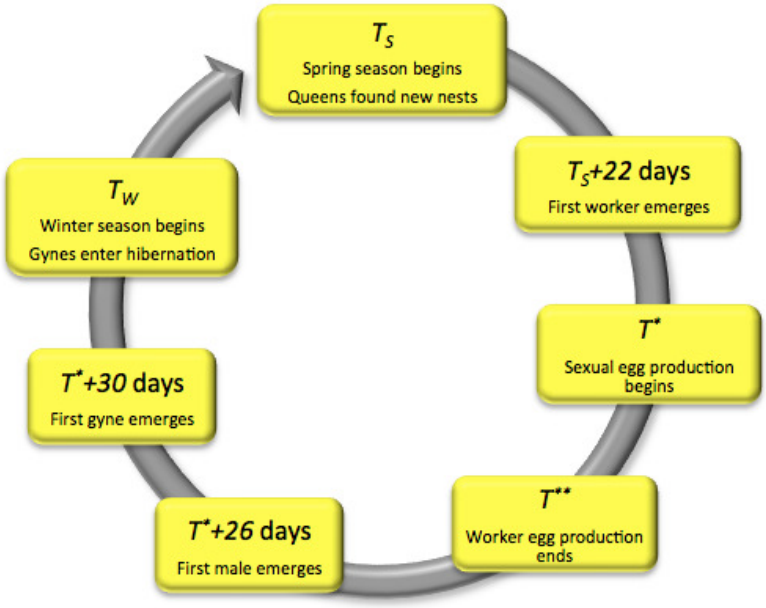

Figure 2.1 Timeline of bumblebee seasonal dynamics

We assume that the founding queen, workers, as well as worker, male and gyne larvae consume both nectar and pollen [63]. We explicitly assume that nectar and pollen consumption in the nest is negligible for adult males and adult gynes; [84] notes that males leave the colony a few days after reaching adulthood and that gynes may stay in the nest and forage for some time before finding a place to hibernate. In the absence of estimations for the resource consumption by emerging males and gynes in a colony, we assume that this short period of consumption is negligible and do not include it in the current model. We also assume that all colony members have a mortality rate, which encompasses mortality by aging and mortality during foraging trips. Although we assume that adult workers and queens consume resources, we do not model their mortality as a function of resources. We now present the mathematical model as well as the pre-spring history information in (2.1) and (2.2). Because of the previously described changes in seasonal dynamics, some differential equations are piecewise defined. All model variables, switch times, and parameters are described in Table 2.2. In addition, to elucidate the definitions of $\frac{dA}{dt}$ and $\frac{dB}{dt}$, we have included a description of seasonal resource (nectar and pollen) consumption and collection changes in Table 2.1. Resource

consumption by larvae, given by the functions l_W, l_M, and l_G in (2.1), and its functional dependence on $Q_t(a) = Q(t-a), a \in [\alpha, \beta]$ will be described later in more detail.

$$
\begin{aligned}
\frac{dA}{dt} &= \left(b_{AW} - \mu_{AW}\right) W - \mu_{AQ} Q - 2(l_W(t,Q_t) + l_M(t,Q_t) + l_G(t,Q_t)) \\
\frac{dB}{dt} &= \left(b_{BW} - \mu_{BW}\right) W - \mu_{BQ} Q - (l_W(t,Q_t) + l_M(t,Q_t) + l_G(t,Q_t)) \\
\frac{dQ}{dt} &= -\mu_Q Q \\
\frac{dW}{dt} &= b_W(t-22)Q(t-22)\frac{1}{9}\int_{t-18}^{t-9} L(\gamma_W W(s)) L\left(\frac{A(s) + \frac{B(s)}{d_B}}{Q(s)\left(A_{max} + \frac{B_{max}}{d_B}\right)}\right) ds - \mu_W W \\
\frac{dM}{dt} &= b_M(t-26)Q(t-26)\frac{1}{11}\int_{t-22}^{t-11} L(\gamma_M W(s)) L\left(\frac{A(s) + \frac{B(s)}{d_B}}{Q(s)\left(A_{max} + \frac{B_{max}}{d_B}\right)}\right) ds - \mu_M M \\
\frac{dG}{dt} &= b_G(t-30)Q(t-30)\frac{1}{13}\int_{t-26}^{t-13} L(\gamma_G W(s)) L\left(\frac{A(s) + \frac{B(s)}{d_B}}{Q(s)\left(A_{max} + \frac{B_{max}}{d_B}\right)}\right) ds - \mu_G G
\end{aligned}
\tag{2.1}
$$

$$
A(t) = \begin{cases} 0 & t < T_S + 22; \\ A_0 & t = T_S + 22; \\ 0 & t \geq T_W; \end{cases}
\qquad
W(t) = \begin{cases} 0 & t < T_S + 22; \\ W_0 & t = T_S + 22; \\ 0 & t \geq T_W; \end{cases}
$$

$$
B(t) = \begin{cases} 0 & t < T_S + 22; \\ B_0 & t = T_S + 22 \\ 0 & t \geq T_W; \end{cases}
\qquad
M(t) = \begin{cases} 0 & t < T^*; \\ M_0 & t = T^* + 26; \\ 0 & t \geq T_W; \end{cases}
\tag{2.2}
$$

$$
Q(t) = \begin{cases} 0 & t < T_S; \\ G(T_S - 1) & t = T_S; \\ 0 & t \geq T_W; \end{cases}
\qquad
G(t) = \begin{cases} G_0 e^{-\mu_{G_W} t} & t < T_S; \\ 0 & t = T_S; \\ G_1 & t = T^* + 30; \end{cases}
$$

Table 2.1 Seasonal time intervals and corresponding effects of colony members on resources, nectar and pollen.

Time interval	Resource collection and consumption
$[T_S, T_S+22)$	queen collecting and consuming resources worker larvae consuming resources after T_S+4 negligible accumulation of in-nest resources
$[T_S+22, T^*)$	workers collecting and consuming resources queen consuming resources worker larvae consuming resources
$[T^*, T^{**}+22)$	workers collecting and consuming resources queen consuming resources worker larvae consuming resources until $T^{**}+13$ male larvae consuming resources after T^*+4 gyne larvae consuming resources after T^*+4
$[T^{**}+22, T_W)$	workers collecting and consuming resources queen consuming resources male larvae consuming resources until T_W-11 gyne larvae consuming resources until T_W-13

Table 2.2 Model variables and parameters. The selected value for simulations is given in the last column; we include a source reference for values drawn from the literature.

Variable	Description	Units	Estimate
t	time	days	
$A(t)$	amount of nectar in colonies	ml	
$B(t)$	amount of pollen in colonies	g	
$Q(t)$	number of queens	individuals (queens)	
$W(t)$	number of workers	individuals (workers)	
$M(t)$	number of males	individuals (males)	
$G(t)$	number of gynes	individuals (gynes)	
Timeline			
T_S	first day of spring		$T_S := 0$
T^*	first day male/gyne eggs laid		40 [134]
T^{**}	end of worker eggs laid		44 [134]
T_W	beginning of winter		120
Parameters			
μ_{AQ}	queen nectar consumption rate	$\frac{\text{ml}}{\text{day·individual }(Q)}$	1
μ_{BQ}	queen pollen consumption rate	$\frac{\text{g}}{\text{day·individual }(Q)}$	0.8
μ_Q	queen death rate	$\frac{1}{\text{day}}$	0.0154 [79]
b_{AW}	worker nectar collection rate	$\frac{\text{ml}}{\text{day·individual }(W)}$	0.6[87, 146]
b_{BW}	worker pollen collection rate	$\frac{\text{g}}{\text{day·individual }(W)}$	0.4[87, 68]
μ_{AW}	worker nectar consumption rate	$\frac{\text{ml}}{\text{day·individual }(W)}$	0.15
μ_{BW}	worker pollen consumption rate	$\frac{\text{g}}{\text{day·individual }(W)}$	0.15
$b_W(t)$	worker birth rate	$\frac{\text{workers}}{\text{queen·day}}$	2.4
μ_W	worker death rate	$\frac{1}{\text{day}}$	0.05
γ_W	worker-worker larvae survival coefficient	$\frac{1}{\text{individual }(W)}$	0.0025
$b_M(t)$	male birth rate	$\frac{\text{males}}{\text{queen·day}}$	1.2
μ_M	male death rate	$\frac{1}{\text{day}}$	0.01
γ_M	worker-male larvae survival coefficient	$\frac{1}{\text{individual }(W)}$	0.0025
$b_G(t)$	gyne birth rate	$\frac{\text{gynes}}{\text{queen·day}}$	0.8
μ_G	in-season gyne death rate	$\frac{1}{\text{day}}$	0.01
μ_{G_W}	hibernation gyne death rate	$\frac{1}{\text{day}}$	
γ_G	worker-gyne larvae survival coefficient	$\frac{1}{\text{individual }(W)}$	0.0025
A_{max}	in-nest nectar maximum (per nest)	$\frac{\text{ml}}{\text{individual}(Q)}$	150
B_{max}	in-nest pollen maximum (per nest)	$\frac{\text{g}}{\text{individual}(Q)}$	150
d_B	pollen grain density	$\frac{\text{g}}{\text{ml}}$	1[37]
P_0	initial larval pollen consumption	$\frac{\text{g}}{\text{individual}(W)\text{·day}}$	0.001 [158]
$\bar{r}$	larval pollen consumption growth rate	$\frac{1}{\text{day}}$	0.25 [158]

2.2.2 Model and Parameter Considerations

For our simulations, additional model and parameters considerations were necessary. We searched the literature to determine reasonable values for various model assumptions and parameters. Other parameters in the model, such as the death rate of adult bees, are difficult to empirically assess in natural environments. Even parameters for which a measured value can be found in the literature may be scenario dependent and expected to vary between applications. For these remaining parameters, we select values which are feasible in the defined units and, for the purpose of demonstrating the interplay between resources, workers, and sexual bees, do not result in total population loss. In Table 2.2 all model variables, time points, parameters and initial conditions are reported with corresponding units and literature comments. We now comment further on these choices.

The function L used at several places in (2.1) is defined by

$$L(x) = \frac{1-e^{-x}}{1+e^{-x}}.$$

This is an increasing, saturating sigmoid function depending on the argument x (much like a cumulative distribution function to describe probability of survival) [108]. The function L is bounded in $[0,1]$ and used to describe various daily survival rates of worker, male and gyne larvae, where x depends on the population of worker bees which tend to the larvae or in-nest resources. In (2.1), the product of the two daily survival rates are averaged (using a weighted integral) over the time frame for which members of a class would be in their larval state. For example in $\frac{dW}{dt}$, emerging workers are in their larval state between $t-18$ and $t-9$ which are the bounds for the integral and the weight $1/9$ is required for the 9 days these workers spent in the larval phase.

In our model equations for workers, males and gynes, we see the term $A(s)+d_B^{-1}B(s)$, quantifying the net resources at time s. Because A is measured in milliliters, and B is measured in grams, it is reasonable to use a unit of either ml or g, so without loss of generality, we choose the unit ml. We can convert the mass of pollen B into volume using the density of pollen. In other words,

$$B_V(t) = d_B^{-1}B(t),$$

where $B_V(t)$ denotes the volume of pollen and d_B denotes its density (a constant). There are various species of pollen, each with different specific material densities. According to [37], an estimated value for pollen grain density is 1g/ml. So we choose $d_B = 1$ for the preliminary simulations.

When modeling resource consumption we use the fact that a bumblebee goes through three sequential stages: egg, larval, and pupal before becoming an adult. Larvae consume resources but eggs and pupa do not; we note the effect this has on seasonal resource consumption in Table 2.1. Larval stage length can be modified based on food availability [174] or in-nest temperature. For

simplicity, we assume that bumblebees have constant incubation schedules, seen in Table 2.3 [63].

Table 2.3 Bumblebee incubation breakdown by caste

Caste	Total no. incubation days	Egg (days)	Larva (days)	Pupa (days)
Workers	22	4	9	9
Males	26	4	11	11
Gynes	30	4	13	13

Our model tracks resources (pollen and nectar) and adult colony members (queens, workers, males and gynes). However, all larvae contribute to resource consumption as well and this dynamic must be included in the model. In Table 2.1, we summarize the effects of all colony members on resources at all phases of the season. We tentatively assume, for sake of simplicity, that the last worker emerges when the first male emerges (because of our knowledge of incubation times of 22 and 26 days for workers and males, respectively, and our estimate that $T^* = 40$ and $T^{**} = 44$, as seen in Table 2.2). With these assumptions, we have three functionals $l_W(t,Q_t)$, $l_M(t,Q_t)$ and $l_G(t,Q_t)$, in (2.1), which reflect larval pollen consumption and require definition.

According to [158, 159, 148] daily pollen intake (measured in mass of pollen per larvae per day) increases exponentially as age increases. Therefore, we can model daily pollen intake per worker larvae by $P_0 e^{\bar{r}a}$ where a measures age with unit [day], for some positive constants P_0 and $\bar{r}$. The expected number of worker larvae of age a at time t is given by $b_W(t-a)Q(t-a)$, for $4 \le a \le 13$. Therefore, we can model pollen consumption per day by worker larvae as

$$l_W(t,Q_t) = \int_4^{13} b_W(t-a)Q(t-a)P_0 e^{\bar{r}a}\,da. \tag{2.3}$$

A simple change of variables can be used to express this in terms of hysteretic dependence on Q given by

$$l_W(t,Q_t) = \int_{t-13}^{t-4} b_W(s)Q(s)P_0 e^{r(t-s)}\,ds.$$

Note that this functional $l_W(t,Q_t)$ depends on the values of $Q(s)$, $t-13 \le s \le t-4$. Similarly, we have

$$l_M(t,Q_t) = \int_4^{15} b_M Q(t-a)P_0 e^{\bar{r}a}\,da, \tag{2.4}$$

for pollen consumption by male larvae which can be written as

$$l_M(t,Q_t) = \int_{t-15}^{t-4} b_M(s)Q(s)P_0 e^{r(t-s)}\,ds,$$

and

$$l_G(t,Q_t)=\int_4^{17} b_G Q(t-a)P_0 e^{\bar{r}a}\,da, \tag{2.5}$$

for pollen consumption by gyne larvae which can be written as

$$l_G(t,Q_t)=\int_{t-17}^{t-4} b_G(s)Q(s)P_0 e^{r(t-s)}\,ds.$$

We note that the functional dependence on $Q(s)$ is different in each of (2.3), (2.4) and (2.5). We will however simply denote the dependence by Q_t in a slight abuse of notation which should not result in confusion for the reader.

By examining data in [158], we assume that initial larval consumption (per larva) P_0 is constant across castes, along with exponential consumption rate $\bar{r}$. In addition, according to [147], larval diet consists of approximately 34% pollen, and the rest is a combination of nectar and a trivial amount of digestive enzymes. Consequently, we can assume an approximate 2:1 ratio of nectar to pollen for larval consumption, which explains the larval consumption terms in the model for $\frac{dA}{dt}$. We note, however, that the functionals l_W, l_M, and l_G assume consumption by larvae with total survivability into adulthood, while (2.1) assumes some proportion of all larvae do not survive to adulthood. Our model underestimates the store of in-nest resources available to hives by overestimating the consumption of these resources by larvae. Furthermore to capture the first brood (W_0) dynamics of the colony [63], the first brood is assumed to have the necessary resources and size to grow to adulthood, while larval consumption (and the necessary resource collection) controls the hive dynamics for all larvae after the initiation of a queen's first brood.

Since different colonies within a region can exhibit different growth and reproductive strategies [84], the initial conditions in (2.2) may be non-zero valued in order to capture the appropriate dynamics. To accurately simulate first brood dynamics, the initial condition $W_0 = 192$ accounts for the number of workers produced at $T_S + 22$ [63] corresponding to the number of beginning colonies, $G_0 = 20$. Similarly, M_0 and G_1 allow for large emergence of males and gynes respectively. The non-zero initial values A_0 and B_0 may represent in-nest stores of pollen and nectar which remain after the queen rears the first brood. As indicated previously, we assume no in-nest stores when workers emerge at $T_S + 22$. We also assume no large emergence of males and gynes, taking $M_0, G_1 = 0$.

In addition, we simplify the model by letting the worker, male and gyne birth rates $b_W(t)$, $b_M(t)$, and $b_G(t)$ respectively, be time dependent expressions given by

$$
\begin{aligned}
b_W(t) &= \begin{cases} \overline{b}_W & T_S \le t \le T^{**} \\ 0 & \text{else} \end{cases} \\
b_M(t) &= \begin{cases} \overline{b}_M & T^* \le t \le T_W - 26 \\ 0 & \text{else} \end{cases} \\
b_G(t) &= \begin{cases} \overline{b}_G & T^* \le t \le T_W - 30 \\ 0 & \text{else.} \end{cases}
\end{aligned} \tag{2.6}
$$

This allows for proper simulation of the phases described in Table 2.1 by equations (2.3) - (2.5).

To determine the seasonal switch times (T^*, T^{**}), we use the following information taken from [134]. Let the term “first egg" denote the first egg laid in the colony, regardless of caste determination. In the experiments conducted in [134], the average time from first egg to last worker emergence was approximately 66 days; assuming a 22 day incubation time, this implies that $T^{**} = 44$. The average time from first egg to first emergence of gynes and males was 70 and 65 days, respectively. Assuming 30 and 26 day incubation periods for gynes and males, respectively, this provides two estimates for T^*: $T^* = 40$ or $T^* = 39$. Because these values are so similar, we assume $T^* = 40$ for our simulations.

Also from the literature, values for b_W and μ_Q were determined; the reference [134] provides an estimate for the average number of workers produced per day in a given colony, which gives us a direct estimate: $b_W = 2.4$. Then by [79], we used the information that 14 out of 40 total colonies saw mother queen loss (hence 26 queens survived) in a given experiment lasting 28 days. We performed a simple inverse problem for the model

$$
\frac{dQ}{dt} = -\mu_Q Q, \quad Q(0) = 40
$$

with the sole data point $Q(28) = 26$. This returns the best fitting estimate $\mu_Q = 0.0154$. We initially use these values in our simulations.

Last, we note that the state variables may be properly viewed as components of the 6×1-vector $\mathbf{x}$ satisfying delay differential equations [9, 10, 11, 16, 20, 53, 105, 104, 83, 168] which have been widely used over the last several decades in population models. As is known, these delay equations require not only the initial values, η, of the states at time 0 ($t \equiv T_S$), but also the history information, ϕ for all $t \in [-\overline{\tau}, 0)$, for $\overline{\tau}$ defined by the model (in this case, $\overline{\tau} = 30$). For now, we further simplify the model by changing the history information for the gyne population, G. Instead of the exponential decay we see in (2.2) for $t < T_S$, we will first assume that G remains a non-zero constant value G_0 for $t < T_S$. Initially, we made these choices of history information,

$$
\eta = [A_0, B_0, Q_0, 0, 0, 0]^T
$$

where $Q_0 = G(T_S - 1) = G_0$ (i.e., the number of queens when spring begins is the number of gynes at $t = -1$, i.e., at the end of last season), and

$$\phi = [0, 0, 0, 0, 0, G_0]^T,$$

for some constants A_0, B_0, and G_0. With these choices of history information, all history functions are continuous except at $t = 0$ where there is a jump discontinuity in four of the six variables. While this is theoretically acceptable for our numerical solution method of using spline approximations (discussed briefly below and in more detail in [15, 13]), in practice this jump discontinuity creates a computational error in our model that is propagated over time (because solving delay equations requires iteratively solving large linear systems, which are described in detail in [15]). To alleviate this, we instead chose a continuous history function by incorporating "ramp" functions for nectar, pollen, queens, and gynes. For example, let $\phi_A(t)$ and η_A denote the history function on $t \in [-\overline{\tau}, 0)$ for nectar and $A(0)$, respectively. Then we have

$$\phi_A(t) = \begin{cases} 0 & -\overline{\tau} < t < -2; \\ \eta_A(\frac{t}{-2} + 1) & -2 \leq t < 0; \end{cases}.$$

Defining similar ramp functions and incorporating them into our history for pollen, gynes and queens alleviates the computational error faced with the jump discontinuities at $t = 0$.

The Banks-Kappel spline methodology, described in [10, 20, 11, 13], is used to find a linear spline approximation to the solution of the system of equations in (2.1)-(2.2). This method is useful since our model is defined piecewise (in terms of reproduction) and when solving in phases (see Table 2.1), history functions can easily be determined from prior phases. The linear spline solutions also allow for easy approximation of the integral expressions found in the model. The Banks-Kappel spline methodology produces auspicious results for our model as shown below.

2.3 Results

In Figure 2.2 we plot the solution to the system with the default parameter set described in Table 2.2. In the collection of colonies, the total number of workers decreases throughout the season, with the slowest rate of decrease occurring between days 40 and 60. The workers enter a phase of purely exponential decay towards the end of the season, driven by our definition of the period in which new workers are produced. The males and gynes both experience growth, but this growth is slow and levels off quickly. Resource levels increase significantly after workers emerge, with pollen growing at a slower rate than nectar by choice of parameters. In the colonies, the nectar and pollen resources level off toward the end of the season.

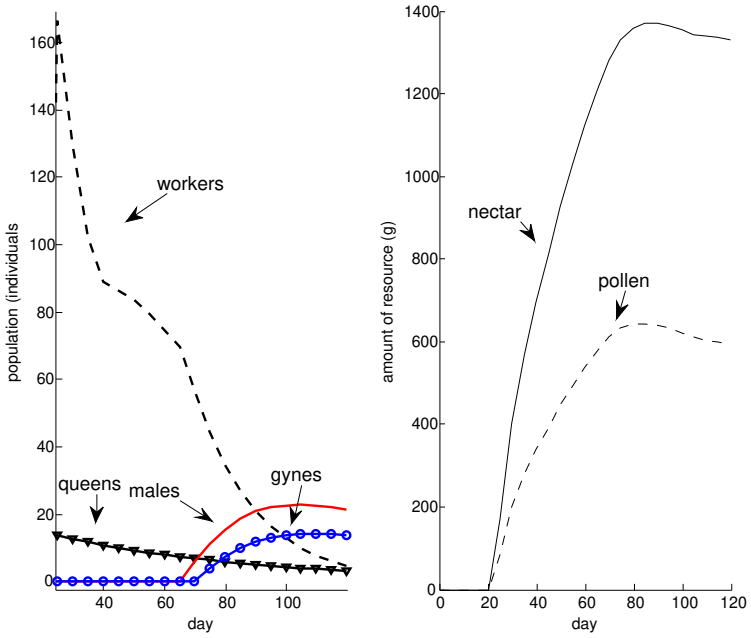

Figure 2.2 Population levels simulated with the default parameter set. Bee castes are plotted in the left graphs and resource levels are plotted in the right graphs.

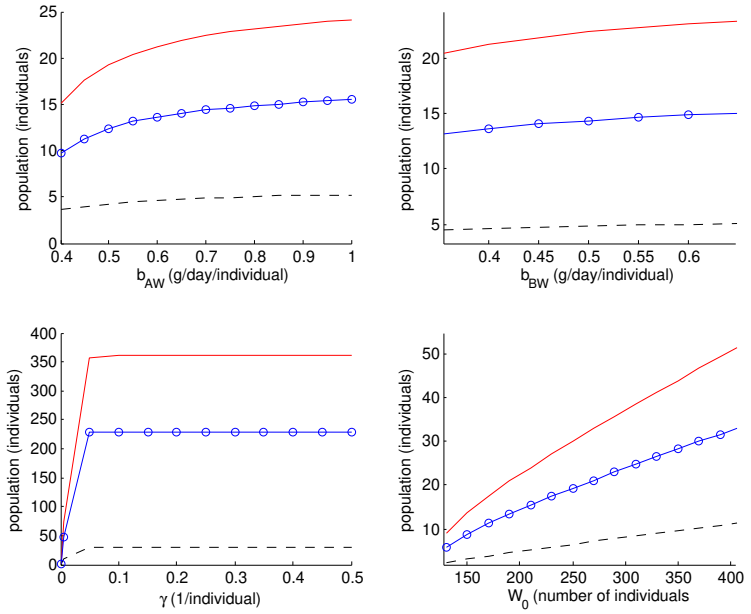

Figure 2.3 Sensitivity of the final populations of workers, males, and gynes to changes in b_{AW}, b_{BW}, γ, and W_0.

In Figure 2.3 we plot the final population levels of the workers, males, and gynes as functions of parameters b_{AW} (worker nectar collection rate), b_{BW} (worker pollen collection rate), γ (worker to larvae survival coefficient), and W_0 (size of initial worker brood). In Figure 2.4, we plot the final nectar and pollen levels as functions of the same parameters.

The final worker, male, and gyne populations do not appear to be sensitive to b_{AW} or b_{BW}. However, these parameters have significant impacts on the amount of nectar and pollen available to bumblebee larvae; the final amount of nectar increases with b_{AW} and, similarly, the final amount of pollen increases with b_{BW}.

The final level of all populations and resources share a positive, saturating relationship with γ. We note that for $\gamma = .4$, we have $L(\gamma W) \geq .999$ for all $W \geq 25$. That is, we have almost no larval mortality due to worker neglect while $W \geq 25$. Since $W_0 = 192$, there are sufficient worker bees for much of the season to guarantee that $L(\gamma W) \geq .999$. It is not surprising that increasing the value of γ beyond this value does not significantly affect the final state of the system.

All states share a positive, linear relationship with W_0. We note that the final worker population does not exhibit high sensitivity to any of the tested parameters. This is not surprising; because workers enter a phase of exponential decay around $t = 70$, they may be highly sensitive to the parameters, but this effect is diminished by the end of the season.

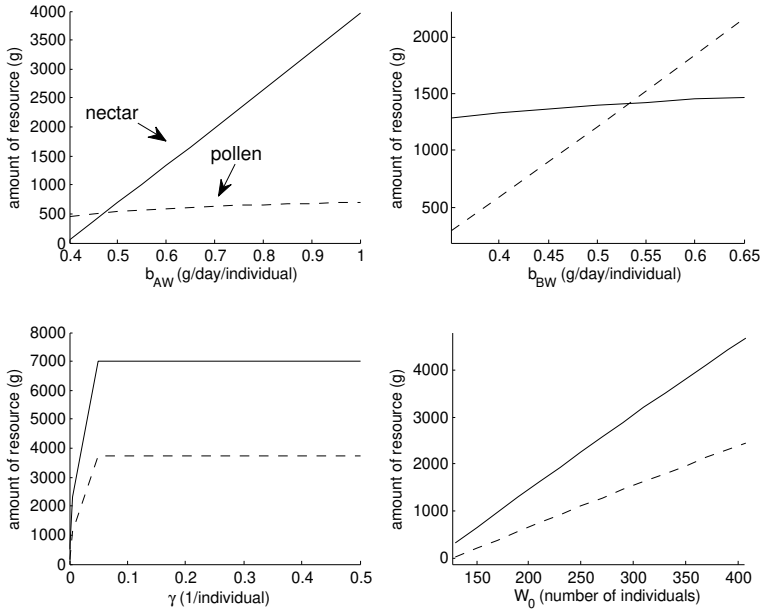

Figure 2.4 Sensitivity of the final nectar and pollen levels to changes in b_{AW}, b_{BW}, γ, and W_0.

2.4 Discussion

In this paper, we present a delay differential equation model to describe population dynamics of a collection of bumblebee colonies. Following [51], we place significant importance on the colonies' collection of nectar and pollen in determining larval survival and hive dynamics. We chose the natural use of delay equations to accurately capture the incubation times and dependence on the history of resource availability in bumblebee birth rates. We present the solutions to the model in a season where a lack of resources does not cause significant environmental pressure and the switch to production of bees occurs at a fixed time, independent of bee populations.

Without data, we cannot conclude that our model captures the behavior of a particular collection of bumblebee colonies. We find that compared to other theoretical works, our model performs adequately in describing bumblebee dynamics. In [51], total colony weight was expected to increase exponentially and subsequently decrease once workers begin to die and sexuals begin to leave the nests. Without modeling subadult stages, we cannot quantify colony weight for a direct comparison; we do note, however, that prior to the emergence of sexuals we see rapid growth of in-nest resources, measured in grams. Rates of birth into subadult classes are assumed to be constant, but we cannot draw conclusions about larval contributions to hive weight due to assumed mortality and adult emergence. Furthermore, queen production in [51], as in our model, was driven by multiple mechanisms, including floral resources. The general trend of increased total population until worker death and sexual dispersal seen in the model and experimental data of [51] lended further support to our proposed model, though Poitrineau et al. and others emphasize that this may be mitigated by worker efficiency and queen egg-laying rates [30, 152].

Our simulations capture late-season death of workers and the emergence of sexual bees, although nectar and pollen levels do not decrease late in the season, making it unlikely that colony weight decreases as observed in [51]. This is far from an optimal strategy for hive consumption of resources and may be an artifact of uncertainty in our parameters instead of a likely population dynamic; it is necessary in future work that we corroborate model output with available data in order to calibrate our assumed parameters for resource collection and consumption. Due to the manual selection of critical model parameters and the inherent uncertainty in those taken from the literature, we do not necessarily conclude that the model cannot replicate this weight pattern. Instead, we must in future efforts better estimate model parameters in order to match this classically assumed behavior.

The authors of [152, 121] model bumblebee reproductive switch times by optimal strategies; as explained in our model development, we assume an overlapping switch in which queens lay worker and sexual eggs simultaneously. Our choice of reproductive strategy is in line with the behaviors modeled in [152], but our model's assumed incubation times for sexual bees results in dynamics similar to those in [121], where the worker population is in complete decline when sexuals begin to emerge. With data, we can calibrate model parameters to obtain resource and population outputs

at physically reasonable levels.

We can see in the sensitivity results that the size of the first brood of workers has a more significant impact on the male population than the gyne population. This may be affected by the birth rate of the males, which is higher than the gyne birth rate. However, the fact that males have a shorter development time (4 days less) may also enhance this effect; the history that affects an emerging male bee at time t overlaps with, but is distinct from, the history that affects a gyne emerging at that same time. These types of delay dynamics are uniquely captured by our choice of model. Although the use of a DDE produced a more complex mathematical and computational problem to solve, we suggest that an ODE-based model would be insufficient to describe seasonal bumblebee population dynamics in this way.

The results from the sensitivity analysis also indicate that changes need to be made to the model in future simulations. We would expect that parameter values which can cause low levels of nectar or pollen in the hive (such as b_{AW} and b_{BW}) would have a significant impact on larval survivability and therefore the final populations of males and gynes, but our model does not capture this behavior. This may be caused by considering the quantity $A + B/d_B$ in larval survivability; even when pollen resources are near zero, larval survivability can be high if nectar resources are sufficiently high. At the default parameter set presented here, resources are plentiful and the lack of resource-dependent mortality does not play a significant role. Resource scarcity also has no effect on adult mortality in the current model, which may contribute to the lack of sensitivity to b_{AW} and b_{BW}. However, at extremely low resource levels, a persistent worker bee population may cause a rebound effect for resources, where total colony collapse would be more realistic. We note that the conflation of uncertainty in model assumptions and parameters makes it difficult to determine a single cause of model dynamics.

2.5 Research Contributions

As mentioned previously, it is important to understand bumblebee population dynamics in the presence of various environmental pressures, including resource scarcity and insecticide exposure. The model developed in this work is the first delayed differential equation model in the literature that focuses on individual classes of bumblebees within a colony and in addition addresses resource management. This amount of detail describing the processes which occur inside the hive is not found in other modeling attempts of bumblebee colonies (with the exception of an agent-based model [29] developed simultaneously with our work). Our results indicate that our model holds high promise for better understanding bumblebee population dynamics, especially in response to anthropogenic disturbance. For instance, there are multiple ways to incorporate both lethal and sub-lethal effects of insecticide-exposure into population models of this sort, including changes in worker death rate, worker collection rate, worker productivity rates, queen death rate, and queen

reproduction rates. In [40] the authors show that varying parameterizations of an ODE model can result in colony loss under sub-lethal stresses. Next, we progress to the motivating problem of understanding how pressures such as neonicotinoid exposure may have lethal and/or sublethal effects on bumblebee colonies.

CHAPTER

3

LETHAL AND SUBLETHAL EFFECTS OF TOXICANTS ON BUMBLEBEE POPULATIONS: A MODELING APPROACH

Adopted from Open Access publication: Ecotoxicology, February 2020 [22]

3.1 Introduction

The protection of ecosystem services has become a major focus of applied ecology, with one emphasis on understanding population processes of pollinators and biological control agents. Pollinator conservation in particular has received much attention due to their well-documented decline coupled with their ability to significantly contribute to crop pollination [110, 195]. Globally, chemical pesticides (especially the class known as neonicotinoids) have been implicated in hymenopteran decline [59, 86, 120, 163]. Exposure to pesticides has been implicated in deficits in both short- and long-term learning as well as memory and sensory capabilities, all of which can affect foraging efficiency and provisioning [178, 111]. Within-colony behavior related to caretaking, which can have implications for thermoregulation and colony survival, may also be affected by pesticide exposure [49]. Despite our increased understanding of the effects of pesticide exposure on bee physiology and behavior, the overall effects of pesticides on population dynamics of bees remain poorly understood. Furthermore, much of what we do know about population processes of pollinators stems from work conducted with honeybees (*Apis melifera*); recent simulation models have identified the potential for sublethal effects on honeybees stemming from varroa mites and

other stressors [28, 182], while other models have underscored the complex relationships between food availability and honeybee foraging and survival [108, 149].

More recently, attention has increasingly focused on non-*Apis* bees, especially wild bees. In particular, declines and shifts in community composition of bumblebees (*Bombus sp.*) have been documented in North America and Europe [33, 36, 27]. A suite of lethal and sublethal effects of pesticides on bumblebee populations have been demonstrated, including reductions in foraging ability and other behavioral changes [38, 68, 26, 169, 175, 150, 115]. A population-level perspective is critical in linking what we know about individual toxicant effects to the long-term effects of pesticide exposure on bumblebee populations.

Pesticide risk assessment in the United States for all arthropods is based on acute toxicity tests (LC_{50}) on a single species – the European honeybee (*A. mellifera*) – making that organism an ideal starting point for understanding the effects of chemical stressors for other bees. However, we have shown that, due to subtle differences in life histories, even closely related hymenopteran species can exhibit markedly different population responses to the same toxic insults [25, 24]. Further complicating matters, work done at the physiological level reveals that different bee species exhibit different levels of susceptibility to the same chemical pesticides [125]. Taken together, what we know about the effects of toxicants on one species (e.g., honeybees) does not necessarily translate to a good understanding of the effects of toxicants on other even closely related species such as bumblebees; responses to toxicants need to be evaluated for each species. Furthermore, it is now well established that acute tests such as LC/LD_{50}, historically the gold standard for comparing toxicological effects, fail to capture longer-term population outcomes (including sublethal effects) and could be woefully misleading [23, 170, 171, 59, 72, 34, 173]. Finally, most studies of chemical toxicity related to bumblebees have focused on a single toxicant or pesticide, when in practice in the field bees are subjected to multiple toxicants acting in both lethal and sublethal ways [172] Here we seek a better understanding of toxicant effects on a developing colony of bumblebees over time, as well as insights into how acute and sublethal effects (either from the same or different chemical toxicants) may combine to affect population outcomes.

The utilization of computational models in bumblebee research has increased in recent years although it still has not been as exhaustive as efforts on honeybees. Many models have focused on foraging dynamics by workers as they influence different metrics of colony growth [143, 141, 51, 91]. Becher et al. (2018) used agent-based modeling to understand hive dynamics, examining the influence of pesticides on multi-generational colony dynamics, though they did not explore effects on colony interior dynamics. Other similar models indicate that pesticides and other stressors can impact colony dynamics, for example by impairing worker bee productivity or queen fecundity [40, 50]. These studies rely on differential and difference equations, in which changes to the colony at any time depend on the current state of the colony. However, changes to a colony might also depend on prior states of the colony, for example due to the length of larval incubation or history

of resource availability. We describe these dependencies with a delay differential equation model, parameterized with values taken from the literature.

3.2 Methods and Materials

A delay differential equation (DDE) framework is appropriate to use in age structured population models [137, 90, 12, 14]. We modeled a single colony of bumblebees using a non-linear system of delay differential equations that describe twelve state variables: in-nest nectar abundance N(t), in-nest pollen abundance P(t), workers W(t) and their larvae (modeled as a two-stage population, $L_1^{(w)}$,$L_2^{(w)}$), males M(t) and their larvae (modeled as a two-stage population, ($L_1^{(m)}$,$L_2^{(m)}$), and gynes (new queens) G(t) and their larvae (modeled as a three-stage population, ($L_1^{(g)}$, $L_2^{(g)}$, $L_3^{(g)}$). These variables are described in (3.1) - (3.12) and we note that the expressions $\exp[x] = e^{[x]}$ for easier reading.

Bumbleebee Colony Model

Resources:

$$\frac{dN}{dt} = (b_{NW} - \mu_{NW})W - 2[c_1(L_1^{(w)} + L_1^{(m)} + L_1^{(g)}) + c_2 L_2^{(w)} + c_3 L_2^{(m)} + c_4 L_2^{(g)} + c_5 L_3^{(g)}] \tag{3.1}$$

$$\frac{dP}{dt} = (b_{PW} - \mu_{PW})W - [c_1(L_1^{(w)} + L_1^{(m)} + L_1^{(g)}) + c_2 L_2^{(w)} + c_3 L_2^{(m)} + c_4 L_2^{(g)} + c_5 L_3^{(g)}] \tag{3.2}$$

Workers:

$$\frac{dW}{dt} = b_W^*(t-22)\exp[\Phi^{(w)}(t-18) - \Phi^{(w)}(t-9)] - \mu_W W \tag{3.3}$$

$$\frac{dL_1^{(w)}}{dt} = b_W^*(t-4) - \mu^{(w)}(t)\, L_1^{(w)} W - b_W^*(t-10)\exp[\Phi^{(w)}(t-6) - \Phi^{(w)}(t)] \tag{3.4}$$

$$\frac{dL_2^{(w)}}{dt} = b_W^*(t-10)\exp[\Phi^{(w)}(t-6) - \Phi^{(w)}(t)] - \mu^{(w)}(t)\, L_2^{(w)} W - b_W^*(t-13)\exp[\Phi^{(w)}(t-9) - \Phi^{(w)}(t)] \tag{3.5}$$

Males:

$$\frac{dM}{dt} = b_M^*(t-26)\exp[\Phi^{(m)}(t-22) - \Phi^{(m)}(t-11)] \tag{3.6}$$

$$\frac{dL_1^{(m)}}{dt} = b_M^*(t-4) - \mu^{(m)}(t)\, L_1^{(m)} W - b_M^*(t-12)\exp[\Phi^{(m)}(t-8) - \Phi^{(m)}(t)] \tag{3.7}$$

$$\frac{dL_2^{(m)}}{dt} = b_M^*(t-12)\exp[\Phi^{(m)}(t-8) - \Phi^{(m)}(t)] - \mu^{(m)}(t)\, L_2^{(m)} W - b_M^*(t-15)\exp[\Phi^{(m)}(t-11) - \Phi^{(m)}(t)] \tag{3.8}$$

Gynes:

$$\frac{dG}{dt} = b_G^*(t-30)\exp[\Phi^{(g)}(t-26)-\Phi^{(g)}(t-13)] \tag{3.9}$$

$$\frac{dL_1^{(g)}}{dt} = b_G^*(t-4)-\mu^{(g)}(t)\,L_1^{(g)}W - b_G^*(t-10)\exp[\Phi^{(g)}(t-6)-\Phi^{(g)}(t)] \tag{3.10}$$

$$\frac{dL_2^{(g)}}{dt} = b_G^*(t-10)\exp[\Phi^{(g)}(t-6)-\Phi^{(g)}(t)]-\mu^{(g)}(t)\,L_2^{(g)}W - b_G^*(t-13)\exp[\Phi^{(g)}(t-9)-\Phi^{(g)}(t)] \tag{3.11}$$

$$\frac{dL_3^{(g)}}{dt} = b_G^*(t-13)\exp[\Phi^{(g)}(t-9)-\Phi^{(g)}(t)]-\mu^{(g)}(t)\,L_3^{(g)}W - b_G^*(t-17)\exp[\Phi^{(g)}(t-13)-\Phi^{(g)}(t)] \tag{3.12}$$

Larval Mortality:

$$\frac{d\Phi^{(k)}}{dt} = \mu^{(k)}(t)W(t), \qquad \text{where index } k \text{ denotes class w, m, or g} \tag{3.13}$$

For $\theta \in [T_s-8, T_s+22]$,

$$\begin{aligned}
&N(\theta)=N_0 && W(\theta)=R(W_0).\\
&P(\theta)=P_0 && L_1^{(w)}(\theta)=R(L_0^{(W)})\\
&M(\theta)=0 && L_2^{(w)}(\theta)=0\\
&L_1^{(m)}(\theta)=0 && G(\theta)=0\\
&L_2^{(m)}(\theta)=0 && L_1^{(g)}(\theta)=0\\
&L_2^{(g)}(\theta)=0 && L_3^{(g)}(\theta)=0\\
&\Phi^{(k)}(\theta)=0,
\end{aligned} \tag{3.14}$$

where k indicates class w,m, or g and $R()$ is a ramp function.

The model describes the development of the reproductive classes by means of important colony functions such as resource management, worker caregiving, and population control. It utilizes larval development as the link between colony resources and the adult bumblebee members. Parameter values are given in Table 3.2. Solutions of the bumblebee colony model are found using the Matlab delay differential equation solver *dde23* [126]. This solver was chosen over the Banks-Kappel spline method [20, 11] for three reasons: results have a higher order solution, integrals are no longer present

in the description of the dynamics and lastly, the increase of unique discrete delays from 7 to 15 are easier to manage with *dde23*.

Here we model a bumblebee colony over a single year capturing the behavior of a colony from its initiation in the spring (T_s) until hive functions cease in winter (T_w). With limited information in the literature regarding the behavior of queens prior to the emergence of the first brood, our simulated colony begins 22 days after hive initiation in the spring ($T^s + 22$), when the first brood of workers emerge to begin gathering nectar and pollen as well as larval feeding and ejection (if necessary). This is observed in the necessary history functions of model defined on the time domain $\phi \in [T_s - 8, T_s + 22]$ in (3.14). This choice reflects the longest fixed delay in the model of 30 days which represents the time for complete metamorphosis of gynes, see Table 3.1. The switch time, which represents the time when a colony changes from producing worker offspring to male and gyne offspring, is a distinguishing event in a colony's development [63]. We fixed a late switch time at $T^* = 40$, so that male and gyne larvae appear at day $T^{**} = 44$, coincidentally the same day the last worker eggs are laid (see Figure 2.1). Development time for each larval subclass was assumed to be fixed as described Table 3.1.

In order to model the bumblebee life cycle, it is important to understand that bumblebees develop over a series of life stages for which we have made certain assumptions in the model. Eggs are introduced into the hive by the queen at fixed rates (b_w, b_m, b_g), require minimal care from the workers, and under the stress of resource limitation are removed by oophagy thereby decreasing the size of the brood prior to its larval phase. During the larval phase, workers care for and feed juveniles under normal conditions. When the hive is under stress either by resource limitation or insufficient worker population, larval ejection by the workers can occur as an additional population control on juveniles [160]. Each of the juvenile phases have fixed duration in the model and once a larva pupates it will emerge as an adult after the fixed time delay, see Table 3.1.

The primary sources of nourishment in a bumblebee colony includes in-nest stores of pollen and nectar. Once the first workers emerge, some members commence foraging for the resources (b_{NW}, b_{PW}) while others act as caregivers, remaining in the hive to distribute resources to the larvae and consume stored resources (μ_{NW}, μ_{PW}). Larval consumption is the primary draw from the stored resources where nectar is consumed at twice the rate of pollen [147]. Each of the larval subclasses grow at different rates which is directly related to the amount of resources that are consumed at each stage [158]. This is reflected in the five different consumption parameters, c_i's as seen in expression $c_1(L_1^{(w)} + L_1^{(m)} + L_1^{(g)}) + c_2 L_2^{(w)} + c_3 L_2^{(m)} + c_4 L_2^{(g)} + c_5 L_3^{(g)}$ from (3.1) and (3.2). Note the first stage of each subclass is defined such that their members share the same consumption rate but members of $L_1^{(w)}$, $L_1^{(m)}$, and $L_1^{(g)}$ consist of different age groups. Consumption of stored resources by the queen was considered but due to a lack of quantifying information for queen behavior in the literature this mechanism was omitted in carrying out the simulations.

The driving force of the model is larval population control in the presence (or lack thereof) of

resources and worker caregivers. To enter into the initial larval stage for any class their eggs must have been laid 4 days prior as can be seen in the egg laying expression $b_W^*(t-4)$ in (3.3).The model also includes time varying larval ejection rates per worker ($\mu^{(w)}$(t), $\mu^{(m)}$(t), $\mu^{(g)}$(t)) which are found in (3.13) and based on past values of the worker, pollen and nectar variables. These expressions allow for the calculation of brood development independent of each other over a continuous spectrum. To calculate the cumulative effect of larval ejection over time, the ejection rates ($\mu^{(k)}W(t)$)can be integrated over fixed temporal bounds in the delay differential equation (3.13), with a delay of zero days ($t-0$). The basis for this idea follows that given a particular brood $L^{(k)}(t;a)$, the maximum number of members are present at time $t=a$ when this brood enters one of the larval stages, $L_1^{(k)}$, $L_2^{(k)}$ or $L_3^{(k)}$. Loss of larval members can only occur for this particular brood and is described by the decay dynamics below where larval ejection is described by an interaction between available workers and brood members,

$$\frac{dL^{(k)}(t;a)}{dt} = -\mu^{(k)}(t)W(t)L^{(k)}(t;a). \tag{3.15}$$

The workers present to perform the ejection $W(t)$ do not depend on the current brood $L^{(k)}(t;a)$ so solving (3.15) yields that any particular brood can be described as the following with a constant, B and variable Φ defined in the model equation (3.13),

$$\begin{aligned}
L^{(k)}(t;a) &= B\exp\left[\int_a^t -\mu^{(k)}(s)W(s)ds\right],\\
L^{(k)}(t;a) &= B\exp\left[\int_a^t \frac{d\Phi^{(k)}}{dt}(s)ds\right],\\
L^{(k)}(t;a) &= B\exp\left[\Phi^{(k)}(t)-\Phi^{(k)}(a)\right]
\end{aligned}$$

Since the size of a brood can only decrease after all eggs have been laid, an expression such as $\exp[\Phi^{(m)}(t-8)-\Phi^{(m)}(t)]$ (see (3.8))represents the proportion of decay of a specific male brood over the previous 8 days by larval ejection. We multiply this expression by the number of male eggs that entered the larval state 8 days ago, $b_M^*(t-12)$, to determine how many male larvae survived and are entering the second male larvae state $L_2^{(m)}$ in (3.8). Considering Table 3.1, male juveniles would be entering state $L_2^{(m)}$ at the precise time of 12 days post the laying of their eggs given they had not been ejected during the prior 8 day period in the $L_1^{(m)}$ state. Essentially, delays in states $\Phi^{(w)}$, $\Phi^{(m)}$, and $\Phi^{(g)}$ allow the model to compute the survival of individual broods (defined by the day their eggs were laid) without having to track them explicitly. This functionality makes delayed differential equations a more appropriate method for this system as opposed to ordinary differential equations.

The larval mortality rate represents the rate at which larvae are ejected from the hive per worker. Larval Ejection is a biological mechanism in bumblebee colonies which controls the number of larvae present. This behavior is not well studied; we propose this behavior could occur when not enough workers are present to care for the larvae and when the hive is under stress by a resource

deficiency [160, 180, 154, 181, 78]. With regard to the resource criteria for ejection, a comparison between desired pollen consumption and the available pollen P(t) at that time is required. By defining the amount of pollen that existing larvae want to consume as

$$C = c_1(L_1^{(w)} + L_1^{(m)} + L_1^{(g)}) + c_2 L_2^{(w)} + c_3 L_2^{(m)} + c_4 L_2^{(g)} + c_5 L_3^{(g)}, \tag{3.16}$$

we recognize this as the larval consumption term for our resources in (3.2). A corresponding version for nectar can be found in (3.1). It follows from P being the available amount of in-nest pollen that a shortage of pollen would be represented by positive values of the expression $C-P$. To determine the severity of the resource deficiency, we use the expression:

$$\frac{C-P}{C+\epsilon} = \frac{\text{deficiency}}{\text{consumption}}, \tag{3.17}$$

where ϵ is a small value to ensure the factor is well defined particularly in case where all larval classes become too close to zero. This deficiency factor for pollen will be negative anytime $C < P$ and can fall within the range $(0,1)$ when $C > P$. The deficiency factor is designed on the range $(0,1)$ to scale the maximum larval ejection when there is a resource shortage. A similar factor is used for nectar deficiency as well.

Now in order to design a mechanism for neglect, consider that there exists an optimal larvae to worker ratio Z.Then the sustainable larval population is ZW which determines the number of larvae that receive proper feeding and care by the available workers within the colony [154, 181]. It follows that the total larval population in the colony is the sum of its larval subclasses, $L = \sum_{i,k} L_i^{(k)}$ where $i = 1,2,3$ and k indicates class w,m, or g. Using the terms above, we define the excess larvae (i.e. those that cannot be cared for) as $L-ZW$ and can create a scaling factor for neglect here:

$$\frac{L-ZW}{L+\epsilon} = \frac{\text{excess larvae}}{\text{total larvae}}. \tag{3.18}$$

This factor is negative when $L < ZW$ and approaches 1 as L exceeds ZW. Putting all the scaling terms together with maximum larval ejection rates per worker (α and β), we produce an expression for the actual larval ejection rate per worker,

$$\mu^{(k)}(t) = \alpha \max\left[\frac{L-ZW}{L+\epsilon}, 0\right] + \beta \max\left[\frac{C-P}{C+\epsilon}, \frac{2C-N}{2C+\epsilon}, 0\right]. \tag{3.19}$$

It is reasonable to assume that negligence and resource deficiency have different contributions in the larval ejection behavior, hence the equation has 2 different maximum larval ejection rates, α and β. This can be justified by considering that in the case of resource deficiency without any negligence where at least a sufficient number of workers are present inside the hive to care for all the larvae. A resource shortage that triggers larval ejection in the colony would have a large number of workers, relatively, to assist in performing this behavior. By contrast in the case of larval neglect with sufficient resources, not enough works are present in the hive to care for all the larvae which triggers

ejection to occur. Here the behavior of ejecting larvae may be more taxing on the existing workers as opposed to a sufficient number of workers were present. We note here that in our simulations α and β are set to the same value but future research would help determine the differences between these two maximum ejection rates.

Another form of population regulation within a hive was exhibited through oophagy, or the consumption of eggs by the workers or queen. Although this behavior is not strictly a population control measure, it can be a significant behavior when malnourishment occurs in the hive. Although this mechanism is not well studied, oophagy has been observed in relation to bumblebee pollen diets. For example, low pollen quality or low amounts of protein available for the colony appears to correlate with high amounts of oophagy [78]. The degree of oophagy was calculated using a factor derived from desired resource consumption and availability of resources, in the same way that larval ejection was calculated from (3.17) and also the nectar counterpart. We expect high oophagy when the factor is close to 1 and no oophagy when it's negative. To model oophagy, these expressions are not used directly in the system of DDE's but rather are incorporated directly into egg survival rates $b_W^*(t)$, $b_M^*(t)$, and $b_G^*(t)$. This is accomplished by scaling the egg laying rates (b_W, b_M, b_G) within corresponding egg survival rates.The egg survival rates are defined as follows:

$$b_k^*(t-\tau) = b_k\left(1-\max\left[\frac{C(t-\tau)-P(t-\tau)}{C(t-\tau)+\epsilon}, \frac{2C(t-\tau)-N(t-\tau)}{2C(t-\tau)+\epsilon}, 0\right]\right). \tag{3.20}$$

which represents the number of eggs laid at the time $t-\tau$ that become larvae at time t; k denotes the worker, male or gyne class of bumblebee.Overall, these mechanisms yield model expressions such as $b_W^*(t-22)\exp[\Phi^{(w)}(t-18)-\Phi^{(w)}(t-9)$, which represented new workers on day t whose eggs were laid 22 days prior, having begun the second larval phase 18 days prior and survived to undergo pupation for the previous 9 days.

With the foundation of model as described above, we are able to explore pesticides effects on bumblebees. We used the model to simulate toxicant effects in different scenarios that reflect well-documented impacts of pesticide exposure in the literature. In particular, we simulated (i) acute direct effects on workers, (ii) sublethal effects via reduced foraging abilities, (iii) lethal and sublethal effects on larvae via reductions in development/survival. We ran simulations for each of these, incorporating acute and sublethal effects into the model and measuring the reproductive output (number of males and gynes) as our primary metric of population effect. In order to explore these toxicant effects, we parameterized the model using values from the literature where possible to use as a baseline/control. Then we modified the parameters to simulate toxicant effects.

First, we simulated an acute effect of pesticides acting directly on worker survivorship, corresponding to an LD_{50} . We varied the time of exposure to the pesticide, noting the impact that delaying exposure may have on reproductive output. Second, we simulated the sublethal effect of reduced foraging ability, reducing pollen and nectar resources available to the colony and measuring the resulting reproductive output. Third, we simulated reductions in new brood, corresponding to a

sublethal effect on the queen's egg-laying rate, and noted especially the effects of brood reduction on subsequent broods and overall reproductive output. Finally, we simulated both acute and sublethal effects and noted their combined effects on reproductive output.

Table 3.1 Fixed Duration (in Days) of Bumblebee Life Stages for Model.

Class	Egg	$L_1^{(k)}$	$L_2^{(k)}$	$L_3^{(k)}$	Pupa	Total Age
Worker	4	6	3	-	9	22
Male	4	8	3	-	11	26
Gyne	4	5	4	4	13	30

3.3 Results

Control: In the absence of toxicological insult, the model produced an increase in the number of workers until around day 60, after which workers decline and males and gynes (reproductives) increased nearly exponentially before plateauing off around 100 days after the start of the simulation. Pollen and nectar resource levels also declined between 70 and 80 days after the simulation, corresponding roughly with the decline in the worker population, see Figure 3.1.

Table 3.2 Model variables and parameters. The selected value for simulations are given in the last column.

Variable	Description	Units	Estimate
t	time	days	
$N(t)$	amount of in-nest nectar	ml	
$P(t)$	amount of in-nest pollen	g	
$W(t)$	number of workers	individuals (workers)	
$L_1^{(w)}(t), L_2^{(w)}(t)$	number of worker larvae	individuals (larvae)	
$M(t)$	number of males	individuals (males)	
$L_1^{(m)}(t)$, $L_2^{(m)}(t)$	number of male larvae	individuals (larvae)	
$G(t)$	number of gynes	individuals (gynes)	
$L_1^{(g)}(t), L_2^{(g)}(t), L_3^{(g)}(t)$	number of gynes larvae	individuals (larvae)	
Timeline			
T_S	first day of spring		0
$T_S + 22$	first workers emerge		22 [63]
T^*	first day male/gyne eggs laid		40 [134]
T^{**}	end of worker eggs laid		44 [134]
T_W	beginning of winter		120
Parameters			
b_{NW}	worker nectar collection rate	$\frac{\text{ml}}{\text{day·individual }(W)}$	0.6 [87];[146]
b_{PW}	worker pollen collection rate	$\frac{\text{g}}{\text{day·individual }(W)}$	0.4 [87]; [68]
μ_{NW}	worker nectar consumption rate	$\frac{\text{ml}}{\text{day·individual }(W)}$	0.35 [181]
μ_{PW}	worker pollen consumption rate	$\frac{\text{g}}{\text{day·individual }(W)}$	0.25 [181]
c_i	larval pollen consumption rates	$\frac{\text{g}}{\text{day·individual }(L)}$	(0.01, 0.25) [158]
$b_W(t)$	worker birth rate	$\frac{\text{workers}}{\text{day}}$	8.5 [63]
$b_M(t)$	male birth rate	$\frac{\text{males}}{\cdot\text{day}}$	2 [63]
$b_G(t)$	gyne birth rate	$\frac{\text{gynes}}{\cdot\text{day}}$	2.6 [63]
μ_W	worker death rate	$\frac{1}{\text{day}}$	0.05
Z	larvae to worker ratio		4 [63]
α	max ejection rate (negligence)	$\frac{\text{individual }(L)}{\text{day·individual }(W)}$	0.75
β	max ejection rate (malnutrition)	$\frac{\text{individual }(L)}{\text{day·individual }(W)}$	0.75
ϵ	roundoff correction factor		0.001

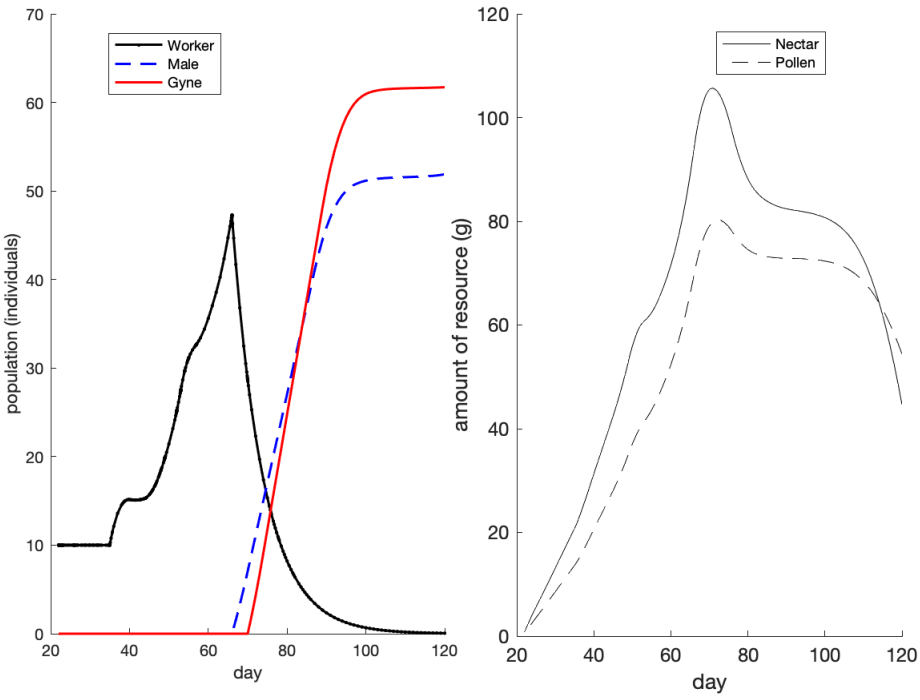

Figure 3.1 Bumblebee colony simulation over 120 days, including dynamics for both resources, adult workers and cumulative adult reproductive members (males and gynes).

Lethal pesticide effects: Acute pesticide effects were characterized as immediate reductions in the worker population corresponding to the LD_{50} dose of pesticide applied. We varied the time of exposure, noting the impact that delaying contact to pesticide may have on reproductive output. Simulation of an acute effect of pesticides on workers – corresponding to the LD_{50} – resulted in a marked decline of reproductive output when exposure to the toxicant occurred during the first 30 days of the simulation. However, results varied as a function of the timing of the exposure; application of the toxicant at 36 days after the start and beyond resulted in much less severe effects, see Figure 3.2.

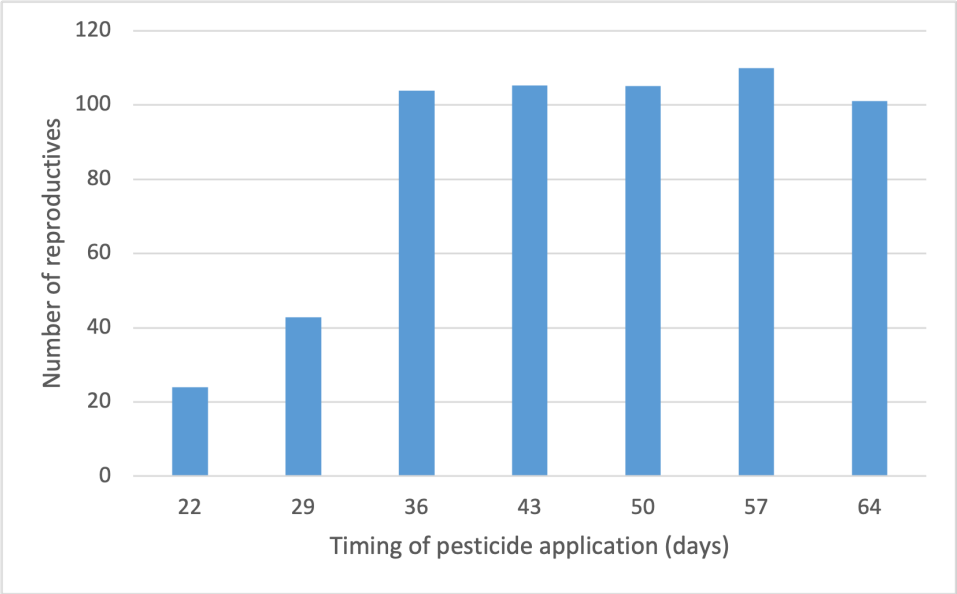

Figure 3.2 Acute effects of LD_{50} dose on cumulative males and gynes produced in the colony as a function of the timing of pesticide application.

Sublethal pesticide effects: The effect of resource reduction was severe for both pollen and nectar reduction levels above 20%. Though these effects were independent of each other, pollen reduction had a slightly more severe impact on reproductive output than nectar reduction as shown in Figure 3.3. Reductions in new brood (first and second broods together) greater than 10% corresponding to a sublethal effect on the queen's egg-laying rate resulted in severe declines in reproductive output. Also apparent, reductions in the first brood due exposure exacerbated the effects seen by a reduction in the second brood (workers that emerge on day 35) in Figure 3.4. We emphasize this is an effect of fewer workers produced by the queen as opposed to any lethal exposure of workers to a pesticide.

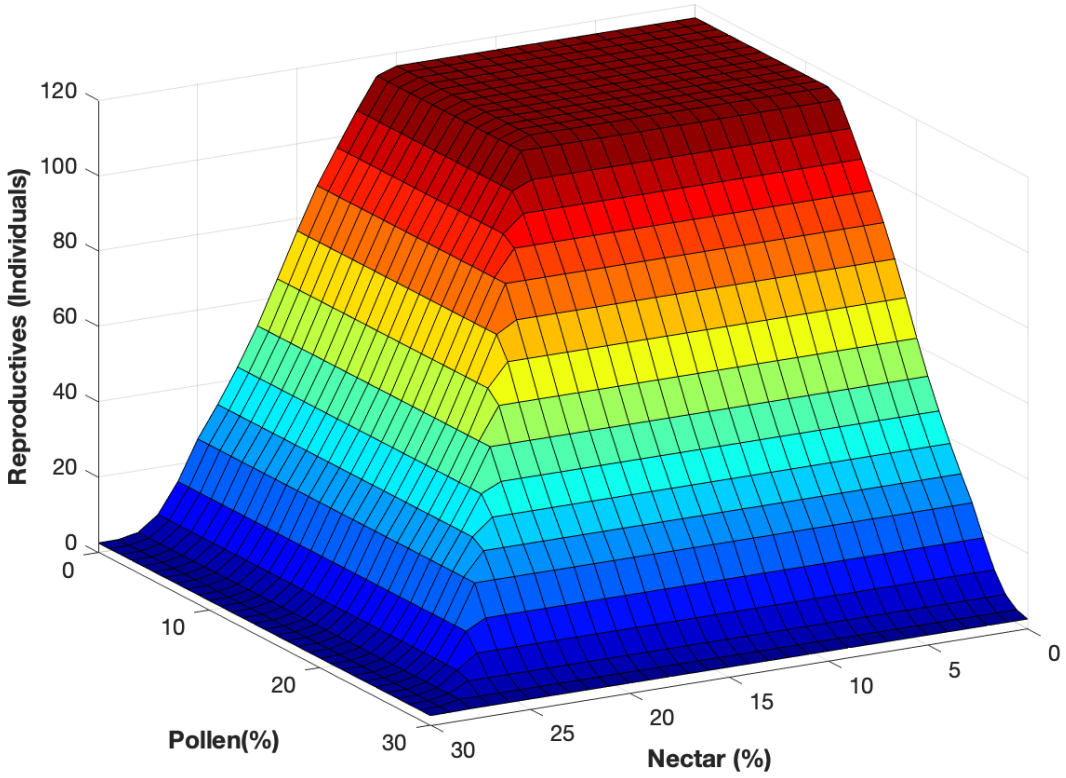

Figure 3.3 Influence of sublethal effect of reducing foraging ability (by percentage) on bumblebee reproductive output (males + gynes).

Lethal and sublethal effects combined: Simulations of combinations of lethal and sublethal effects resulted in a non-linear interaction, demonstrating a synergistic effect. Declines in reproductives occurred after approx. 30% reductions solely due to lethal effects, or 20% solely in pollen reductions; the combination of these two levels resulted in nearly double the decline of reproductives as observed in Figure 3.5.

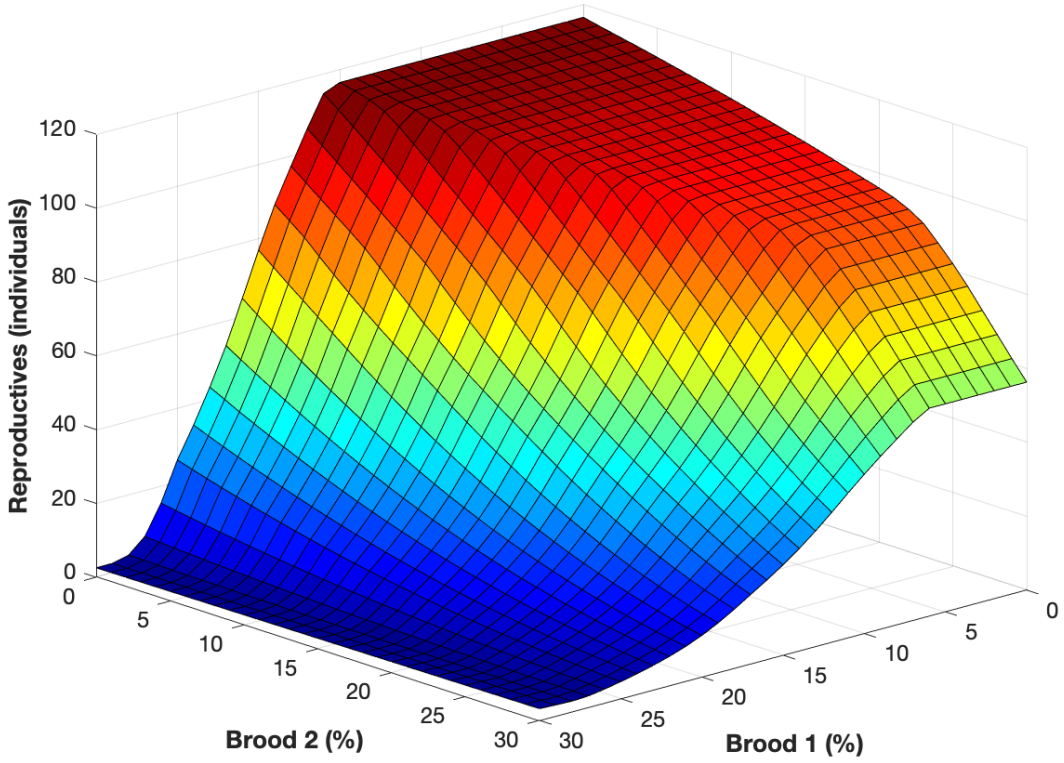

Figure 3.4 The effect of sublethal reduction to egg laying rates (on 1st and 2nd broods) on cumulative reproductive output of the colony.

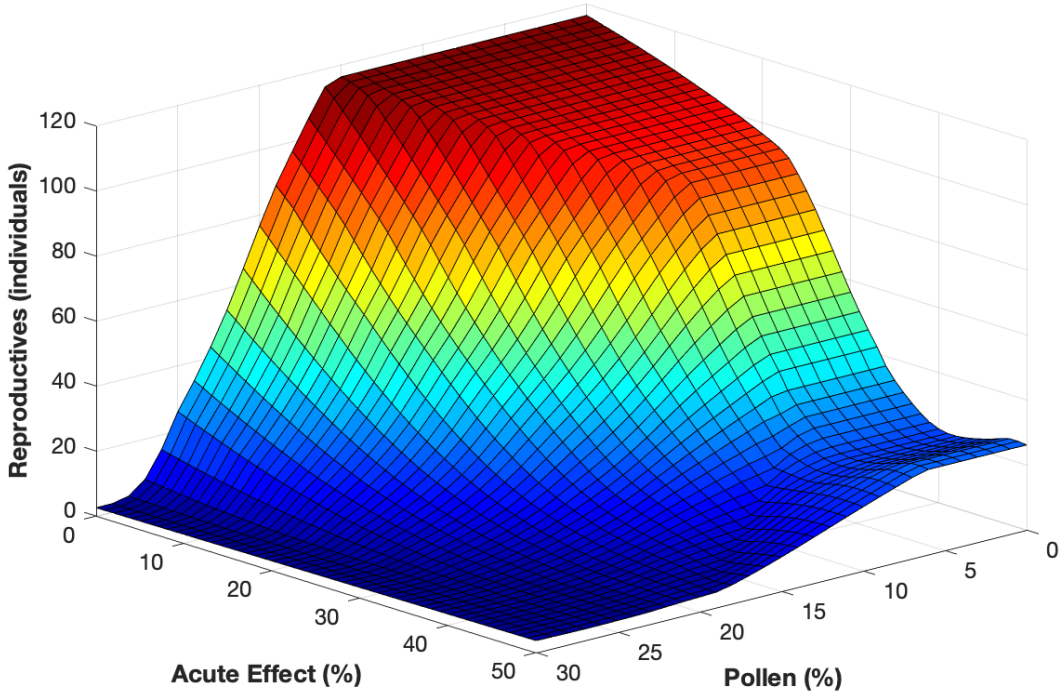

Figure 3.5 Effects of combined lethal ("Acute") and sublethal ("Pollen" reduction) toxic insults on bumblebee reproductive output.

3.4 Discussion

The Millennium Ecosystem Assessment (2005) provided a conceptual framework for linking environmental health and human well-being; protection of ecosystem services such as biocontrol and crop pollination are central themes. In the past decade, significant efforts aimed at better understanding the effects of toxicants such as pesticides on hymenoptera – especially honeybees – have been made [120]. Although empirical studies on the effects of toxicants on non-*Apis* hymenoptera are increasing (e.g., [163, 169], assuming that our knowledge of one species' responses can be applied directly to other species risks creating confusion and misunderstandings [24]. Recent physiological studies have corroborated this, demonstrating that pesticides such as pyrethroids affect honeybees (*A. melifera*) and bumblebees (*B. terrestris*) in fundamentally different ways (e.g., [102]). Assessment and maintenance of the protection of ecosystem services relies fundamentally on a deep understanding of population dynamics; both empirical and theoretical approaches are important tools in this effort. Explorations of bumblebee population dynamics that incorporate our understanding of biological processes with predictive mathematical models provide a powerful means of prescribing protective measures and best practices. Here we have used a mechanistic model tailored to bumblebee colony

development in an attempt to better understanding the response of bumblebees to toxicants such as pesticides. Our use of a delay differential equation model enables us to explicitly describe the effect of larval incubation and colony history on population outcomes. This level of detail allows us to demonstrate the sensitivity of colony viability to the timing and severity of pesticide sprays. Furthermore, the DDE model requires far fewer parameter estimations than approaches that use agent-based or individual-based models (e.g., [28, 29]). Empirical efforts that track real- time survivorship and behavior of larvae, workers and queens over a longer time period (similar to those conducted by Crall et al. [48, 49] but extended to larvae and for longer time periods would be useful for validating the DDE model presented here.

Understanding the mechanisms underlying the effects of resource availability on bumblebee population growth is an increasing focus of field and theoretical studies [192, 191]; a recent study by Crone and Williams (2016) illustrates the importance of parsing out the relative importance of putatively important drivers (e.g., colony growth rates and floral resource availability) of bumblebee population outcomes. Less is known about combinations of reduced resource provisioning and diminished survivorship that may result from exposure to pesticides or mixtures of pesticides that have both lethal and sublethal effects, though the potential for multiplicative effects have been demonstrated in recent elegant experiments (e.g., [79]). Our simulations suggest that, even at low levels, sublethal effects such as reduced pollen foraging ability may result in severe declines in reproductive output if combined with lethal effects over 40%, for instance (see Figure 3.5). This underscores the importance of better understanding the effects of exposure to mixtures of toxicants.

In the current analysis, our model highlights several important aspects pertaining to population implications of pesticide exposure in bumblebees. First, the overall impact of acute effects such as those exhibited by an LC_{50} or LD_{50} dose varies greatly with timing of exposure, with pesticides applications later in the development of the colony having relatively little effect compared with applications imposed within the first 30 days (Figure 3.2). The immediate reduction in workforce size prevents the same level of foraging as seen before pesticide exposure, thereby limiting the resources available to rear future broods. In addition, the reduced number of workers also results in neglected larvae which ultimately limits future brood sizes and further impacts the production of reproductive bees. Perry et al. (2015) similarly found that early reductions in foraging ability in honeybees could have dramatic impacts at the population level later on; they suggest that these types of delayed responses due to early stressors may help explain field observations and experiments documenting colony collapse disorder. Our model results likewise suggest that delays in pesticide applications could significantly lessen deleterious effects on bumblebee populations.

Second, sublethal effects on the population output due to reduced egg-laying rates may be lessened if reductions are kept below 10%. However, higher levels of reduced egg-laying rates in the first brood may interact synergistically with subsequent brood exposure (due to repeated exposure to the same pesticide, or exposure to another, different chemical), wreaking havoc on the population

at higher levels even for low levels of reductions on the second brood (Figure 3.4). Field studies exploring combinations of pesticides on bumblebee colony outcomes have revealed similar effects (e.g., [79]). Because bees in farmland mosaics are often exposed to multiple spray events, sometimes with multiple pesticides, these types of knock-on effects may be difficult to mitigate in practice.

3.5 Research Contributions

In this work, we redesigned the bumblebee colony model to address a single hive and include more accurate larval dynamics and the primary population controls found in colonies. The model dynamics shown in the control closely resemble the description of bumble colonies presented by Duchateau and Velthuis [63], one of the most comprehensive research articles on colony development. The mathematical model presented in this work is the first individual specific differential equation model to address mixed sublethal and lethal effects of toxicants on a bumblebee colony. The only other individually detailed model currently that can address pesticide effects is an agent-based model which is much more sophisticated and contains significantly more parameters than our model which need to be calibrated particularly for North American species of bumblebees [29]. Our bumblebee colony model presents an alternative for researchers interested in testing the effects of toxicants on colonies. The reduced parameter set should allow for easier calibration and in addition, the DDE model can be used in an inverse problem framework with sufficient data to help determine values for those parameters which are studied less in literature.

The synergistic effects revealed in our simulations emphasize the need to carefully consider population endpoints when gauging risk to bumblebees from pesticides and other toxicants; none of these effects would be detectable from simple LC_{50} analyses. Taken together, our results suggest that more sophisticated mathematical treatments of population processes are critical for assessing mechanisms underlying the effects of pesticides on bumblebees. Particular attention should be paid to timing of pesticide exposure, as well as the specifics of combinations of pesticides to which bumblebee colonies might be exposed. Finally, empirical data should be generated to test and validate the specific outcomes predicted by the model.

CHAPTER

4

MODELING IMMUNOSUPPRESSION IN RENAL TRANSPLANT PATIENTS USING OPTIMAL CONTROL THEORY AND KALMAN FILTERING

4.1 Introduction

Chronic kidney disease (CKD) affects 37 million American adults and millions of others remain at risk [61]. CKD is most prominent in individuals over age 65 with approximately 38% of the group affected while as many as 90% of people with CKD are unaware of its presence until significant loss of kidney function occurs. CKD is characterized by conditions which damage the kidneys and impair kidney function in the body. Many different conditions are known to cause chronic kidney disease, yet the leading causes are diabetes and high blood pressure which account for 66% of cases [73, 74]. Treatment options for CKD focus on controlling risk factors to slow the progression of the disease since only a few forms of kidney disease have cures [43]. In the most severe cases of CKD, the disease is no longer manageable and kidney failure is imminent.

Although studies are showing promise with regenerative therapies for patients with acute kidney impairment, individuals suffering from CKD remain unable to restore kidney function [132, 144].

The kidneys are a pair of bean-shaped organs located in the abdomen responsible for removing waste products and excess fluid from the body while also regulating electrolytes. An adult kidney includes approximately one million structures called nephrons where the removal and regulation of the blood takes place. Inside each nephron, blood is filtered by the glomerulus to begin the removal process and subsequently passes through a renal tubule which further removes wastes and excess fluids to complete the process before returning the blood to the body, refer to Figure 4.1 [60]. Damaged renal tubules and subsequently nephrons result in irreversible impaired kidney function since kidneys are unable to replace or regenerate nephrons [43]. The glomerular filtration rate (GFR) is a widely accepted assessment of kidney function on a range from 0 to 90+ mL per minute. The best approximation to GFR is the estimated GFR test which takes into account an individual's concentration of creatinine in the blood and personal characteristics such as age, gender, weight, height, and race [187, 129]. As a significant component of that test, creatinine is a waste product related to muscle metabolism that kidneys remove from the blood with a typical range of 0.6 to 1.35 mg per dL in healthy adults [89, 88]. Since creatinine concentration is included in the determination of the estimated GFR, blood tests for serum creatinine levels are often used as a surrogate for GFR and can be used as a biomarker for renal health [135]. Patients that suffer from CKD experience loss of kidney function and an increase of serum creatinine resulting in GFR values below 90 mL per minute.

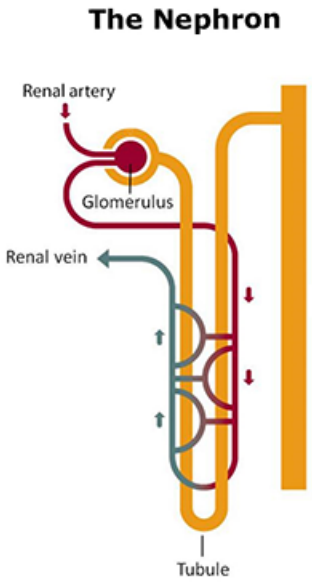

Figure 4.1 Diagram of a Healthy Nephron [60].

Chronic kidney disease can progress through 5 stages of deteriorating kidney functionality, each described by a decreasing range of GFR values. The final stage of CKD, known as end stage renal

disease (ESRD) occurs at GFR values below 15 indicating kidney failure has occurred or is highly likely [74]. Treatments for ESRD are limited to primarily two options: routine dialysis at a clinic or solid organ transplantation. In March 2018, 95,301 people were awaiting a kidney transplant representing approximately 80% of people awaiting a solid organ transplant [142, 135]. If a compatible kidney is available, transplant recipients see an increased chance of survival and lower costs compared to the alternative hemodialysis [176]. Post transplant, recipients need to continue a cautionary lifestyle to prevent CKD from reoccurring and resulting in allograft nephropathy.

Long-term allograft survival is a challenging goal for renal transplant patients. Transplant recipients require daily drug treatments to suppress their immune system since it will regard the allograft as foreign tissue resulting in an immune response that attacks the allograft [151]. Standard immunosuppression therapies involve first an induction therapy to prevent acute rejection of the organ immediately following the procedure. Maintenance therapy is also used which involves combinations of immunosuppressive drugs in an effort to prevent chronic allograft nephropathy and allograft loss [103]. In the case where drug doses are prescribed lower than a particular patient needs, the immune response may not reject the allograft outright but will result in chronic allograft injury which is common among transplant recipients. This under-suppression of the patient's immune system can result in reduction of kidney function. Alternatively, when prescribed drug doses are too high the immune system becomes incapable of protecting the patient from pathogens.

The unintended consequence of the immunosuppression treatment is the susceptibility of the patient to pathogens and in particular, naturally latent viruses. There are a variety of viruses,such as cytomegalovirus, human herpes virus and human polyomavirus 1, that can infect patients while most often they remain in a latent state until the individual becomes immunocompromised [185]. The human polyomavirus 1, also known as BK virus (BKV), is present in over 80% of the worldwide population and in a latent state in the majority [6]. BK virus is particularly problematic to renal transplant recipients since no known antiviral treatments exist to combat it. When BKV becomes active in an immunocompromised individual, the virions target the cells of the renal tubules inside the nephrons. Persistent BKV infection ultimately results in the loss of the ability for nephrons to function. Understandably, two of the three leading causes of organ failure in renal transplant patients are organ rejection and BKV nephropathy [166, 76].

Currently, optimal protocols for immunosuppression treatments have yet to be established given the dependence on a variety of individual patient factors (e.g., age, diabetes, etc.) [139]. Treatment protocols are typically based on physicians' understanding of current literature and a patient's data in response to treatment. We expand upon a methodology which utilizes mathematical modeling and optimal control theory to simulate immunosuppression for patients following a renal transplantation. A number of mathematical and statistical modeling approaches have been taken to assist in understanding different aspects of renal transplantation since the 1970's [189, 113, 183, 8, 123]. Ordinary differential equations have been used previously for modeling immunosuppression in humans

in relation to both HIV and transplantation applications [55, 186, 17]. In addition, many different biological systems have seen control theory methodologies applied in mathematical models of their systems, including areas such as cellular and chemical interactions, circadian rhythms in mammals, and immunosuppression [47, 138, 1]. Following the findings of [136], we propose changes to their approach of the receding horizon control in their mathematical model and demonstrate the utility of using an alternative method for feedback, the ensemble Kalman filter.

4.2 Methods

Currently, protocols for immunosuppressant treatments in renal transplants vary by treatment center and are inconsistent, differing based on the experience and interpretation of literature by professionals at each center [139, 69, 5]. Dynamical systems models for immunosuppression therapy in renal transplant patients can assist in developing more effective protocols for this therapy. The ordinary differential equation model utilized in this work is the result of multiple iterations by Banks et al. and Murad et al. [18, 136]. Mathematical methods from optimal control theory can assist physicians in finding the desired balance of suppression necessary to prevent severe BK viral infection (due to over-suppression) and allograft rejection by the immune system (due to under-suppression). By using a closed loop control system, immunosuppression dosing can be determined automatically by satisfying desirable biological criteria such as maintaining a healthy functioning kidney and limiting BK viral loads below a threshold. Patient data can be introduced into this mathematical framework by applying a Kalman filter into the model. The Extended Kalman Filter (EKF) and Ensemble Kalman Filter (EnKF) are two methods implemented to provide direct patient feedback in the model and create more personalized immunosuppression treatments.

4.2.1 Ordinary Differential Equation Model

An initial ordinary differential equation model for immunosuppression in renal transplant patients was developed by Murad et al. (2018) and was chosen for this research because of two important assumptions: the BK virus is the pathogen of interest and the kidney is unable to regenerate or replace damaged cells within the nephrons. Under the first assumption, BK virus is important in part because there are no known antiviral treatments available for it, thus BK virus is primarily controlled by the patient's immune system which is influenced by the efficacy of immunosuppression treatments. Additionally, BKV specifically targets renal tubule cells inside the nephrons. In pathogens that do not target the kidney, severe viral infection is the consequence of over-suppression, but with BKV a severe viral infection results in reduced kidney functionality which can also be captured in the model. The second assumption follows from the widely held understanding that adult kidneys are composed of all the nephrons an individual will ever have and while under the stress of CKD, the kidney is unable to regenerate or repair damaged nephrons at any rate that affects kidney function

[99]. As nephron damage occurs (due to infection), reduced kidney functionality can be observed through increases of the waste products in the blood such as serum creatinine levels later observed in this model.

Table 4.1 State Variables in the Mathematical Model

State	Description	Unit
H_S	Concentration of susceptible graft cells	cells/mL
H_I	Concentration of infected graft cells	cells/mL
V	Concentration of free BKV	copies/mL
E_V	Concentration of BKV-specific CD8+ T-cells	cells/mL
E_K	Concentration of allo-specific CD8+ T-cells	cells/mL
C	Concentration of serum creatinine	mg/dL

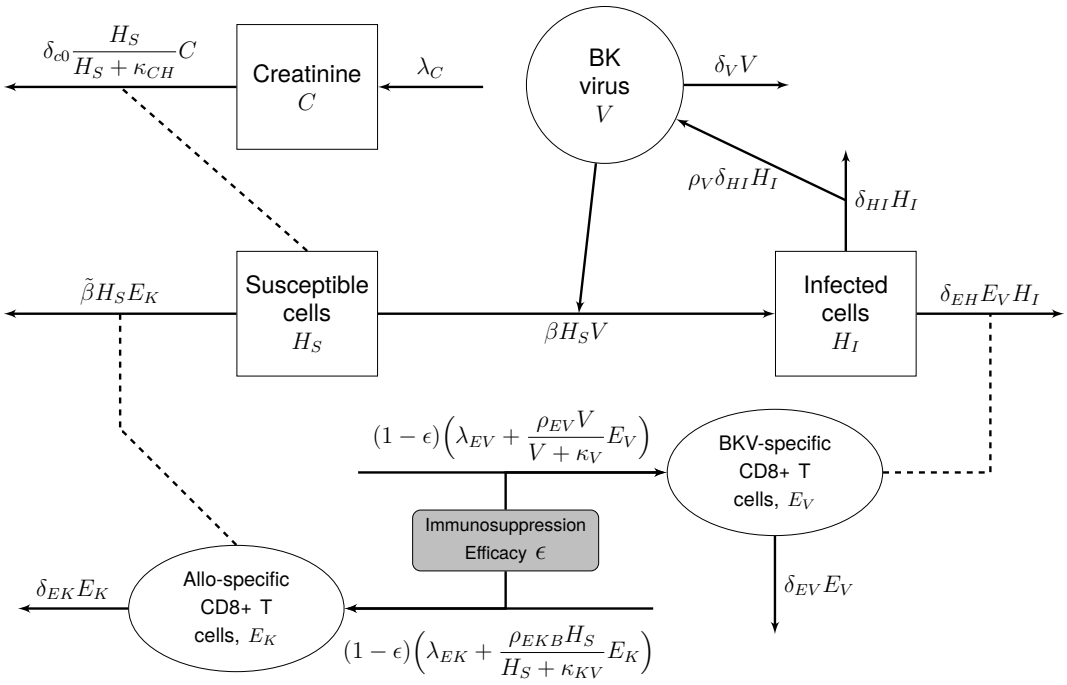

Figure 4.2 Compartment diagram for immunosuppression in a renal transplant patient

The mathematical model reduces the complexity of this biological system into 6 states as shown in Table 4.1. It follows the template of a Susceptible-Infected model with dynamics between healthy

(H_S) and infected (H_I) kidney cells (of the transplant) while also including a single pathogen, (V) and the immune response split into two states. Since the immune system uniquely targets threats using CD8+ T cells, 2 states are used to represent concentrations of the CD8+T cells specific to BKV (E_V) and the allograft (E_K). The model also includes a state for accumulation of serum creatinine indicating kidney functionality (C). Figure 4.2 gives a visual relationship between these states. For simplicity, the model chooses to focus on a single pathogen although a variety of of latent viruses may be present within a transplant patient. Expanding the model, would require additional states and specific immune responses for each pathogen to be included. The mathematical model is shown in the system of equations (4.1) - (4.6) [136].

Renal Model:

$$\dot{H_S} = -\beta H_S V \chi_{(V>V^*)} - \tilde{\beta} H_S E_K \chi_{(E_K>E_K^*)} \tag{4.1}$$

$$\dot{H_I} = \beta H_S V \chi_{(V>V^*)} - \delta_{HI} H_I - \delta_{EH} E_V H_I \chi_{(E_V>E_V^*)} \tag{4.2}$$

$$\dot{V} = \rho_V \delta_{HI} H_I - \delta_V V - \beta H_S V \chi_{(V>V^*)} \tag{4.3}$$

$$\dot{E_V} = (1-\epsilon)\left(\lambda_{EV} + \frac{\rho_{EV} V}{V+\kappa_V} E_V\right) - \delta_{EV} E_V \tag{4.4}$$

$$\dot{E_K} = (1-\epsilon)\left(\lambda_{EK} + \frac{\rho_{EK} H_S}{H_S+\kappa_{KH}} E_K\right) - \delta_{EK} E_K \tag{4.5}$$

$$\dot{C} = \lambda_C - \delta_{C0} \frac{H_S}{H_S+\kappa_{CH}} C \tag{4.6}$$

Equation (4.1) represents the interactions that affect the decrease in the healthy cell population. The concentration of healthy susceptible cells (H_S) are measured in cells per mL which can be reduced by two different interactions. The first loss term $\beta H_S V$ of (4.1) represents free flowing virus in the blood interacting with the healthy cells within the nephron which results in infection of these susceptible cells. The parameter β represents the frequency that the interactions between healthy cells and virus result in infection of the cell and thereby removing these kidney cells from the susceptible population. The second loss term $\tilde{\beta} H_S E_K$ of $\dot{H_S}$ takes place in regards to the immune response. Since the immune system responds to the allograft as foreign tissue, E_K represents allo-specific CD8 +T cells which target the healthy kidney tissue. The interactions between these allo-specific CD8 +T cells and the susceptible cells results in healthy cell death at a rate $\tilde{\beta}$. We recognize the lack of a source for healthy kidney cells which follows from our initial assumption that the body cannot replace or regenerate the healthy cells. This means the initial population of susceptible cells H_S at time $t = 0$ is the maximum number of cells the patient will ever have.

In equations (4.1) - (4.3), the characteristic function is utilized to represent dynamics when certain

states only exist in trace amounts. By using the characteristic function of the form:

$$\chi_{(X>X^*)} = \begin{cases} X \leq X^*, \ \chi = 0 \\ X > X^*, \ \chi = 1 \end{cases} \tag{4.7}$$

where X^* is a threshold parameter, associated interactions will be active when a particular state exceeds the threshold. According to Murad, work with this model and its earlier iterations showed that some interactions were negligible when trace amounts of virus or CD8 +T cells were present [135]. The thresholds E_K^* and E_V^* are set to 2500 cells per mL and 500 cells per mL respectively as determined by Murad. We assume that concentrations of CD8 +T cells below the thresholds do not represent an active immune response and therefore will not reduce healthy kidney cell concentration. Similarly, V^* is set to 1000 copies per mL, a choice made in [135] to represent BKV in its latent state. We note this level is below the lower limit of quantification (1750 copies per mL) for the assay performed by the Mayo Clinic Laboratories [114, 179]. Observing the characteristic terms in (4.1), $\chi_{(V>V^*)}$ indicates healthy cells will not be infected while the BK virus remains in its latent state, i.e. when $V < V^*$. In the case of allo-specific CD8 +T cells (E_K), the concentration can occur in trace amounts, for instance when the patient is immunosuppressed, and satisfy the criteria $E_K < E_K^*$. When this occurs, rejection of the allograft by the patient's immune response will cease as shown in the second loss term of (4.1).

The change in the infected kidney cell concentration occurs in (4.2) which contains expressions resembling those described in $\dot{H}_S$. The source for infected cells follows from the expression presented in (4.1) as expected since β represents the rate at which healthy cells become infected by virus when it is active. These infected cells may also be targeted by the BKV-specific CD8 +T cells when there is an immune response. This interaction occurs in the final loss term at the rate δ_{EH} where infected cells are removed from the patient. Upon infection, the cellular machinery begins producing copies of the virus called virions. The cell will continue to make virions until lysis eventually occurs. This natural cell death of the infected cells is found in the first loss term, occurring at rate δ_{H_I} and results in virions being released into the bloodstream.

The free virions are found in the patient's bloodstream where some remain until they pass through nephrons in the kidney providing the potential to infect susceptible cells. These virions are represented by V in the model and measured by copies per mL of blood plasma. New copies of the virus are introduced to the bloodstream during the lysis of infected cells as shown in $\rho_V \delta_{HI} H_I$. Over the course of the infection, each infected cell will produce ρ_V copies of the virus on average. The BK virus can also be cleared from the body and may be found in the urine. This natural clearance of virions from the body occurs in the first loss term of (4.3) at the exponential rate δ_V. When infecting susceptible cells, a single virion is removed from the blood for each susceptible cell infected. Since there is a 1:1 ratio between virions and infected cells, the expression for infection seen in

(4.1) is also repeated in (4.3). This loss of BKV due to infection occurs at rate β as shown in the loss expression $\beta H_S V$. These dynamics complete the virus-nephron interaction loop which is the principal system when over-suppression is present in patients. This can be observed in Figure 4.2 between compartments H_S, H_I, and V.

Modeling the immune response in a renal transplant patient is presented in equations (4.4) - (4.5). As described earlier, the immune system uniquely responds to the BK virus and the allograft in $\dot{E}_V$ and $\dot{E}_K$, respectively. Both equations follow the same framework and rely on similar assumptions but differ in the values of their corresponding parameters. In Murad et al. (2018), (4.4) - (4.5) follow the assumption that the immune system maintains a low level defense before any threat arises as represented by constant source terms λ_{EV} and λ_{EK}, respectively. The immune response reacts to the magnitudes of present threats such as increase in active virus in the bloodstream or introduction of foreign tissues to the body which are described in the fractional source terms of (4.4) - (4.5). These source terms provide a simple framework that captures sufficient complexity of BKV-specific CD8 +T cells response to changes in the quantity of virions with a half-saturation constant κ_V for viral level and maximum growth rate of ρ_{EV} for the CD8 +T cells. A similar expression is used in (4.5) characterizing the relationship between the allograft and the allo-specific immune response. In both immune responses, exponential decay is exhibited with the natural death rates of δ_{EV} and δ_{EK}.

The initial expression for both equations (4.4) and (4.5) is $(1-\epsilon)$ and formulates the idea behind immunosuppression for the patient. The parameter, ϵ represents the efficacy of the immunosuppression treatment on a scale from 0 to 1 where a value of 0 indicates no suppression (fully competent immune system) and 1 indicates full suppression (completely compromised immune response). This choice generalizes the model to any variety of treatments based on their effectiveness at suppressing the patient's immune system. This immunosuppression expression is multiplied by both sources of the immune response thereby reducing production of the CD8 +T cells that make up the immune system in the model. In the case of full suppression ($\epsilon = 1$) this expression completely nullifies CD8 +T cell production resulting in decay of the initial quantity of cells. Alternatively, setting the suppression treatment to $\epsilon = 0.5$, indicates the treatments are suppressing the immune system by 50% and therefore only producing half of the cells in a typical response to both BKV and the allograft.

The model also includes serum creatinine levels, C, as a surrogate for determining healthy levels of kidney function (as mentioned in section 4.1). Serum creatinine can be collected at regular checkups through blood and/or urine analysis thus providing data about the patient. Including the serum creatinine state in the model provides the benefit of allowing collected data to be utilized for model validation or the implementation of patient feedback mechanisms as we will show in a later section. The creatinine state has a single constant source term that comes from the natural metabolic process of breaking down creatine which ranges from 0.6 to 3 mg/dL in adults without ESRD [44, 89]. Clearing of serum creatinine is also modeled as an interaction between the healthy

functioning renal cells and the amount of metabolite in the blood. Here the half-saturation is κ_{CH} and the maximum clearance rate of creatinine is δ_{C0}. As the allograft loses healthy cells due to infection and rejection, the deterioration of kidney function is characterized by a reduced clearance rate of serum creatinine. The difference between the clearance rate and constant source produces serum creatinine accumulation as is observed in renal transplant recipients.

Table 4.2 Parameters and values used in the Mathematical Model [135]

Parameter	Description	Unit	Value
$\tilde{\beta}$	Attack rate on H_S by E_K	mL/(cells·day)	0.0001
β	Infection rate of H_S by V	mL/(copies·day)	8.22×10^{-8}
δ_{HI}	Death rate of H_I by V	/day	0.085
δ_{EH}	Elimination rate of H_I by E_V	mL/(cells·day)	0.0018
ρ_V	Virions produced by H_I before death	copies/cells	15000
δ_V	Natural clearance rate of V	/day	0.05
λ_{EV}	Source rate of E_V	cells/(mL·day)	285
ρ_{EV}	Maximum proliferation rate for E_V	/day	0.36
κ_V	Half saturation constant	copies/mL	10^6
δ_{EV}	Death rate of E_V	/day	0.17
λ_{EK}	Source rate of E_K	cells/(mL·day)	285
ρ_{EK}	Maximum proliferation rate for E_K	/day	0.137
κ_{KH}	Half saturation constant	cells / mL	10^3
δ_{EK}	Death rate of E_K	/day	0.09
λ_C	Production rate for C	mg/(dL·day)	0.01
δ_{C0}	Maximize clearance rate for C	/day	0.2
κ_{CH}	Half saturation constant	cells/mL	10^4
E_K^*	Threshold concentration of allo-specific CD8+ T-cells	cells/mL	2500
V^*	Threshold concentration of BKV	copies/mL	1000
E_V^*	Threshold concentration of BKV-specific CD8+ T-cells	cells/mL	500

It is important that this model captures the extremes of immunity over- and under-suppression. When complete over-suppression occurs ($\epsilon = 1$), the immune systems ability to produce CD8+ T cells is significantly impaired and can be seen by the nullification of source terms in both (4.4) and (4.5). This results in initial quantities of both immune response cells ($E_K(0) = E_{K0}$ and $E_V(0) = E_{V0}$) being left to decay at their specific rates and essentially negates their influence on healthy and infected cells. This can be observed in the loss terms of both (4.1) and (4.2) where E_K and E_V become smaller over time. Uninhibited accumulation of infected kidney cells leads to increasing amounts of virions in the bloodstream (i.e. V grows quickly) and severe BKV infection with reduced kidney function

Table 4.3 Initial Values for the system of ODE's [135]

State	Value	Reasoning
H_{S0}	1025 cells/mL	Value from [135]
H_{I0}	2×10^{-16} cells/mL	Trace concentration given BKV is latent
V_0	1200 copies/ mL	Limited detectable level [92, 114]
C_0	0.7	Value from [135]
E_{V0}	100 cells/mL	Limited level given BKV is latent
E_{K0}	2×10^{-16} cells/mL	Trace concentration pre-transplantation

(i.e. reduced H_S), the ultimate consequence. Table 4.4 shows these dynamics in the case where ϵ is high with increasing infection and serum creatinine. Alternatively during under-suppression ($\epsilon = 0$), all sources for CD8 +T cells are fully active providing state growth relative to the size of V for E_V and H_S for E_K. This results in low V populations as E_V removes a majority of infected cells in (4.2). The unfortunate consequence of under-suppression occurs in (4.1) where initially the H_S cell population is at its largest quantity leading to the highest growth of allo-specific CD8 +T cells at day 0. This results in a quick loss of healthy kidney cells to the immune response driving increased serum creatinine levels. Table 4.4 presents the dynamics where CD8 +T cells at their highest push both virions in the blood and susceptible allograft cells to significantly low levels thus high amounts of creatinine accumulate in the blood.

Table 4.4 State dynamics in terms of immunosuppression [135]

ϵ	CD8+ T cells	BKV	Infected Cells	Susceptible Cells	Creatinine
High	↓	↑	↑	↓	↑
Balanced	↓	↓	↓	↑	↓
Low	↑	↓	↓	↓	↑

This model is simulated using the MATLAB 2018a software package [127]. The built-in integrator *ode15s* is used to solve the system of ordinary differential equations described in the (4.1) - (4.6) with *'RelTol'* $= 1e-12$, *'MaxOrder'* $= 4$, and *'MaxStep'* $= 0.1$. These settings are necessary to balance numerical error and runtime. For forward simulations, the mathematical model is solved over the time interval $t_0 = 0$ to $T = 280$ days. The 280 day final time is chosen since it allows a reasonable amount of simulated patient data to be used as feedback while keeping simulation runtimes (which include feedback) under 24 hours. Descriptions of the model states, initial values, and parameters used in the simulations are provided in Tables 4.1, 4.2, and 4.3 respectively.

4.2.2 Log Transform Model

A notable feature of immunosuppression in renal transplant patients is the difference in scale of the important quantities such as viral load (copies per mL), susceptible/infected kidney cells (cells per mL), and serum creatinine levels (mg per dL). Following [135], our work assumes the initial kidney cell population begins below 1500 cells per mL while infected cell counts remain below 100 cells per mL at any moment due to the relatively short duration cells spend in this state. On the other hand, viral levels can change very rapidly and approach hundreds of thousands of copies when a severe BK viral infection occurs placing this state orders of magnitude larger than kidney cells populations. Furthermore, serum creatinine levels for new ESRD patients range from 4 to 16 mg per dL, therefore these levels for renal transplant patients can be as much as 5 orders of magnitude lower than viral loads [70]. Due to these differences in magnitude of the state variables along with the potential of drastic changes in quantities such as viral load, it is common for researchers to treat these quantities on a log scale especially in viral dynamics [94, 95, 145].

A log transformation of mathematical models has been used in other viral dynamics research for a variety of benefits; see [2, 18, 135]. Log transformation will restrict the numerical solutions of the states to non-negative values. This quality is advantageous in biological modeling where negative states are often unrealistic and numerical solutions can be affected by round-off error. Log transforming the model standardizes the scale of the solutions making optimization more efficient when the stopping criteria involves state variables. Large differences in the scale of model quantities can increase condition numbers causing slower convergence in the numerical methods. Additionally from a statistical perspective, a log transformation of observations provides a more normally distributed grouping [18]. This property will assist in the discussion on Kalman Filtering and feedback in section 4.4.

The mathematical model described in equations (4.1) - (4.6) can be rewritten by defining the solution vector $\bar{y}(t) = [H_S(t), H_I(t), V(t), E_V(t), E_K(t), C(t)]^T$. Here the bar notation on $\bar{y}$ represents an unscaled vector. Furthermore the model takes the form

$$\dot{\bar{y}} = \bar{g}(t, \bar{y}; q) \tag{4.8}$$

with initial conditions $\bar{y}(0) = [H_S(0), H_I(0), V(0), E_V(0), E_K(0), C(0)]^T$. Here $\bar{g}$ is the vector of differential equations ((4.1)-(4.6)) and q is the vector of parameters as described in Table 4.2. For the dynamics of an individual state, let the scaled state y_i be such that $y_i = log_{10}\bar{y}_i$. The base-10 logarithm scaled model equations for $i = 1, .., 5$ can be written as

$$\frac{dy_i}{dt} = \frac{\bar{g}_i(t, \bar{y}; q)}{\ln(10)10^{y_i}}. \tag{4.9}$$

This formulation for the log transformed model is chosen since the transform is applied to the first

five state variables (H_S, H_I, V, E_V, E_K) while the final state, C remains unscaled and in the original form from equation (4.6). The scaling of serum creatinine is unnecessary since quantities occur at a magnitude comparable to the other transformed states and changes occur slowly over time. We can further generalize the model combining the transformed states with the unscaled creatinine state into the vector $y(t) = [x_1, x_2, x_3, x_4, x_5, \bar{x}_6]^T$ and similarly their corresponding derivatives in the vector valued function f such that

$$\frac{dy}{dt} = f(t, y; q) \tag{4.10}$$

with the appropriate transformed initial values where $y(0) = y_0$.

4.3 Control Methodology

4.3.1 Optimal Control of Immunosuppression

Optimal control theory provides the framework for finding the ideal outcome in an application and is particularly useful in nonlinear systems of ordinary differential equations. In practice, given a mathematical model and cost functional to describe an optimal outcome, a controller can be designed to achieve this outcome when the cost functional is minimized. Optimal control strategies have seen extensive use in finding effective immunotherapies most notably in research with HIV, cancer, and solid organ transplant [167, 17, 1]. Here, the optimal controller is designed to find immunosuppression treatment strategies that keep creatinine and BK viral levels low while preventing the loss of allograft cells.

Almost every transplant recipient requires a lifetime of daily anti-rejection treatments. Treatment comprises a combination of drugs which are used to prevent acute rejection of the allograft and chronic allograft nephropathy [103]. The prescribed treatments are at the discretion of the attending physicians and are often based on the physicians' observations and knowledge of the literature. These selections for immunosuppression treatments may be sufficient, but are likely suboptimal. Some experts in the field acknowledge that optimal therapies still have not been established for renal transplant recipients [139]. For generality, we focus on the effectiveness of nondescript treatment strategies since various combinations and dosages of anti-rejection drugs could produce similar subduing effects on the immune system. As discussed in section 4.2.1, the model uses treatment efficacy ϵ to determine the activity of the immune system. The continuous controller will take the place of ϵ in the model allowing drug prescriptions to change over time in response to the patient's condition.

There are two types of nonlinear control systems: open loop control (feedforward) and closed loop control (feedback) systems. In open loop control systems, the controller depends on the initial state

and either a fixed final state or fixed final time, i.e. , the final state of the optimal control is unknown but lies within an acceptable range of values. This control does not depend on intermediate values of the state variables. The closed loop control system in contrast depends on both the initial state and intermediate states allowing for feedback to be utilized when finding the optimal controller.

Managing immunosuppression is best accomplished using a closed loop control problem since the precise final states are less important than maintaining low BK viral and serum creatinine levels, while the number of healthy functioning cells within the nephrons must remain as high as possible. The dependence of the closed loop control on intermediary state values also allows for patient data to be introduced into the model as feedback; this will be discussed in detail in section 4.4.

The open loop optimal control problem is set up initially in the following manner. Let the drug efficacy controller be a continuous function in time, $u(t)$. Consider the vector $s \in \mathbb{R}^{T+1}$, where s_k is the efficacy of the prescribed treatment on day $k = 0, 1, \ldots, T$. Using a linear spline approach, the controller u is defined as

$$u(t) = s_k + (s_{k+1} - s_k)(t - k). \tag{4.11}$$

More advanced functions could be chosen for the controller but that is left for future work. We update the general model in (4.10) to include the controller as follows

$$\frac{dy}{dt} = f(y(t), u(t), t; q) \tag{4.12}$$

with the same initial conditions y_0 to describe the dynamics for the continuous nonlinear control problem. This control problem has a free final state at a fixed final time T since an infinite number of solutions will have final states $y(T)$ that yield favorable results: a healthy kidney and controlled BK viral levels and serum creatinine concentrations. The general cost functional has the form

$$J(t_0) = \phi(y(T), T) + \int_{t_0}^{T} L(y(t), u(t), t) dt. \tag{4.13}$$

The optimal controller can be found by solving the 2-point boundary problem using Lagrange multipliers (λ) as described in [118]:

$$\text{Hamiltonian: } H(y, u, t) = L(y, u, t) + \lambda^T f(y, u, t; q) \tag{4.14}$$

$$\text{State: } \dot{y} = \frac{\partial H}{\partial \lambda} = f(y, u, t; q), \qquad t \geq t_0 \tag{4.15}$$

$$\text{Costate: } -\dot{\lambda} = \frac{\partial H}{\partial y} = \frac{\partial f^T}{\partial y}\lambda + \frac{\partial L}{\partial y}, \quad t \leq T \tag{4.16}$$

$$\text{Constraints: 1) } y_0 \text{ given}$$

$$2)\ (\phi_y - \lambda)^T|_T \, dy(T) = 0. \tag{4.17}$$

We wish to satisfy Pontryagin's Minimum Principle

$$H(y^*, u^*, \lambda^*, t) \leq H(y^*, u, \lambda^*, t), \tag{4.18}$$

with * representing optimal quantities and controllers, u, are taken from the space of all admissible controllers, $\mathscr{U}$ [56]. Thus we find the optimal controller (where $0 \leq u(t) \leq 1$) that satisfies

$$u^*(t) = \underset{u \in \mathscr{U}}{\operatorname{argmin}}\ H(y^*(t), u(t), \lambda^*(t), t).$$

We choose a cost functional that penalizes two conditions: high levels of BKV in the blood and deteriorating kidney function. The cost functional to achieve this objective is

$$J(t_0) = \int_{t_0}^{T} \omega_V V(t)^2 + \omega_C \bar{C}^2(t) + \omega_{HS}(log_{10} H_{S0} - H_S)^2, \tag{4.19}$$

where the ω's are weights and the bar notation represents an unscaled quantity. This functional penalizes the controller for all virus present in the blood and rising levels of creatinine in the blood. These are important quantities because not only are serum creatinine levels a surrogate for kidney function, but both viral concentrations in the blood and serum creatinine concentrations can be obtained during routine checkups to assess changes in treatment [187]. The benefit provided by the inclusion of these states is the ability of the cost functional to react to patient data which translates into a patient specific optimal controller. Serum creatinine levels in the blood are not always sufficient to control the loss of kidney function so the final term of (4.19) with respect to H_S is included to increase the cost for loss of kidney function by penalizing a diminished quantity of susceptible kidney cells. We note that in comparison to (4.13), our $J(t)$ sets $\phi(y(T), T) = 0$ since a penalty for deviation from a final state is unnecessary. In addition, the form of (4.19) and the free final state assumption affect the boundary condition described in (4.17). It follows that $dy(T) \neq 0$ given that the final state is free, hence $(\phi_y - \lambda)^T|_T = 0$ in (4.17) which implies $\lambda(T) = 0$ for our final constraint.

Only the simplest of nonlinear control problems have closed form solutions. Numerical methods provide a means for solving the 2-point boundary problem. We employ the algorithm in [56] to find our optimal controller:

1. Solve the state equation (4.15) forward in time over the interval (t_0, T) using the initial state y_0.
2. Solve the costate equation (4.16) backward in time from T to t_0 using the constraint $\lambda(T) = 0$.
3. Compute the cost $J(u)$ and gradient $H_u = \nabla J$ using a first order approximation [153].
4. Provide the J and ∇J to the numerical optimization function.
5. Determine the optimal controller until convergence tolerances are met.

The MATLAB optimization function *fmincon* is chosen to find the optimal control using settings *'TolFun' = 0.1* and *'TolX'* $= 1e-4$. This method requires the choice of an initial guess for the controller denoted u_0, a continuous function in time. Since we have no prior knowledge of the form of the optimal controller, u_0 is chosen as a fixed controller such that $0 < u_0(t) < 1$ for all $t \in [t_0, T]$. This follows from $u(t)$ representing drug efficacy defined specifically on this range.

4.3.2 Receding Horizon Controller Scheme

Renal transplant recipients attend regular post-transplant visitations with their transplant physicians while the duration between these appointments may vary patient to patient. These routine check-ups often involve blood analyses and may include urine analysis [45]. The medical tests can provide patient data regarding serum creatinine levels and BKV blood levels at the time of the appointment. This data can be used as feedback to update the nonlinear control problem in the search for a controller that provides the best immunosuppression treatment for specific patients. We employ this feedback mechanism (and create a closed loop control system) by using the receding horizon control (RHC) methodology as described in [57].

The time frame of interest for this problem is from t_0 to T days. The discrete days for which routine check-ups take place is the set of t_i for $i = 1, 2, 3, ...$ such that $t_i < T$. The control horizon, $t_{ch,i}$ is the fixed amount of time over which an optimal controller will be determined, such that $t_{ch,i} \geq t_{i+1} - t_i$. The RHC problem can be seen as a sequence of nonlinear control problems, $\mathcal{O}_i$, over their respective intervals $[t_i, t_{i+1}]$. For each interval, the 2-point boundary control problem will be solved with initial time t_i and fixed final time $t_i + t_{ch,i}$, where the cost functional is

$$J_i = \phi(y(t_i + t_{ch,i}), t_i + t_{ch,i}) + \int_{t_i}^{t_i + t_{ch_i}} L(y, u, t) d\,t, \tag{4.20}$$

with initial condition $y(t_i)$ and boundary condition $\lambda(t_i + t_{ch,i}) = 0$. The process for finding the optimal control with feedback at times, t_i for $i = 1, 2, 3...$ is an iterative process that follows these steps [57]:

1. Given the constraints $y(t_i)$ and $\lambda(t_i + t_{ch,i}) = 0$, solve the control problem $\mathcal{O}_i$ on the interval $[t_i, t_i + t_{ch,i}]$.
2. Use the controller defined on $[t_i, t_i + t_{ch,i}]$ and forward solve the model on the time interval $[t_i, t_{i+1}]$.
3. Use observation or state estimator to update $y(t_{i+1})$.
4. Repeat steps 1-3 over the next time interval $[t_{i+1}, t_{i+2}]$ using $y(t_{i+1})$ as the initial condition.

The process described here finds the optimal controller over a time interval defined by the control horizon, $t_{ch,i}$. The portion of that optimal control used for the model solution lies over the interval $[t_i, t_{i+1}]$ which represents the time between the initialization of the controller at t_i until the next observation is available at t_{i+1}. The observation can be introduced as feedback into our system to update $y(t_{i+1})$. The next optimal control problem is then solved using this new information and the process repeats until the final time of interest T is reached. An example of this method can be observed in Figure 4.3, where this example sets $t_{ch,i} = T$. The blue controller in this figure represents the collected portions of each optimal controller used over their respective time intervals.This yields a controller for the problem from time t_0 to T as desired with feedback at the discrete t_i's.

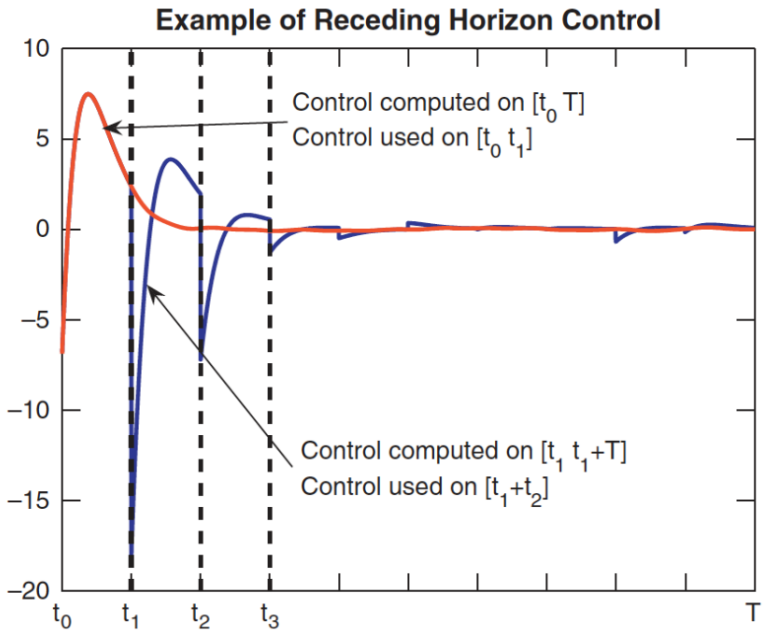

Figure 4.3 RHC example with control horizon, T [57]

In our nonlinear control problem, routine visits with transplant physicians are chosen to occur every 20 days, yielding a set of discrete observation time points as $t_i = 20, 40, 60, ...260$ with simulations concluding at $T = 280$ days. We chose these time points due to the unavailability of a dataset with sufficient observations which would otherwise dictate the values for t_i. Following [135], the control horizon is chosen as $t_{ch,i} = 200$ days since no benefit appeared for exceeding this value. The implementation of the receding horizon control requires a mechanism to introduce observations (simulated data) or state estimators as feedback for the controller which is explained in the following section.

4.4 Kalman Filtering Model Feedback

Feedback driven control is a primary focus for this modeling effort which suggests the inclusion of patient data into model. Solid organ transplant patients require routine post-transplant visitations with their physicians for continued assessment of allograft success and patient health. Renal transplant patients typically undergo blood and/or urine analysis with each visit to check allograft function, general immune response, and presence of infection [45]. Since tests account for total immune system health, determining the portion of the response related to allograft rejection or a particular disease is unlikely since determining BKV specific CD8+ T cells is extremely difficult even in healthy subjects [188].Therefore, this data is not reliable for use as feedback since our model focuses on specific components of the immune system and not the complete response on a cellular level.

However, assays are presently in use to provide the concentration of BKV in a patient's blood [114, 92]. Serum creatinine levels are also collected which provide the GFR surrogate assessment of kidney function which can be compared to model output. Our ideal dataset would comprise of regular viral and creatinine data points. Since a dataset is unavailable, patient data was simulated using the model output for both viral and creatinine levels drawn from a normal distributions with means $V(t_i)$ and $\bar{C}(t_i)$ respectively. The covariance for the data is represented by R. A method for introducing patient data as feedback into the receding horizon control problem is called Kalman filitering. Maybeck offers the apt description, "a Kalman filter combines all available measurement data, plus prior knowledge about the system and measuring devices, to produce an estimate of the desired variables in such a manner that the error is minimized statistically" [128]. The Kalman filter uses a predictor-corrector framework to produce a state estimator that utilizes the mathematical model solution and the patient data taking into account the uncertainty of both. Variations of the Kalman filter have been developed and applied to control problems in biology [57, 135, 130]. The extended Kalman filter and ensemble Kalman filter are variations of the Kalman filter for nonlinear systems and both are applied individually to the RHC in this research.

The general form of a continuous-discrete nonlinear Kalman filter requires system dynamics and an observation process as described by:

$$\dot{y} = f(y(t), u(t), t, \omega(t)), \quad \omega \sim N(0, Q), \tag{4.21}$$

$$z_k = H(y_k) + \nu_k, \quad \nu \sim N(0, R), \tag{4.22}$$

where $\omega(t)$ and ν_k are white noise processes [117]. Here the uncertainty in the mathematical model is Q which can be understood as inherent error of the model given that it approximates a real phenomenon. Although Q can be obtained through model validation with an appropriate dataset, it can also be used as a tunable quantity for filter. The uncertainty in the data is labeled R and can be determined by the statistics of the dataset and accuracy of the data collection techniques.

To characterize the uncertainty in our state information, first consider the mathematical model which simplifies a complex system by making assumptions and captures most of the driving dynamics of the system. This simplification inherently includes an amount of uncertainty. In addition, the numerical solutions to the mathematical model include generalized amounts of error based on the numerical methods used and the behavior of the solution. Although the numerical error can somewhat be quantified, the uncertainty due to model assumption is less clear. There is also uncertainty in the methods used to obtain patient data, precisely in the collection and analysis of blood and urine. The error in the precise methods used in gathering the data can be determined through literature.

Just as in section 4.3.2, the set of t_i with $i = 0, 1, 2, ...$ represents discrete time points for which complete patient data is available. The continuous dynamics between any time points t_i and t_{i+1} can be determine using (4.21) since no data exists between the endpoints of this interval. The predictor step of the method (also referred to as the *Time Update*) requires finding the state estimate at t_{i+1} using the system dynamics. The corrector step of the method (also called the *Measurement Update*) generates the Kalman gain K_k using the uncertainty in the model (Q), data (R) and states (P). The Kalman gain is a matrix that adjusts the state estimates and is scaled by the difference between the estimate and the data. This process corrects the state estimate from the model using the data. The contrast in scale between values in Q and R provides confidence that the source (model or data) with the lower uncertainty is a better approximation of the true state values. In the case where less uncertainty is in the data than the model, the Kalman gain corrects the model output (state estimates) to a level closer to the data. The updated state estimate includes feedback from the model and the predictor-corrector process can continue on the next time interval from t_k to t_{k+1}. This process repeats until the final time of the simulation is reached.

4.4.1 Extended Kalman Filter

The Extended Kalman filter (EKF) is an extension of the original Kalman filter for use in nonlinear problems and can be applied to problems with continuous dynamics and discrete data points as in our problem [117]. The EKF simplifies the problem of nonlinearity by linearizing the dynamics and observation process around the mean state estimate at the discrete sample times t_i when data is introduced as feedback. The uncertainty in the model is a weighted white noise process with $\omega(t)$ that is described by a 0 mean and covariance Q. The uncertainty in the data is a white noise process v_k described by mean 0 and covariance R. These processes for our problem are described as:

$$\dot{y} = f(y(t), u(t), t) + \omega(t), \text{ where } \omega(t) \sim N(0, Q) \tag{4.23}$$

$$z_k = h(y(t_k), k) + v_k, \text{ where } v_k \sim N(0, R). \tag{4.24}$$

For the time update step, both the mean state and covariance are propagated forward in time between the previous time data was collected, t_k and next introduction of data at t_{k+1} using

$$\dot{y} = f(y(t), u(t), t) \tag{4.25}$$

$$\dot{P} = P\nabla f(\hat{y})^T \nabla f(\hat{y})P + Q. \tag{4.26}$$

We observe in (4.26) the Jacobian matrix of f which is a result of linearizing the nonlinear problem. This system of equations will be solved iteratively with initial values $\hat{y}(t_{k-1})$ and $P(t_{k-1})$. The result includes both the state and covariance estimates yielded by the model dynamics at t_k which are $\hat{y}_k^- = \hat{y}(t_k)$ and $P_k^- = P(t_k)$, notationally. In the measurement update, the Jacobian matrix of the observation process (∇h) is used when working with observation estimates in the linearized methods. To calculate the Kalman gain, the state covariance estimate, uncertainty in collected data R, and observation Jacobian are used:

$$K_k = P_k^- \nabla h(\hat{y}_k)^T [\nabla h(\hat{y}_k) P_k^- \nabla h(\hat{y}_k)^T + R]^{-1}. \tag{4.27}$$

This matrix determines how much the observed and unobserved states should be adjusted and will be scaled based on the error between the data and the observation estimates. We also include the gain when updating the state covariance estimate. The measurement update concludes with finding the mean state estimate and covariance based on feedback from the data (z_d)as follows:

$$\hat{y}_k = \hat{y}_k^- + K_k[z_d - h(\hat{y}_k^-, k)] \tag{4.28}$$

$$P_k = [I - K_k \nabla h(\hat{y}_k^-, k)]P_k^-. \tag{4.29}$$

The values obtained from (4.28) and (4.29) represent a shift from the output of model at time t_k toward the data in the observed states and estimates for corresponding unobserved states given the known uncertainties. The new estimates reflect the source with the most certainty, i.e., the lower covariance values. To demonstrate this idea, the model is considered to capture important dynamics with immunosuppression in a renal transplant patient but we recognize it does not capture all of the processes influencing the dynamics. Instead, we believe the data captures a representation the dynamics missing from the model within a specific patient even with the uncertainty in data collection methods. Since a sufficient dataset is unavailable to obtain a realistic scale of Q or R, in our work the scale of the covariances is adjusted in an attempt to determine a reasonable amount of noise the model can process given available computation power and time.

By utilizing the Kalman gain, the EKF adjusts the model output closer to the data collected from individual patients when R is close to or greater than Q thereby personalizing the treatment to the individual. These more personalized estimates of the mean state and covariance are then used as the initial conditions for the model dynamics until the next patient data is available at t_{k+1} where a new Kalman gain can be calculated and utilized. We provide the EKF algorithm in Algorithm 1.

Algorithm 1 Continuous-Discrete Extended Kalman Filter (EKF) [117, 135]

Nonlinear dynamic model with discrete measurements:

$$\begin{aligned} \dot{y}(t) &= f(y(t), u(t), t) + \omega(t), \quad & \omega &\sim N(0, Q) \\ z_k &= h(y(t_k), k) + \nu_k, & \nu_k &\sim N(0, R) \end{aligned}$$

Initialization of state and covariance ($k = 0$):

$$\begin{aligned} y(0) &\sim N(y_0, P_0) \\ \hat{y}(0) &= y_0 \\ P(0) &= P_0 \end{aligned}$$

For k = 1,2,3, ...

Time Update:

1. Find the controller, $u(t)$, over $t_{k-1} < t < t_k$ using the state mean $\hat{y}(t_{k-1})$
2. Compute the Jacobians:

$$A(y, t) = \nabla f(y, t), \quad C(y) = \nabla h(y, k)$$

3. Solve the system over the interval (t_{k-1}, t_k) using $\hat{y}(t_{k-1}) = \hat{y}_{k-1}$ and $P(t_{k-1}) = P_{k-1}$

$$\begin{aligned} \dot{\hat{y}}(t) &= f(\hat{y}(t), u(t), t) \\ \dot{P}(t) &= PA^T(\hat{y}, t) + A(\hat{y}, t)P + Q \end{aligned}$$

Let $\hat{y}_k^- = \hat{y}(t_k)$ and $P_k^- = P(t_k)$

Measurement Update:

4. Compute the Kalman Gain

$$K_k = P_k^- C^T(\hat{y}_k^-)[C(\hat{y}_k^-)P_k^- C^T(\hat{y}_k^-) + R]^{-1}$$

5. Update state mean and covariance

$$\begin{aligned} \hat{y}_k &= \hat{y}_k^- + K_k[z_d - h(\hat{y}_k^-, k)] \\ P_k &= [I - K_k C(\hat{y}_k^-, k)]P_k^- \end{aligned}$$

4.4.2 Ensemble Kalman Filter

In contrast to the EKF, the Ensemble Kalman filter (EnKF) maintains the nonlinear dynamics and observation process throughout the application of the filter. Similar to the EKF, the uncertainty in the model and data are assumed to be related to white noise random variables ω_k and ν_k. The formulation of the state and observation process with weights g_ω and g_ν are:

$$\dot{y} = f(y(t), u(t), t), \qquad \forall t > t_{k-1} \tag{4.30}$$

$$y_k = y(t_k; y_{k-1}, u) + g_\omega(k)\omega_k, \text{ where } \omega_k \sim N(0, Q) \tag{4.31}$$

$$z_k = h(y(t_k), k) + g_\nu(k)\nu_k, \qquad \text{where } \nu_k \sim N(0, R). \tag{4.32}$$

The EnKF assumes initially that the state is normally distributed such that $y(t_0) \sim N(\hat{y}_0, P(t)_0)$. A sample of q points are drawn from the initial distribution creating an ensemble of initial values. Each initial value will produce a solution denoted $y^j(t)$ for $j = 1, ..., q$. The propagation of each element through the nonlinear dynamics and observation process are used to calculate the necessary statistics for the filter. We assume the patient will respond to treatment similar to the sample mean hence the controller $u(t)$ over an interval from t_{k-1} to t_k is determined using $\hat{y}(t_{k-1})$ as the initial value. One might consider finding the set of optimal controllers for each $y^j(t)$ and determining the optimal controller for the patient from the set of optimal controllers. This method would require too much computational power to be feasible and also falls outside the scope of this research.

The time update begins with calculating the solution for each member of the ensemble using the dynamics in (4.30) over the interval from t_{k-1} to t_k (i.e. , between observations). At time t_k when the next patient data is available, the state estimates (y_k^{j-}) and observation estimates (z_k^{j-}) for $j = 1, ..., q$ are calculated using model dynamics, model noise, and the observation process [4]:

$$y_k^{j-} = y^j(t_k, u; y_{k-1}^j) + g_\omega(k)\omega_k \tag{4.33}$$

$$z_k^{j-} = h(y_k^{j-}, k). \tag{4.34}$$

Since simulated data is being used, we assume the patient behaves similar to model dynamics with initial value $\hat{y}(t_{k-1})$ and call this solution $y_d(t)$ over the time interval between data points. Given that q elements are in the ensemble, q data points are generated using the observation process in (4.32) in the following manner [4]:

$$z_d^j(t_k) = h(y_d(t_k)) + \nu_k^j, \quad \text{for } \; j = 1, ..., q. \tag{4.35}$$

The corrector portion of the algorithm occurs in the measurement update where sample statistics are used to determine the Kalman gain. The estimated sample and observation means are calculated

using the state and observation estimates from the time update:

$$\hat{y}_k^- = \frac{1}{q}\sum_j y_k^{j-} \tag{4.36}$$

$$\hat{z}_k^- = \frac{1}{q}\sum_j z_k^{j-}. \tag{4.37}$$

Next, covariance estimates can be determined by finding the necessary differences between the estimated states and observations and their respective mean values:

$$E_k^y = [y_k^{1-} - \hat{y}_k^-, ..., y_k^{q-} - \hat{y}_k^-]^T \tag{4.38}$$

$$E_k^z = [z_k^{1-} - \hat{z}_k^-, ..., z_k^{q-} - \hat{z}_k^-]^T \tag{4.39}$$

$$P_{yz_k} = \frac{1}{q-1} E_k^y (E_k^z)^T \tag{4.40}$$

$$P_{zz_k} = \frac{1}{q-1} E_k^z (E_k^z)^T. \tag{4.41}$$

The Kalman gain is built from these covariance estimates and the uncertainty in the data as follows:

$$K_k = P_{yz_k}(P_{zz_k} + R)^{-1}. \tag{4.42}$$

Now each element of the ensemble is updated using the gain which is scaled by the difference between the observation estimate and the associated data. After the entire ensemble is updated, the sample mean is calculated to be used for finding the control (and simulated patient data) over the next interval from t_k to t_{k+1}. These steps can be seen here:

$$y_k^j = y_k^{j-} + K_k(z_d^j(t_k) - z_k^{j-}), \quad \text{for } j = 1, ..., q \tag{4.43}$$

$$\hat{y}_k = \frac{1}{q}\sum_j y_k^j. \tag{4.44}$$

The ensemble Kalman filter algorithm is provided in Algorithm 2.

4.5 Results

4.5.1 Fixed Efficacy Treatments

In the case where the immunosuppression treatments provide a fixed effectiveness at suppressing the host's immune system, both the optimal control and Kalman filters are not utilized. Examples of fixed efficacy treatments are provided in Figures 4.4 and 4.5 where the dose effectiveness is 40%

Algorithm 2 Continuous-Discrete Ensemble Kalman Filter (EnKF) [66, 106]

Nonlinear dynamic model with discrete measurements:

$$\begin{aligned}
&\dot{y}(t) = f(y(t), u(t), t) \\
&y_k = y(t_k; y_{k-1}, u) + g_\omega(k)\omega_k, \quad \omega_k \sim N(0, Q) \\
&z_k = h(y(t_k), k) + g_\nu(k)\nu_k, \qquad \nu_k \sim N(0, R)
\end{aligned}$$

Initialization of state and covariance ($k = 0$):

$$\begin{aligned}
&\hat{y}_0 = E[y(t_0)] \\
&P_0 = E[(y(t_0) - E[y(t_0)])(y(t_0) - E[y(t_0)]^T)
\end{aligned}$$

Sample q particles from the initial state distribution, $y_0^1, y_0^2, ..., y_0^q$

For k = 1,2,3, ...

Time Update:

1. Find the controller, $u(t)$, over $t_{k-1} < t < t_k$ using the state mean $\hat{y}(t_{k-1})$
2. Propagate the particles through the nonlinear dynamics and observation process over $t_{k-1} < t < t_k$ where $j = 1, ..., q$,

$$\begin{aligned}
&\dot{y}^j(t) = f(y^j(t), u(t), t), \\
&y_k^{j-} = y^j(t_k; y_{k-1}^j, u) + g_\omega(k)\omega_k, \\
&z_k^{j-} = h(y_k^{j-}, k)
\end{aligned}$$

3. Compute the ensemble mean, ensemble state and output deviations

$$\begin{aligned}
&\hat{y}_k^- = \frac{1}{q}\sum_{j=1}^{q} y_k^{j-}, \qquad\qquad \hat{z}_k^- = \frac{1}{q}\sum_{j=1}^{q} z_k^{j-} \\
&E_k^y = [y_k^{1-} - \hat{y}_k^-, y_k^{2-} - \hat{y}_k^-, ..., y_k^{q-} - \hat{y}_k^-] \\
&E_k^z = [z_k^{1-} - \hat{z}_k^-, z_k^{2-} - \hat{z}_k^-, ...z_k^{q-} - \hat{z}_k^-] \\
&P_{yz_k} = \frac{1}{q-1} E_k^y (E_k^z)^T, \qquad P_{zz_k} = \frac{1}{q-1} E_k^z (E_k^z)^T
\end{aligned}$$

Measurement Update:

4. Compute the Kalman Gain

$$K_k = P_{yz_k}(P_{zz_k} + R)^{-1}$$

Measurement Update (cont.):

5. Update state ensemble and compute state mean and covariance

$$y_k^j = y_k^{j-} + K_k(z_d^j(t_k) - z_k^{j-})$$
$$\hat{y}_k = \frac{1}{q}\sum_{j=1}^{q} y_k^i$$
$$E_k = [y_k^1 - \hat{y}_k, y_k^2 - \hat{y}_k, ..., y_k^q - \hat{y}_k]$$
$$P_k = \frac{1}{q-1} E_k E_k^T$$

($\epsilon = 0.4$) and 60% ($\epsilon = 0.6$), respectively. In Figure 4.4 where the treatment suppresses the immune system by 40%, the patient is significantly under-suppressed and the CD8+ T cell populations keep the BK viral levels (mid left) under control and attack the susceptible allograft cells (top left). In the plot of BK virus, the virion concentration is noticeably below the 10,000 copies per mL threshold (red dashes). This threshold represents the detection level for BK viremia, which is a precursor to BKV nephropathy, i.e., noticeable loss of the kidney function [65, 35]. Due to the under-suppressive nature of this treatment level, the immune response is strong enough to significantly impact the allograft. The healthy cell population falls below the lower bound of 15% of initial cells ($\approx$ 154 cells per mL) indicating that nephropathy and more likely allograft loss has occurred. In the creatinine plot, gradual accumulation of serum creatinine levels are observed and due to the sudden loss of kidney function. These levels exceed 1.9 mg per dL (red dashes) which is the upper bound for healthy patients with a single functioning kidney [58]. In normal healthy males the range of creatinine levels is 0.74 to 1.35 mg per dL while normal healthy females range from 0.6 to 1.1 mg per dL due to lower muscle mass [44, 88]. Overall this plot is a good example of the effects from the under-suppression of a recipient's immune system.

Figure 4.5 shows the effects of an immunosuppression treatment which suppresses the immune response by 60% of its maximum. In contrast to Figure 4.4, there are noticeable decreases in the concentrations of the CD8+ T cells, both allo-specific and BKV-specific. This reduction in the immune response leads to BK viremia as shown in the virus plot and suggests that BKV nephropathy is likely which coincides with the significant decrease in the healthy kidney cell population. We point out that not all cases of BK veremia lead to BKV nephropathy instead only up to 50% of patients with viremia develop nephropathy [3, 35]. In Figure 4.5, the infection appears to be taken care of by 280 days (end of simulation) where trace amounts of detectable virus remain in the patient's blood. The healthy kidney cell population approaches a level approximately 35% of the initial concentration which indicates nephropathy and an approximate 35% of kidney function remains, i.e., approximately 65% of renal tubule cells are no longer functioning. This assumption slightly over simplifies this relationship since there could be less function loss if the infected renal

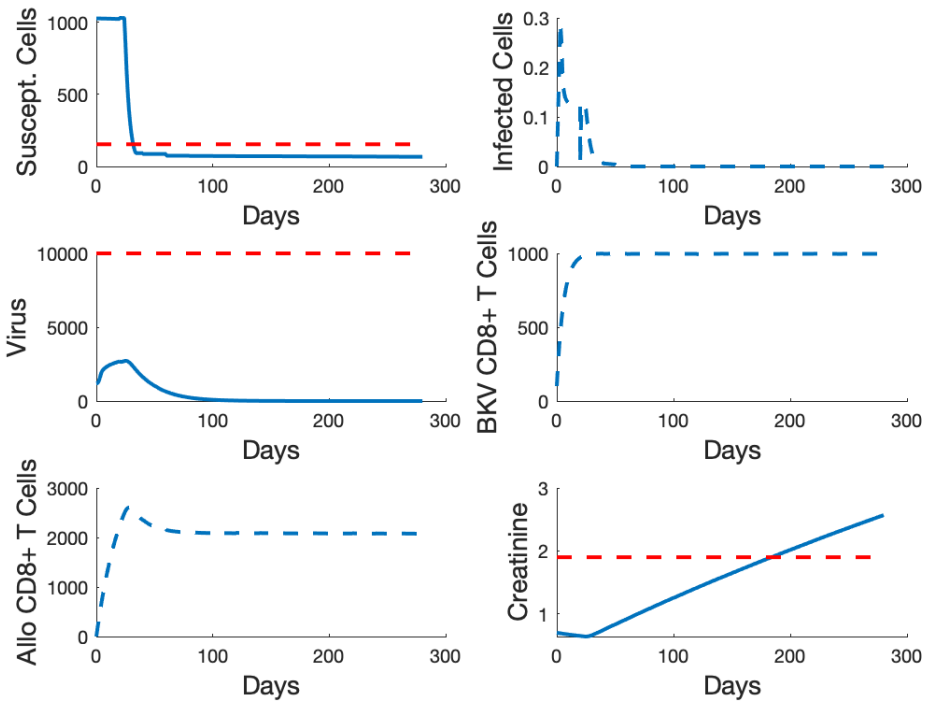

Figure 4.4 Fixed treatment efficacy of 40 % ($\epsilon = 0.4$).

tubule cells are spread among a number of nephrons, although it is more likely the infected cells spread quicker within a nephron than initially infecting many nephrons. Despite this noticeable loss of kidney function, allograft loss has not occurred although it may at some time after the 280 days of the simulation. Since creatinine levels respond slowly to loss of kidney function in the simulations, a rise in serum creatinine levels is observed but remains at acceptable levels. This particular treatment represents a moderate over-suppression of the recipient's immune response and increasing treatment effectiveness ($\geq 70\%$) would ultimately lead to significant over-suppression with a more severe BKV infection and allograft loss.

4.5.2 Receding Horizon Control and Kalman Filtering Calibration

Implementation of the receding horizon control framework requires extensive calibration of the cost functional weights as described in section 4.3. There are three weights of interest associated with viral levels (ω_V), creatinine levels (ω_C), and susceptible kidney cell concentration (ω_{HS}). Each weight takes a positive real number for a value resulting in an infinite number of possible weight combinations. Many simulations were run with both the Extended Kalman filter and Ensemble Kalman filter to determine acceptable weights for the cost functional. The vast majority resulted in allograft loss typically due to extremely large viral concentrations or combinations of BKV and the

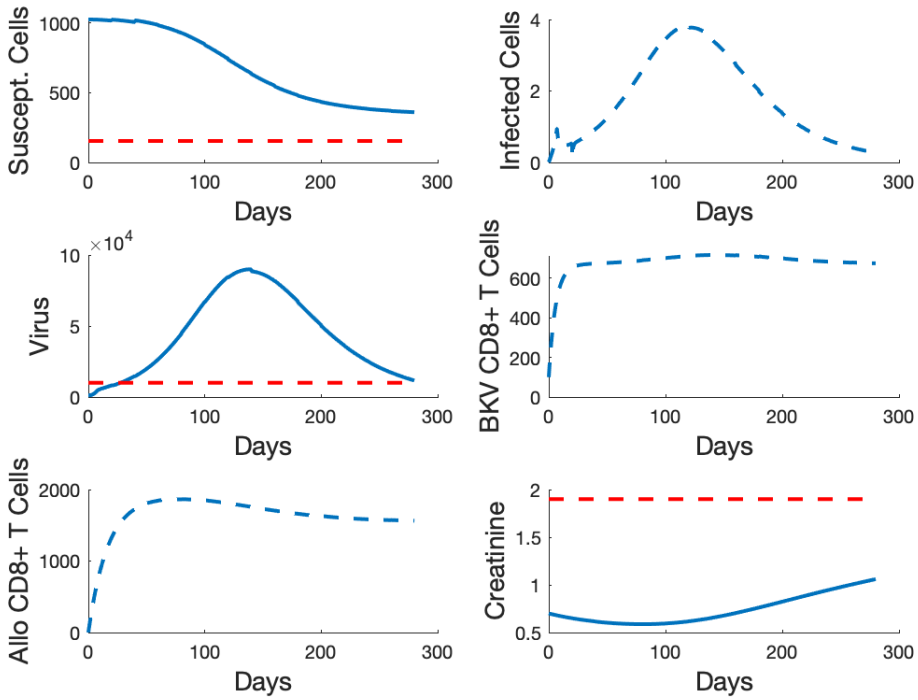

Figure 4.5 Fixed treatment efficacy of 60 % ($\epsilon = 0.6$).

allo-specific CD8+ T cells. In addition to determining a set of acceptable cost functional weights, establishing the best initial guess for the receding horizon control is important. Figures 4.4 and 4.5 from the previous section set respectable bounds for this problem. Fixed treatment efficacy below 40% resulted in severe under-suppression and subsequently allograft loss while fixed treatments of 70% established a boundary for severe over-suppression also leading to allograft loss within 280 days. For simplicity, initial guesses for the receding horizon controller were assumed to be fixed over the initial 20 day interval and were drawn from the range of 0.4 to 0.7 for epsilon. It was determined that cost functional weights $\omega_V = 0.57$, $\omega_C = 0.7$, and $\omega_{HS} = 125$ (for viral, creatinine and susceptible cell levels respectively) produced reasonable results as will be shown in sections 4.5.3 and 4.5.4. The fact that each cost functional weight can take on any positive real number and the long runtime of the model made it difficult to determine the best combination of weights.

In addition to calibration of the control problem, the Kalman filters require that the white noise processes and the covariance of the initial random model states to be known. For the ideal setup, a robust patient data set would be used to determine the variance in the initial state random variables, P_0, and also methods for collecting the data set would establish an appropriate variance for uncertainty in the data, R. A data set was unavailable for this work so values of P_0 and R were chosen as large as possible to determine maximal covariances the model and filter could tolerate with the available computational power. Since the objective of this research is to influence model

output with feedback from patient data, simulated patient data is used in conjunction with the assumption that the model noise covariance, Q, and data noise covariance, R, will be close in magnitude or the magnitude of R will be considerably greater than that of Q. Diagonal matrices are used for Q and R while the best results come from the elements of Q being approximately 1 order of magnitude higher than the elements of R, which was considered as being close. With this criteria the Kalman filters were able to adjust model output based on the proximity of the estimated observable model states and the simulated data while limiting the frequency of runs where the Kalman gain would adjust unobservable states outside biologically realistic model values. This is a common occurrence while calibrating the EnKF. It is also observed that when the elements of P_0, R, and Q were too high, simulations would result in integrator errors where step sizes could not be met or memory problems occurred likely due to large sudden changes in one or more state variables, e.g., virus concentration grows too quickly which also forces susceptible kidney cell concentrations to plummet to zero too quickly. The values in 4.5.2 are taken from Murad [135] for comparing our results with theirs. According to Murad, these variance values were chosen to be close since they felt there would be difficulty determining if more noise is present in the model or measurements. The values used were:

$$P_0 = \begin{bmatrix} 1 & 0 & 0 & 0 & 0 & 0 \\ 0 & 1 & 0 & 0 & 0 & 0 \\ 0 & 0 & 1 & 0 & 0 & 0 \\ 0 & 0 & 0 & 1 & 0 & 0 \\ 0 & 0 & 0 & 0 & 1 & 0 \\ 0 & 0 & 0 & 0 & 0 & 1 \end{bmatrix}, \quad Q = \begin{bmatrix} 0.01 & 0 & 0 & 0 & 0 & 0 \\ 0 & 0.0025 & 0 & 0 & 0 & 0 \\ 0 & 0 & 0.0004 & 0 & 0 & 0 \\ 0 & 0 & 0 & 0.0049 & 0 & 0 \\ 0 & 0 & 0 & 0 & 0.0036 & 0 \\ 0 & 0 & 0 & 0 & 0 & 0.0196 \end{bmatrix} \tag{4.45}$$

$$R = \begin{bmatrix} 0.09 & 0 \\ 0 & 0.0225 \end{bmatrix}$$

4.5.3 Feedback with the Extended Kalman Filter

The initial focus for implementation of the extended Kalman filter is for comparison and extension of the work done by Murad [135]. In Murad's use of the EKF, the cost functional only contained the first two terms found in (4.19) for viral and creatinine levels with weights set as $\omega_V = \omega_C = 1$. Murad's results are show in Figure 4.6. In their work, the patient data was simulated using a fixed immunosuppression efficacy at 60% with additive measurement noise. The utility of these results is a demonstration of the effectiveness of the EKF to adjust state estimates closer to patient data particularly when they did not follow the RHC described treatment. When reproducing the results from [135] for Figure 4.6, we determined that the transplant patient described is in a state of over-suppression given the low BKV levels (mid left) overall and substantial kidney loss (top left). The

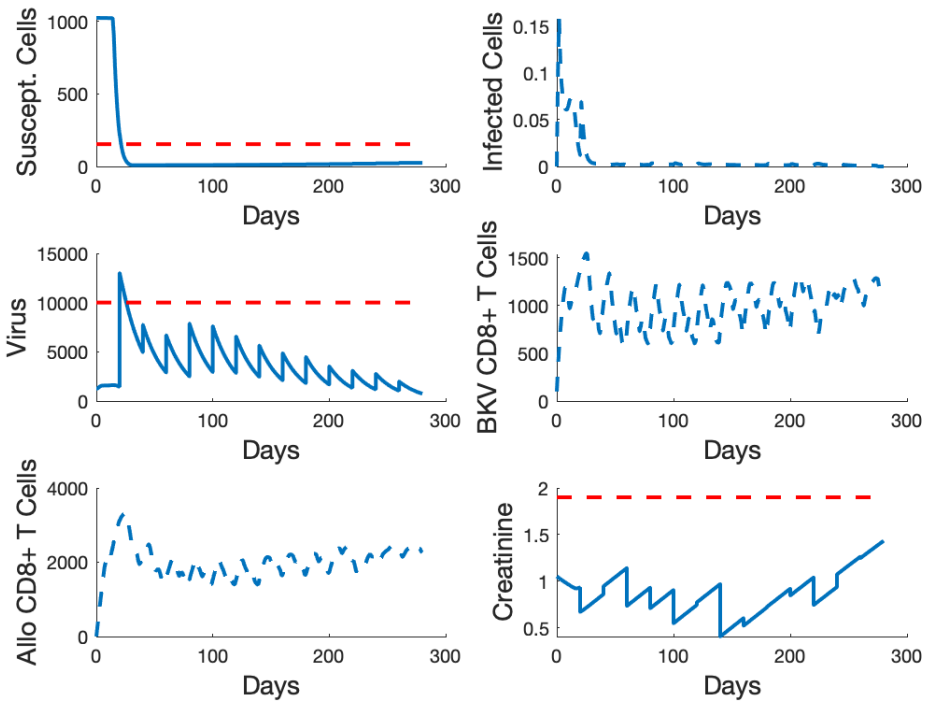

Figure 4.6 Murad Results with all state plots ($\epsilon_0 = 0.45$).

high initial spikes in both allo-specific (bottom left) and BKV-specific (mid right) CD8+ T cell concentrations further support this conclusion. The initial spike in virus also contributes to the loss of kidney cells until the BKV-specific CD8+ T cells begin reducing viral levels. These effects of under-suppression together lead to acute rejection of the kidney which usually occurs within days or weeks of the transplantation and here it occurs at day 21 [184]. We believe the reason for low creatinine concentrations (bottom right) is the fact that creatinine accumulation is a slow process in the model and speculate creatinine levels will cross the 1.9 mg per mL upper bound (red dashed line) sometime after the 280 days shown in the results due to the total loss of kidney function. Figure 4.7 features the receding horizon controller associated with the results in Figure 4.6. Observing the receding horizon controller confirms that initial under-suppression of the patient's immune system is likely the cause for the acute allograft rejection. Within the first 20 days the receding horizon control has treatment efficacies $\leq 20\%$ thereby allowing the immune response to behave closer to normal levels than not. We acknowledge that Figure 4.7 matches the controller in [135] for the initial 60 days and show similar patterns the remainder of the time. Despite the controllers not being identical, they produced the exact same virus and creatinine concentrations as presented in [135]. This discrepancy is most likely related to changes in the MATLAB optimization functions in newer builds since our results were produced on build R2018a (released March 2018) while Murad's results were likely produced on a pre-2018 build since [135] was published in spring 2018 [101].

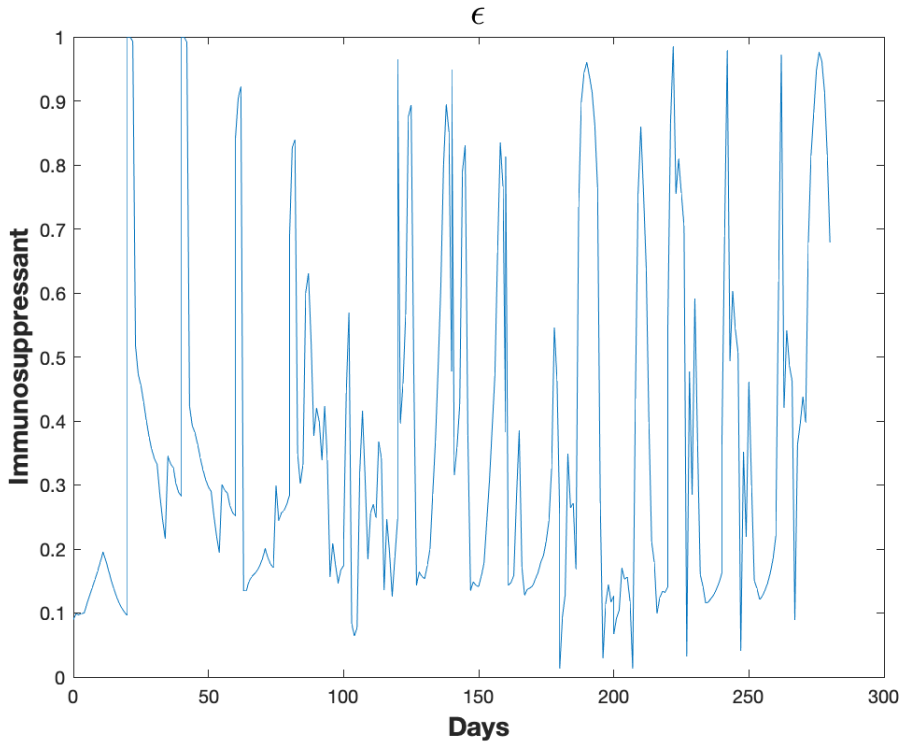

Figure 4.7 Murad receding horizon controller.

For comparison with Murad's results, the cost functional in (4.19) is used instead of the orginial found in [135] while addressing the same renal transplant patient whom follows a fixed 60% dose efficacy instead of the recommended treatment. These results in Figure 4.8 show distinct differences with Figure 4.6 where particularly noticeable differences are seen in the plots for susceptible kidney cell, BKV, and allo-specific immune cell concentrations. In Figure 4.8, the susceptible healthy kidney cell concentration (top left) remains higher throughout the time frame compared to its counterpart in Figure 4.6. Figure 4.8 also displays a significant increase in BK viral cell concentration (mid left) leading to BK viremia with a likelihood of nephropathy (which occurs when exceeding the red dashed threshold) as opposed to Murad's results which show no significant BKV viremia.

Our results using the new cost functional, indicate that the loss of kidney cells occurs predominately due to the BKV infection as opposed to the deterioration of the kidney by allo-specific CD8+ T cells as observed in Figure 4.6. The new cost functional helps determine a controller that prevents treatment schemes which cause acute kidney rejection as shown in Figure 4.8. The receding horizon controller found using this new cost functional is shown in Figure 4.9 and displays a controller with both a higher lower bound and lower upper bound than the controller in Figure 4.7. With less extreme fluctuations, this controller stays close to the treatment efficacy range of 40% to 60% indicating that mid-range treatment efficacies can prevent allograft rejection but possibly lack the ability to completely control BK viral concentrations. Unfortunately, with the controller from

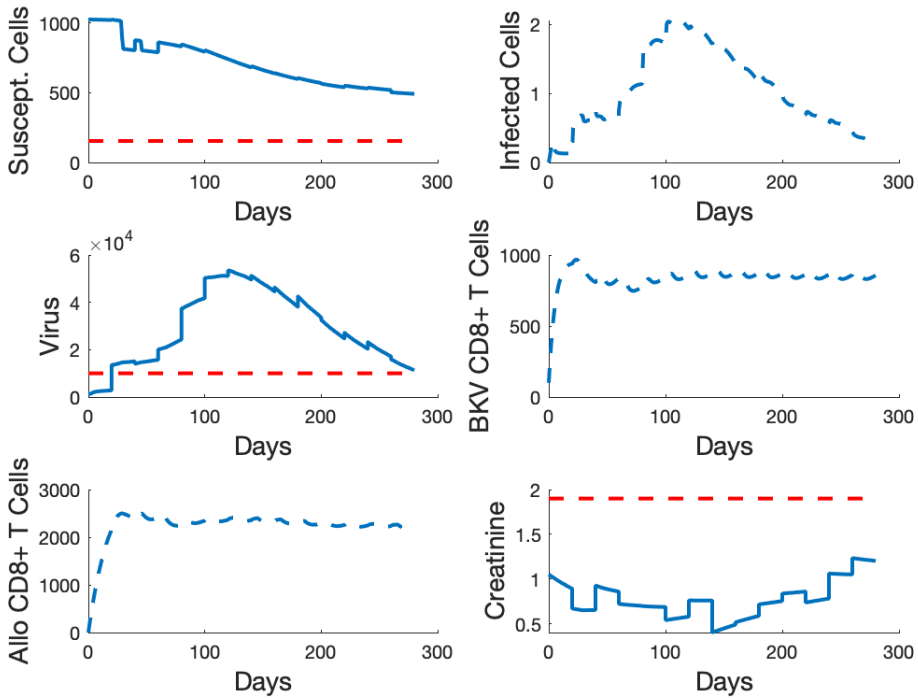

Figure 4.8 EKF model with Murad settings and data using new RHC cost functional (4.19) ($\epsilon_0 = 0.45$).

Murad's work, the allograft rejection at day 21 makes it difficult to determine if periodically higher treatment efficacy values or the significant reduction in susceptible cells are more responsible for the low BK viral concentrations.

In order to focus our EKF method on the behavior of patients that attempt to follow immunosuppression treatments suggested by the controller, we utilize simulated patient data as described in section 4.4.2 equation (4.24) where patient data is generated by solving the system of ODE's using both the updated average state estimate and the receding horizon controller then adding white noise for the measurement variability in the data [4]. First, we note that variance values in (4.5.4) from the next section are used for this application of the model with the EKF since there appeared to be no reasonable upper bound for additive noise. Fixed initial guesses for the controller are used as well. Initially, the case of $\epsilon_0 = 0.5$ (50% immunosuppression) is presented, see Figure 4.10. In these plots, the concentrations of susceptible kidney cells (top left) and BKV (mid left) indicate there is under-suppression of the immune system. The under-suppression of this treatment appears moderate due to the fact that allo-specific CD8+ T cell concentrations (bottom left) are initially kept at a low enough level to prevent acute rejection of the allograft.The treatment is unable to control the BKV-specific CD8+ T cell concentration (mid right) leading to a severe BKV infection with levels significantly above the threshold. In this case, nephropathy occurs as kidney function is reduced by

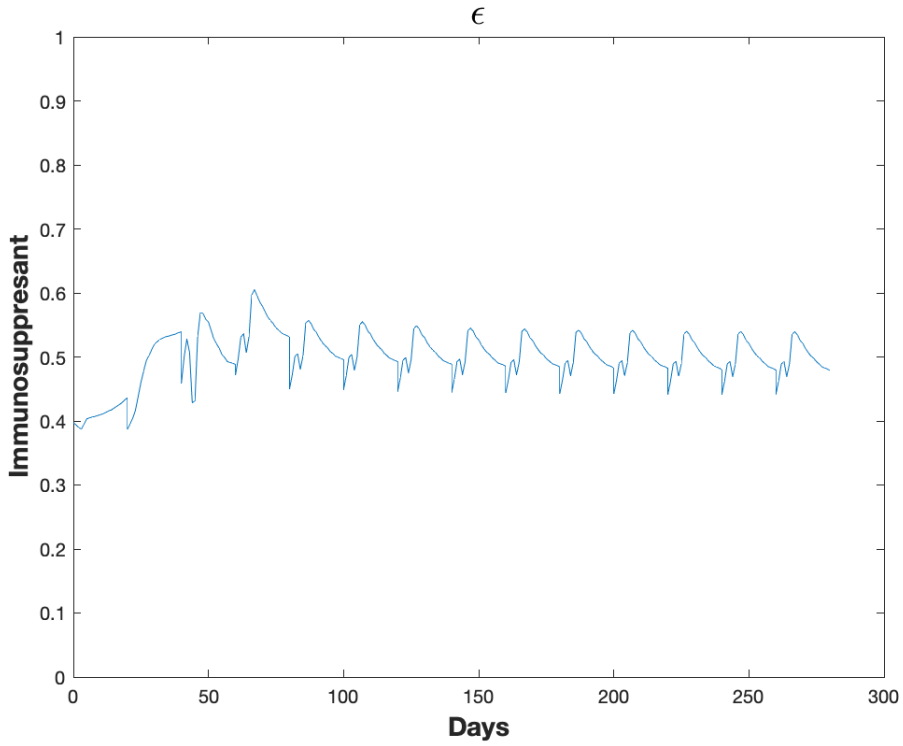

Figure 4.9 EKF model controller when using new cost functional (4.19)

over 60%. It also appears that allograft loss will occur after the 280 days shown in the results. The receding horizon controller that describes the immunosuppression treatment for this patient, in Figure 4.11, begins close to the initial guess which surprisingly is enough immunosuppression to prevent acute transplant rejection but not control BKV. The controller overall displays a periodic form that remains in the range of 36% to 67% with a downward trend. This trend is most likely a result of attempting to control the increase of virus concentration observed in Figure 4.10.

For comparison, an initial guess of $\epsilon_0 = 0.55$ is used with the EKF model. The results for this choice of initial guess are shown in Figure 4.12 where we observe very similar results to those in the $\epsilon_0 = 0.5$ case. Yet the receding horizon controller for the $\epsilon_0 = 0.55$ case, in Figure 4.13, is noticeably different from the previous controller ($\epsilon_0 = .5$). In particular, the first 40 days show a periodic form unseen in Figure 4.11 with lower values overall. The upper bound of the range of the controller is also increased from 67% to over 80% from cases $\epsilon_0 = 0.5$ to $\epsilon_0 = 0.55$, respectively. We note that the choice of initial value plays an important role since changes in initial guesses produce distinct receding horizon controllers as seen Figures 4.11 and 4.13 and will also be seen to more extreme in the next section. This difference in controllers indicates that the space of controllers, which are used to create the receding horizon control, has many local minima creating a difficulty in locating the optimal controller over any time period for our models. We also acknowledge, as is the case with the EKF model, that different receding horizon controllers may produce very similar model results. Lastly,

the decrease in creatinine concentration (bottom right) is unexpected indicating future work with this model should address creatinine as discussed in chapter 5.

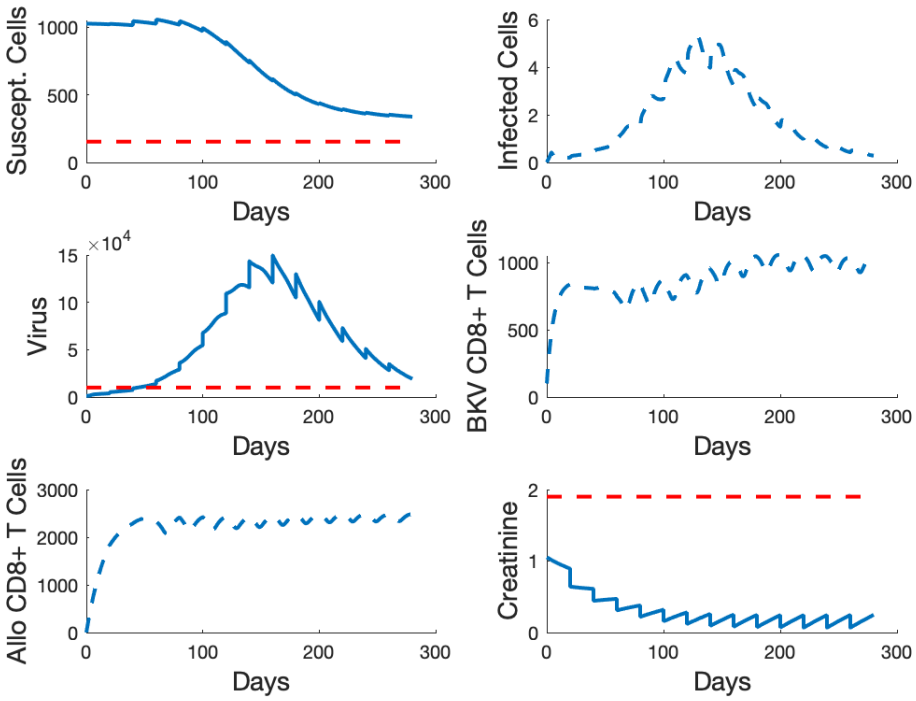

Figure 4.10 Model with the EKF and initial guess $\epsilon_0 = 0.5$.

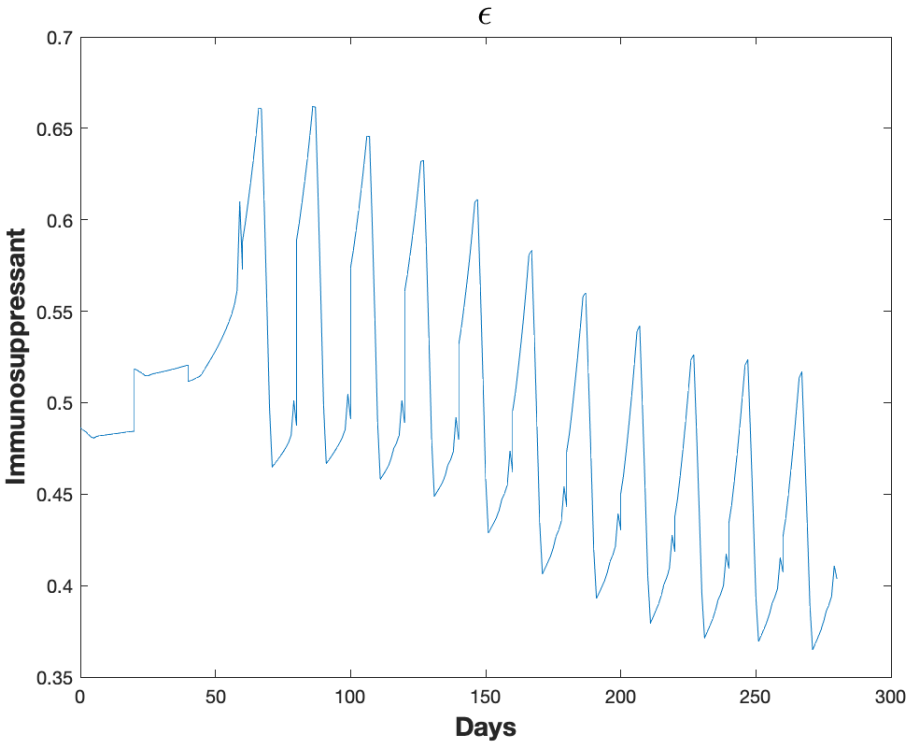

Figure 4.11 EKF model controller when using initial guess $\epsilon_0 = 0.5$.

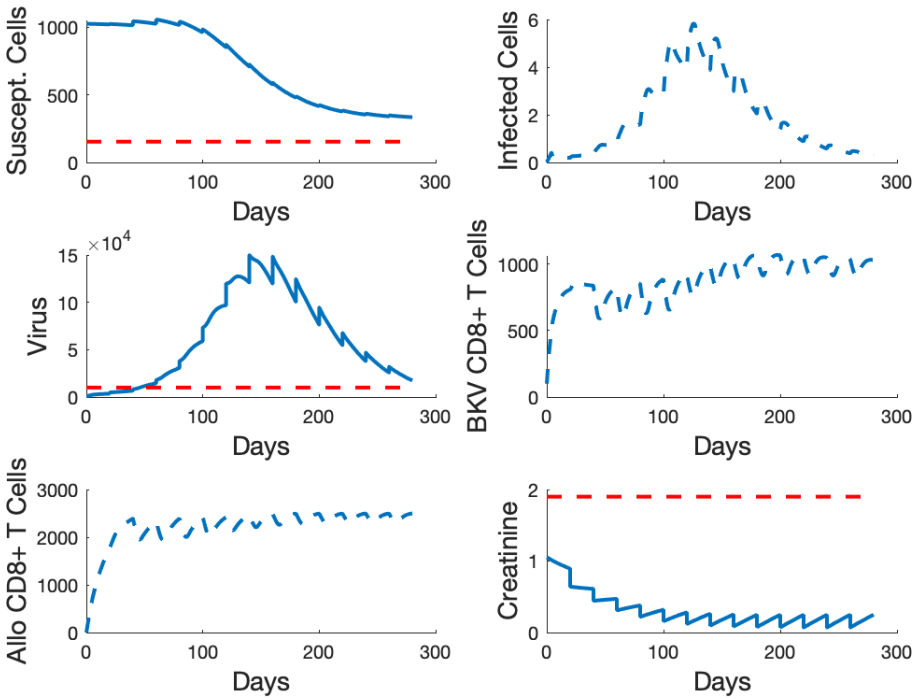

Figure 4.12 EKF model with initial guess $\epsilon_0 = 0.55$.

ϵ

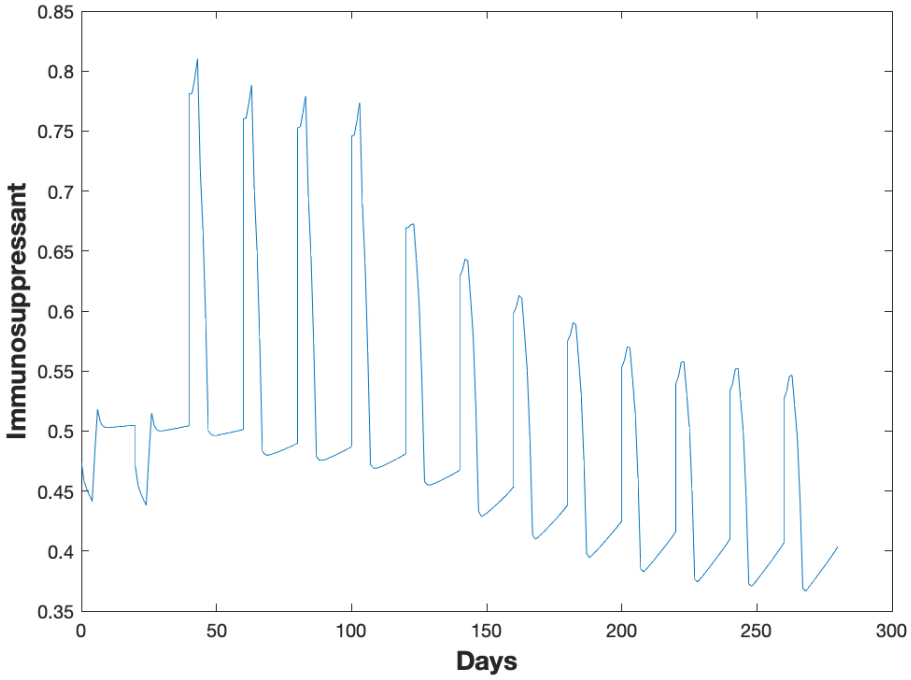

Figure 4.13 EKF model with controller using initial guess $\epsilon_0 = 0.55$.

4.5.4 Feedback with the Ensemble Kalman Filter

The ensemble Kalman filter (EnKF) is the second Kalman filter applied to our receding horizon control problem. The EnKF framework draws a sample of states from the initial distribution of the random state variables to form an ensemble that approximates this initial distribution. By propagating each element of the ensemble through the RHC problem, the ensemble approximates the distribution of the state random variables throughout the solution of the nonlinear control problem particularly at discrete time points where data is collected. Sample mean and covariance can be generated from the ensemble for the EnKF. Data was simulated for use with the EnKF as described in equation (4.32) where the noise is state-dependent. This changes (4.31) and (4.32) in the following way:

$$y_k = y(t_k; y_{k-1}, u) + \omega_k y(t_k; y_{k-1}, u), \text{ where } \omega_k \sim N(0, Q) \tag{4.46}$$

$$z_k = h(y(t_k), k) + \nu_k h(y(t_k), k), \text{ where } \nu_k \sim N(0, R). \tag{4.47}$$

The specific methods and tools utilized for taking measurements vary between medical institutions which influences the sensitivity of their measurements. For instance, PCR methods for detecting BKV

in the blood have lower bound thresholds of 1600 IU/mL and 200 IU/mL for Mayo Clinic Laboratory and Indiana University Health Molecular Pathology Laboratory, respectively [114, 92]. In addition, the laboratories have upper bound detection limits of 16 million IU/mL at Mayo Clinic Laboratories and 20 million IU/mL at Indiana University Health Molecular Pathology Laboratory, thus assuming measurement noise increases with the magnitude of the state is reasonable. A consequence of this choice is that increased noise presents elements of the ensemble that push the limits of the ODE solver and available computational power when solving for them. As the search for upper bounds to the noise variances progressed, the following variances were found to be approaching the upper bound for state-dependent noise when using the control problem with the EnKF:

$$P_0 = \begin{bmatrix} 0.1 & 0 & 0 & 0 & 0 & 0 \\ 0 & 0.1 & 0 & 0 & 0 & 0 \\ 0 & 0 & 0.1 & 0 & 0 & 0 \\ 0 & 0 & 0 & 0.1 & 0 & 0 \\ 0 & 0 & 0 & 0 & 0.1 & 0 \\ 0 & 0 & 0 & 0 & 0 & 0.1 \end{bmatrix}, \quad Q = \begin{bmatrix} 0.0001 & 0 & 0 & 0 & 0 & 0 \\ 0 & 0 & 0.0001 & 0 & 0 & 0 \\ 0 & 0 & 0.0001 & 0 & 0 & 0 \\ 0 & 0 & 0 & 0.0001 & 0 & 0 \\ 0 & 0 & 0 & 0 & 0.0001 & 0 \\ 0 & 0 & 0 & 0 & 0 & 0.0001 \end{bmatrix} \tag{4.48}$$

$$R = \begin{bmatrix} 0.001 & 0 \\ 0 & 0.001 \end{bmatrix}.$$

It was found that increasing any of the following variances by an order of magnitude often resulted in either an integrator step size tolerance error (step size tolerance *'TolX'* $= 0.0001$) or memory limitations in either case no numerical solutions could be determined. If a particular initial guess for the controller did result in a numerical solution there would be one or more state variables (usually unobserved) with biologically unrealistic values, for example, Kalman gain adjustments to healthy cell concentration could elevate this state from a value below the initial value (H_{S0}) to a value ≥ 1.5 times the initial value. When implementing the EnKF methods with the variances from (4.5.4), the numerical optimizing function requires an initial guess for the controller. For the model with the EnKF, different fixed initial guesses are used for their simplicity. Further study could focus on alternatives for initial guesses as discussed in chapter 5 and could lead to successful simulations with higher magnitudes of noise.

Through a variety of fixed initial guesses, we determined that fixed initial guesses $\geq 60\%$ produced limited results since over-suppression often occurred with drastic increases to BKV. Many simulations failed to complete as the integrator appeared unable to progress past the steepest changes in state variables. Similarly for fixed initial guesses $\leq 40\%$, under-suppression with acute transplant rejection as the result took place. Most simulations could not be completed likely due to the extreme decrease in kidney cell concentration leading to integrator problems during runtime. Initial guesses $\epsilon_0 = 0.5$

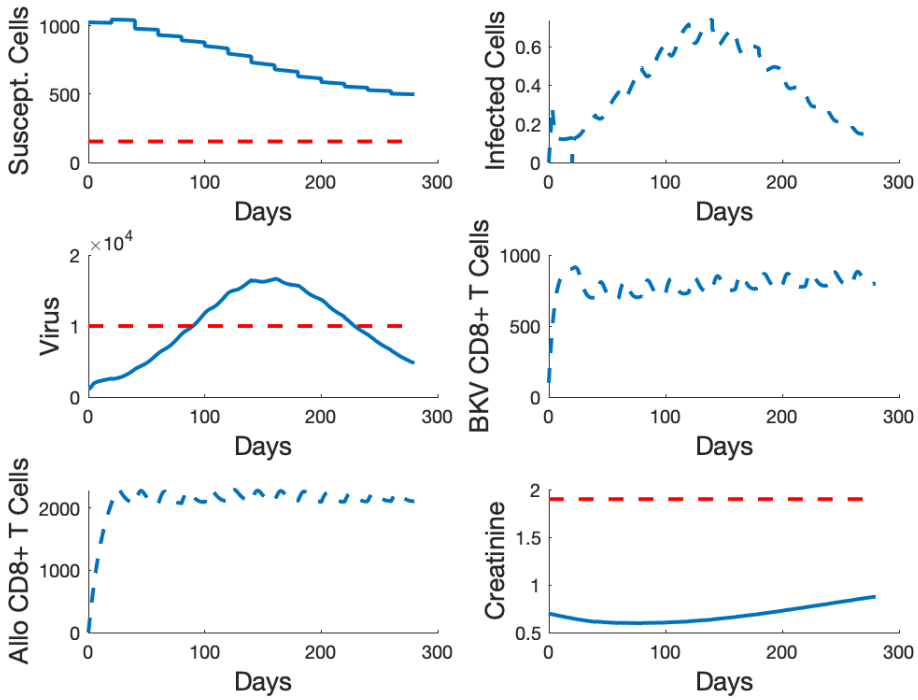

Figure 4.14 Results of the model with the EnKF and initial guess $\epsilon_0 = 0.5$, i.e. 50% suppression.

and $\epsilon_0 = 0.55$ both represent balanced immunosuppression treatments and yielded favorable results. In Figure 4.14, $\epsilon_0 = 0.5$ is used in the EnKF model and produces an immunosuppression treatment that prevents acute kidney rejection as determined by minimal loss of healthy kidney cells (top left) initially. A result of this is low serum creatinine levels (bottom right); the decrease in serum creatinine is peculiar as mentioned previously and is discussed in the next chapter. This treatment also displays some control of BKV. There is viremia with a likelihood of nephropathy as indicated by the virus concentration exceeding the threshold (red dashed line). Examining the susceptible cell concentration (top left), kidney loss has occurred with approximately 50% kidney function remaining. It is difficult to discern if virus or allo-specific CD8+ T cells are more responsible for this loss of susceptible cells. The most important results of this treatment regimen are that kidney rejection has not occurred and that kidney functionally loss is slow which may prevent allograft loss until years later. The results of this treatment appear to coincide with treatment results described in literature where initial anti-rejection is a high priority in treatments and then shifts to maintaining allograft functionality [75]. Chronic allograft nephropathy is not uncommon for renal transplant recipients often leading to allograft loss to occur 2-10 years post-transplant with current treatment regimes. The immunosuppression treatment when $\epsilon_0 = 0.5$ is displayed in Figure 4.15 where immunosuppression remains mostly within a balanced range of 40% to 60% efficacy with periodic form.

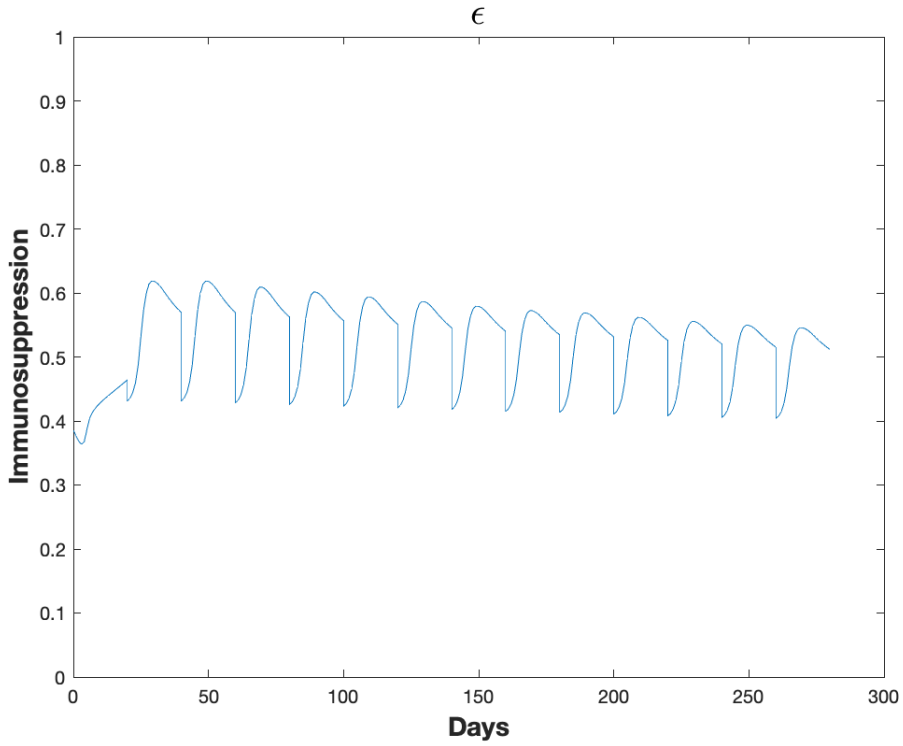

Figure 4.15 EnKF model receding horizon controller for initial guess $\epsilon_0 = 0.5$.

The fixed initial guess of $\epsilon_0 = 0.55$ is used next with the EnKF model and displays a patient experiencing a fairly balanced immunosuppression treatment. In Figure 4.16, the initial suppression of the immune response prevents acute allograft rejection, similar to the results from $\epsilon_0 = 0.5$. The concentration of BKV is also increased for the $\epsilon_0 = 0.55$ case which synergistically pairs with the increase in infected kidney cells (top right), suggesting that BK infection may be more responsible for the reduction in susceptible cells here. Furthermore, the loss of healthy kidney cells occurs more gradually and the change in the slope is decreasing significantly suggesting the allograft could very likely last longer than its counterpart from Figure 4.14 even though they share similar concentrations at 280 days. Additionally, both CD8+ T cell concentrations appear more stable on the daily time scale in Figure 4.16 when compared to the previous results. The changes in model output due to the increase in the initial guess, ϵ_0, appear to follow the trend toward the type of over-suppression seen with the fixed initial guess of 60% suppression particularly with the increasing viral levels which lead to loss of kidney function. In Figure 4.17 the receding horizon control remains in a much narrower range (50% to 55%) when compared to the controller in Figure 4.15 and also lacks the periodicity observed in the previous controller. Like in the EKF cases, the difference in initial guesses produce distinct controllers and in this case vastly different which points to a space of controllers with many local minima thus making the search for the best immunosuppression treatment schemes troublesome.

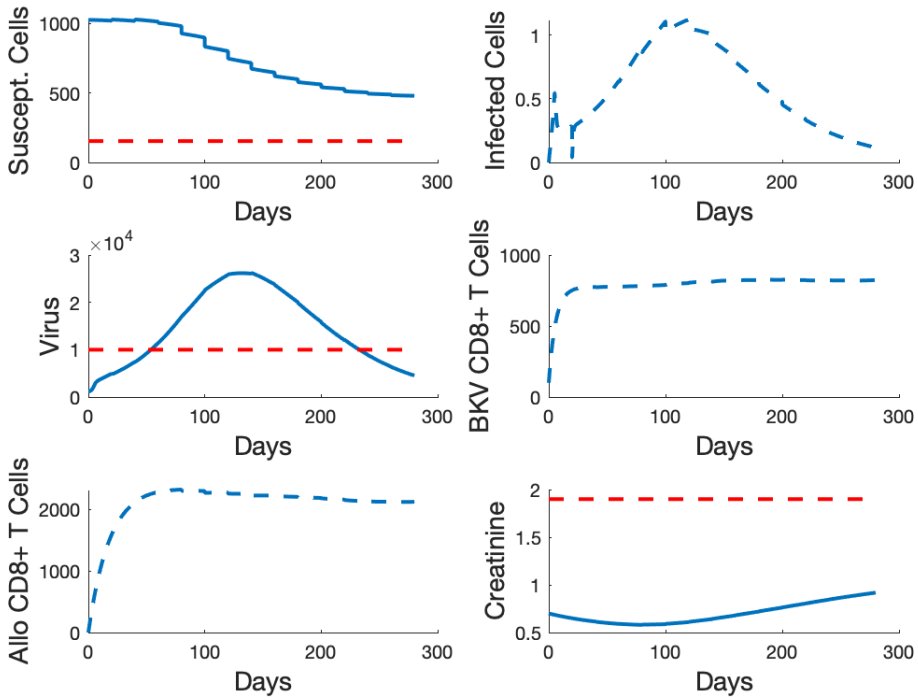

Figure 4.16 Results of the EnKF model with initial guess $\epsilon_0 = 0.55$, i.e. 55% suppression.

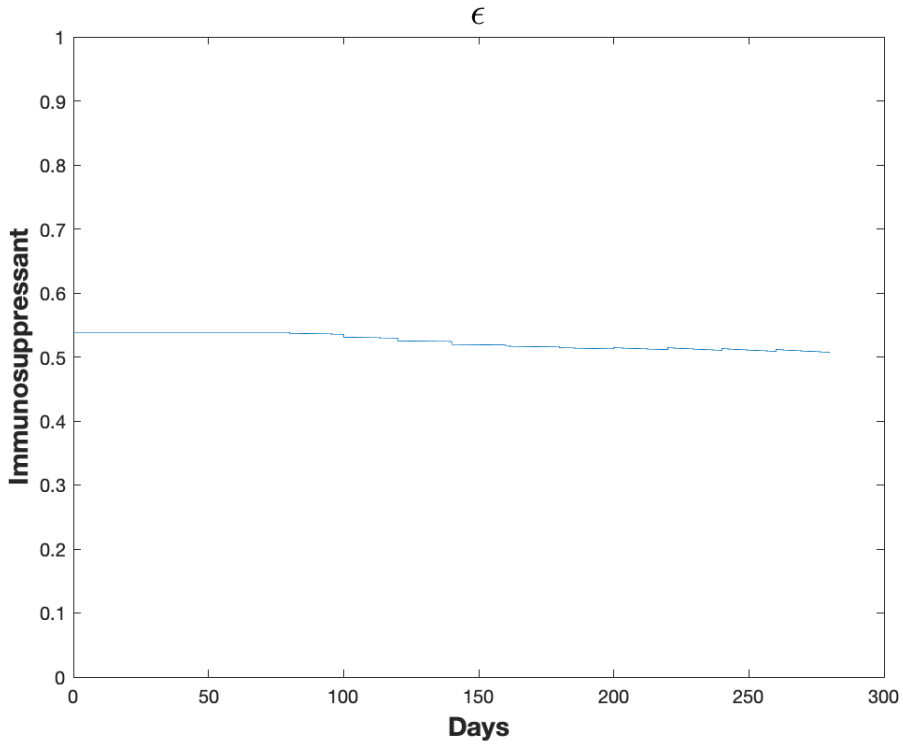

Figure 4.17 Receding horizon controller for the model with the EnKF and initial guess $\epsilon_0 = 0.55$.

4.6 Discussion

The benefit of this research and these results is that our method produced a receding horizon controller that responded to a patient's condition (via data), controls an active BKV infection while preventing/delaying allograph loss, and maintains low concentrations of serum creatinine. With the use of extended Kalman filtering in Figures 4.10 - 4.13, the Kalman gain forces larger adjustments to the state estimates due to the fact that the method linearizes the model while the simulated data is taken directly from the solution of the nonlinear model with the receding horizon control. The substantial infection may be due in part to error accumulating from the linearization used in the EKF which forces large jumps in the viral state estimate. The low concentrations of serum creatinine should be noted since levels remain this way despite the significant loss of healthy functioning kidney cells. These results match the design of the controller (which tries to maintain low creatinine concentration) but growth of this state appears slow to react to changes in the healthy kidney cell state. Model adjustments may be necessary and are addressed in chapter 5. Similar results are observed using ensemble Kalman filtering in Figures 4.14 - 4.17. The state estimates are only adjusted by small amounts likely due to the fact that the distribution of the random state variables is propagated through the nonlinear dynamics by the ensemble. Hence the simulated data (which is

the solution to the nonlinear model using the initial state mean with state-dependent measurement noise added) remains close to the state estimates throughout the 280 days. The drawback to using EnKF for feedback comes from the number of model solves which far exceeds that of the EKF since all the trajectories of the ensemble must be calculated. Also, simulations using the EnKF method were on average 15-18 hours which is not ideal but can still assist physicians in prescribing treatments. The main advantage to the EKF methodology is the access to fairly quick results where simulations were 10 - 20 minutes. The receding horizon controllers can be significantly different as observed in the EnKF results, once again suggesting the space of controller has many local minima.

The results in this work are supported by the literature further strengthening the utility that these models could provide in the future. According to [75] in 2015, acute rejection of allografts in the first year happens in roughly 10% of transplant recipients. This rejection often occurs due to under-suppression of the immune system where donor-specific antibodies, particularly Immunoglobulin G, are allowed to develop post-transplantation [197, 165]. This coincides with the results involving the cost functional from Murad's work in [135] where the receding horizon controller initially did not provide enough suppression of the immune response leading to acute allograft rejection. There is a reasonable connection between the number of B cells of the immune system, which produce antibodies, and the effector cells, e.g., CD8+ T cells, since CD4+ T cells orchestrate rejection using B cells, CD8+ T cells and a variety of others [165, 184]. In our results, the CD8+ T cells for both allo-specific and BKV-specific initially grow towards a steady state and fluctuate around it for the remainder of the 280 days. Weist et al. found that "there were no significant changes in frequencies of BKV-specific CD8+ T cells between the onset of BKV reactivation and during or after the clearance phase" which supports CD8+ T cell concentrations remaining near a steady state once enough cells are present to deal with the specific antigen [188]. They also point out that BKV-specific CD8+ T cells are extremely difficult to detect in patients but as methods improve, we recognize this could be a potential source for additional data in the future.

Much research effort has gone into how BKV affects renal transplant patients given that some view BKV infection as one of the most challenging causes of allograft dysfunction and loss [46]. Multiple studies have shown that the prevalence of BK viremia occurs in approximately 20% percent of patients and agree that a threshold of 10,000 BK viral copies is the criteria many clinics use to begin allograft biopsies for determining if nephropathy is present [54, 46, 35, 96]. In our results, the patients develop nephropathy but have not sustained allograft loss which occurs in approximately 50% of recipients that experience nephropathy [164]. Ultimately, the patients described in our results experience under-suppression as noted by the significant viremia and subsequent nephropathy but remain below the suggested criteria by Elfadawy et al., that nephropathy is certain to occur at approximately 185,000 BK viral copies [65]. Future developments in choosing initial controllers for the model may provide results that resemble a truly balanced suppression scheme and are discussed further in chapter 5.

Although other states in our model agree with conclusions found in other studies, serum creatinine levels are more difficult to validate through literature. The creatinine levels are consistent with the goal of the cost functional to maintain the lowest concentrations possible. Medical standards for healthy creatniine levels in the blood vary between institutions but mostly overlap for healthy men and women with concentration ranges of approximately 0.74 - 1.35 mg per dL in adult men and 0.6 - 1.1 mg per dL in adult women [44, 88]. For individuals with a single functioning kidney such as patients after a kidney transplants but otherwise healthy can see creatinine levels as high as 1.9 mg per dL [58, 89]. For patients with continuing impairment to the allograft, serum creatinine levels can rise above 5.0 mg per dL but it is recommended a physician is consulted if levels exceed 3.0 mg per dL as the likelihood of renal failure becomes greater past this concentration [58, 129]. None of the results from both the EKF and EnKF models where patients follow the recommended treatments approach 3.0 mg per dL despite noticeable loss to susceptible kidney cells. This may be a result of creatinine accumulation in the blood being a slow process. The literature is less clear about how long it would take an individual with kidney damage to approach these levels. In 2002, Hariharan et al. found in patients that saw increases ≥ 0.3 mg per dL of serum creatinine in one year post transplant, a noticeably higher likelihood of kidney loss which got progressively larger as the change in serum creatinine levels increased [89]. In the EnKF model (4.14 and 4.16) and fixed immunosuppression simulations (4.4 and 4.5), there are increasing trends to the serum creatinine levels after loss of kidney function and these levels appear consistent with the findings of Hariharan et al. although higher serum creatinine concentrations may be expected in the EnKF model. At this time, it is unclear if this is due to the ensemble Kalman filter or elsewhere in the model. We acknowledge that the modeling of creatinine in the system of ODE's may need to be re-examined.

4.7 Research Contributions

Given the support of the literature, the model captures the biological dynamics of immunosuppression in renal transplant patients well and also responds to patient data when recommended treatment schemes are followed. A primary benefit of this work is the implementation of the ensemble Kalman filter which preserves the nonlinear dynamics of the system of ODE's. Through the use of the EnKF and the updated cost functional, the model was able to produce results that were better than those of prior research on this problem. In particular, the model provided treatment strategies which showed patients with viremia subsequently having the BKV infection controlled hence slowing the progress of BKV nephropathy so much so that the patient would only have mild to moderate loss of kidney function ($\approx 50\%$) according to the criteria for stage 3 of CKD. This is a promising next step on the journey to fully balanced immunosuppression treatment strategies provided through mathematical modeling. This research has helped pave the way for a collaboration between the Duke Transplant Center, the Duke Center for Human Systems Immunology and the North Carolina State University Center for Research in Scientific Computation which aims to improve

upon the mathematical modeling presented here and acquire a sufficient dataset for their modeling efforts.

CHAPTER

5

CONCLUSION

5.1 Future Work

5.1.1 Directions for Bumblebee Colony Modeling

There are a variety of ways to push forward the modeling of pesticide effects on bumblebees. One of the most important future directions would be assisting field researchers in acquiring an experimental longitudinal dataset. The ideal dataset would likely include frequent measurements quantifying the different classes of bumblebees as well as the larval classes and resource accumulation in a colony from the initiation of the colony until its natural end. This would be a challenging task since many members of the colony remain inside the hive along with all larvae, nectar and pollen. Techniques for data collection observed in Malfi et al. [124] and Kerr et al. [107] indicate that generating an ideal dataset may be possible with minimum colony disturbance. Some novel methods for collecting the data may still need to be developed in order to complete this goal since we are unaware of any such dataset at this time. Ultimately, the collection methods could provide data about both healthy colonies and those exposed to individual and combined pressures including resource limitations, pesticides and habitat loss. Parameter estimation would be possible with this dataset, allowing for more accurate estimates of parameters values which are difficult to determine from the literature alone. The dataset would provide a means for validating the mathematical model under different conditions. Together parameter estimation and model validation could provide more accurate results while also assisting in understanding under studied aspects of bumblebee

colonies such as the switch time.

There are some additions that could be made to our model in future research. The current model is built with a fixed switch time when in reality this feature of the colony is dynamic in the sense that each colony begins producing reproductive members based on internal, external or mixed criteria. The exact triggers that influence a queen to begin producing male and gyne eggs requires further research. Some colonies have short switch times which occur within approximately 2 weeks after colony initiation in contrast to late switching hives where the switch occurs closer to 3 weeks or later [63]. Examining hypotheses about the factors that influence switch times would be interesting research which this model could easily be updated to do. The model could also be modified to be multi-seasonal allowing the gynes to hibernate after the end of the colony and later emerge to begin new colonies. With this functionality, long term examination of the pesticide effects on the progeny of an initial queen would be possible as well as the effects of changing habitats over time. Some studies have focused on the influence of habitat on bumblebee colonies through criteria such as floral abundance [191, 157]. In order to model habitat usage, more mechanics would need to be added to the model in place of the current basic expressions for the foraging of resources. The inclusion of new foraging dynamics would also allow for the examination of additional pesticide effects. In [131], it was shown that imidacloprid reduces the ability of foraging bumblebees to find their way back to the colony when the resources were ≥ 3 meters from the hive. This example could be modeled with the suggestions above. The last suggested addition to the model relates to the method used for modeling the larval classes. Workers and males both have two age classes of larvae while gynes have three age classes and these classes are necessary for the increased consumption of resources with age. In [158], Ribeiro showed a detailed analysis of the growth of bumblebee larvae which influenced the consumption parameters in our model. In that study, the data displays relationships between larval mass, pollen consumption, age and the percentage of body mass which is pollen. Treating the larval states as partial differential equations (PDE) could allow for larvae to be modeled more dynamically. There appears to be a correlation with mass and development of larvae suggesting that periods of resource insecurity could affect development time of larvae. Since development times in the DDE are fixed, the PDE representation may allow for slower larval development when resources are scarce thus lengthening the time to pupation for particular broods. A PDE could also improve how consumption is calculated to provide a more realistic estimate of resources dynamics. Since larvae are the only subadults that are exposed to the workers and resources, shifting from a DDE to PDE for larval dynamics might allow the exploration of direct sub-lethal effects of pesticides on larvae.

5.1.2 Directions for Renal Transplant Immunosuppression Modeling

Similar to section 5.1.1, an ideal dataset for this project was unavailable for parameter estimation or validation. Efforts to assist researchers in determining an ideal dataset for this model and obtaining

that ideal dataset would be incredibly beneficial. In our model, a dataset consisting of periodic measurements of BKV and creatitine concentrations in the blood is expected. For this work, a fixed 20 day period between routine office visits was assumed and further analysis of the model may reveal that an ideal set of data may require shorter or longer delays between physician visits as well as having a variable duration between each visit. With that ideal dataset, a personalized medicine approach could be taken where the dataset is used to parameterize aspects of the model specifically to the patient. Furthermore, future research may reveal methods to gather data for other states of interest. For instance, the most accurate method for determining the onset of nephropathy is performing a biopsy of the allograft to assess the severity of loss of function [35]. Ways to extrapolate concentrations of healthy cells or percentage of kidney function from biopsies could provide additional data about the currently unobserved states for susceptible and infected kidney cell concentrations. Additionally, as research reveals more understanding into the immune response for renal transplant recipients, methods for detecting specific B cells and T cells of the immune response may provide a way to include data for the immune response.

Besides obtaining a robust dataset, improving the base system of ordinary differential equations for the model could prove useful. In chapter 4, the slow reaction of creatinine levels due to loss of kidney function is noted. It is reasonable to consider that creatinine levels may increase quicker due to loss of kidney function than the model indicates despite the evidence that creatinine levels are slow to reduce with a healthy allograft [89]. There could be differences in the rate of accumulation and reduction of creatinine in the blood. If that is the case, improvements to the mechanisms that account for changes in creatinine concentration could assist in producing more successful receding horizon controllers. In addition to creatinine, reexamining the states associated with the immune system could be beneficial. The body of research surrounding a patient's immune response to allografts and BKV has been growing. Current research is examining how antibody levels and types influence acute rejection following the transplant procedure [165, 197]. In some cases, the host may produce antibodies that are less cytotoxic which in turn prevents the production of antibodies more likely to cause significant damage to the allograft. Acute rejection is less likely in these cases. Antibodies, such as Immunoglobulin G may need to be included in future versions of the model given their role in acute rejection [197]. Researchers are also exploring antibody related therapies to assist in preventing acute rejection which indicates this state may be beneficial in determining the receding horizon controller [122, 42, 93, 155]. The host's immune response to BK virus is another aspect of the model which could be explored for possible improvements as researches try to understand the relationship between CD4+ T cells and BKV infection [188]. Literature suggests that CD4+ T cells might be as equally important as CD8+ T cells in controlling BKV clearance [3, 39, 67]. This may result in changes to how allo-specific CD8+ T cells are modeled and/or the addition of an allo-specific CD4+ T cell state variable. We also recognize there may be interest in examining multiple viruses or other viruses related to the immunosuppression of transplant patients. There are a variety of other pathogens that affect immunosuppressed individuals including but not limited to cytomegalovirus, Epstein-Barr virus, and hepatitis viruses [185, 116]. Lastly, much research surrounds regenerative

therapies for CKD patients primarily using stem cells [98, 177, 196]. Therapies derived from this research may change the important assumption that new kidney cells are not produced in any manner that affects CKD patients. These therapies would provide another useful treatment that the model could account for when determining the best treatments for individual patients.

Immunosuppression in the model can also be changed in a few specific ways. To understand immunosuppression treatments designed for renal transplant patients, there are three distinct treatment types: induction treatment, maintenance treatment and rejection treatment [151, 103]. The induction treatments are selected to help heavily suppress the host's immune system to prevent acute rejection in the few weeks after the transplantation. Current induction regimens typically include either rATG or interleukin-2 receptor antagonists[69]. Maintenance therapies are more varied than induction while serving the purpose of maintaining a healthy, immunosuppressed host and preventing chronic allograft nephropathy beyond induction therapy. Maintenance therapy includes a cocktail of drugs which include calcineurin inhibitors such as tacrolimus, corticosteroids, and antiproliferative agents like mycophenolic acid [103, 151, 82, 69]. Adverse side effects from these regimens include overuse of corticosteroids for some patients and drug-toxicity from calcineurin inhibitors. Currently, researchers are trying to determine new and effective treatments for those patients likely to exhibit those negative effects. Rejection treatments are being explored particularly to overcome antibody-mediated rejection which prevents the long-term survival of the allograft in some hosts [151, 103]. These drugs can be taken alongside maintenance treatments to prevent certain long term effects of the host rejecting the kidney. In some cases, they are administered when reduction of maintenance drugs is necessary to prevent drug toxicity.

With the variety of drugs used in immunosuppression treatments, modeling immunosuppression could become more detailed in an updated model. The drug efficacy expression could be revisited in terms of specific drugs or drug categories. This change could explore how treatments may affect allo-specific immune responses differently than the BKV-specific immune responses. An even more challenging change to immunosuppression in the model would be implementing particular drug types directly into the model. This would fundamentally change the nature of the controller in this model but could open the possibility of determining specific doses for standard drug combinations. Realistic next steps for the continuation of this research with our model would be to examine the initial guess for the optimal controller. In this work, fixed initial guesses were chosen for simplicity, but alternative forms of the initial guess might produce better results. As noted previously, induction and maintenance combinations produce a highly suppressed state immediately post transplantation then maintenance therapy sustains a more moderate suppression. Another treatment strategy involves decreasing drugs dosages when significant BK viremia is detected to allow the patient's immune system the opportunity to fight against the virus. These approaches can be used to influence the form of the initial guess and subsequently the receding horizon controller and may yield more balanced results. Altogether the suggestions in this section are possibilities in which this mathematical model could become even more helpful in determining better immunosuppression

treatments.

5.2 Conclusion

In this work, we set out to progress the research in both ecology and medicine by using mathematical modeling methodologies. By using well established mathematical frameworks, we show advancements in both fields. In the case of lethal and sub-lethal effects of pesticides on bumblebee colonies, an individual specific delay differential equation model showed that literature supported results can be obtained. The necessity for including larval dynamics when researching pesticide effects is established. The results displayed the negative impacts that sub-lethal effects theoretically have on bumblebee colonies indicating their importance for future discussions in determining safe levels of pesticides for use in the environment.

For patients suffering from chronic kidney disease and obtaining a kidney transplant, we were able to advance prior research efforts by the Center for Research in Scientific Computation at North Carolina State University. A differential equation model is used that characterizes the interactions between the allograft, BK virus and the patient's immune system. Changes to the cost functional of the control problem and implementation of a new filtering mechanism for feedback show promise for producing reliable treatment schemes. With several avenues for future directions with this project, this framework has the potential to provide a personalized medicine approach to the challenge of determining balanced immunosuppression treatments for renal transplant patients. Through our work, these research projects demonstrate positive steps forward in both fields using mathematical modeling.

BIBLIOGRAPHY

[1] B.M. Adams, H.T. Banks, M. Davidian, H.D. Kwon, H.T. Tran, S.N. Wynne & E.S. Rosenberg. "HIV dynamics: Modeling, data analysis, and optimal treatment protocols". In: *Journal of Computational and Applied Mathematics* **184**.1 (2005), pp. 10–49.

[2] B.M. Adams, H.T. Banks, M. Davidian & E.S. Rosenberg. "Estimation and prediction with HIV treatment interruption data". In: *Bulletin of Mathematical Biology* **69**.2 (2007), pp. 563–584.

[3] G.R. Ambalathingal, R.S. Francis, M.J. Smyth, C. Smith & R. Khanna. "BK polyomavirus: clinical aspects, immune regulation, and emerging therapies". In: *Clinical microbiology reviews* **30**.2 (2017), pp. 503–528.

[4] A. Arnold & H. Tran. "Ensemble Kalman Filtering for Inverse Optimal Control". In: *Center for Research in Scientific Computation Technical Report, CRSC-TR17-27* (2017).

[5] D.A. Axelrod, A.S. Naik, M.A. Schnitzler, D.L. Segev, V.R. Dharnidharka, D.C. Brennan, S. Bae, J. Chen, A. Massie & K.L. Lentine. "National variation in use of immunosuppression for kidney transplantation: a call for evidence-based regimen selection". In: *American Journal of Transplantation* **16**.8 (2016), pp. 2453–2462.

[6] N. Babel, H.D. Volk & P. Reinke. "BK polyomavirus infection and nephropathy: The virus-immune system interplay". In: *Nature Reveiws Nephrology* **7**.7 (2011), p. 399.

[7] B. Baer & P. Schmid-Hempel. "Sperm influences female hibernation success, survival and fitness in the bumble-bee *Bombus* terrestris". In: *Proceedings of the Royal Society of London B: Biological Sciences* **272**.1560 (2005), pp. 319–323.

[8] J.B. Bang, J. Bae & C.-K. Oh. "Mathematical model for early functional recovery pattern of kidney transplant recipients using serum creatinine". In: *Korean Journal of Transplantation* **34**.3 (2020), pp. 167–177.

[9] H.T. Banks. "Delay systems in biological models: approximation techniques". In: *Nonlinear Systems and Applications* : 21–38 (1977).

[10] H.T. Banks. "Approximation of nonlinear functional differential equation control systems". In: *Journal of Optimization Theory and Applications* **29**.3 (1979), pp. 383–408.

[11] H.T. Banks. "Identification of nonlinear delay systems using spline methods". In: *Nonlinear Phenomena in Mathematical Sciences* : 47–55 (1980).

[12] H.T. Banks. *A Functional Analysis Framework for Modeling, Estimation and Control in Science and Engineering*. ISBN 978-1-4398-8084-5. Boca Raton, FL: CRC Press., 2012.

[13] H.T. Banks, J.E. Banks, R. Bommarco, A.N. Laubmeier, N.J. Myers, M. Rundlöf & K. Tillman. "Analysis of nonlinear delay systems with applications in bumblebee population models". In: *Communications in Applied Analysis* **21**.3 (2017), pp. 449–476.

[14] H.T. Banks, J.E. Banks, R. Bommarco, A.N. Laubmeier, N.J. Myers, M. Rundlöf & K. Tillman. "Modelling bumble bee population dynamics with delay differential equations." In: *Ecological Modelling* **351** (2017), pp. 14–23.

[15] H.T. Banks, J.E. Banks, R. Bommarco, M. Rundlöf & K. Tillman. "Modeling bumblebee population dynamics with delay differential equations". CRSC-TR16-06, N.C. State University, Raleigh, NC, June 2016.

[16] H.T. Banks & J.A. Burns. "Hereditary control problems: numerical methods based on averaging approximations". In: *SIAM Journal on Control and Optimization* **16**.2 (1978), pp. 169–208.

[17] H.T. Banks, S. Hu, T. Jang & H.-D. Kwon. "Modelling and optimal control of immune response of renal transplant recipients". In: *Journal of Biological Dynamics* **6**.2 (2012), pp. 539–567.

[18] H.T. Banks, S. Hu, K. Link, E.S. Rosenberg, S. Mitsuma & L. Rosario. "Modeling Immune Response to BK Virus Infection and Donor Kidney in Renal Transplant Recipients". In: *Inverse Problems in Science and Engineering* **24**.1 (2016), pp. 127–152.

[19] H.T. Banks, S. Hu & W.C. Thompson. *Modeling and inverse problems in the presence of uncertainty*. CRC Press, 2014.

[20] H.T. Banks & F. Kappel. "Spline approximations for functional differential equations". In: *Journal of Differential Equations* **34**.3 (1979), pp. 496–522.

[21] H.T. Banks & H.T. Tran. *Mathematical and experimental modeling of physical and biological processes*. CRC Press, 2009.

[22] J.E. Banks, H.T. Banks, N. Myers, A. N. Laubmeier & R. Bommarco. "Lethal and sublethal effects of toxicants on bumblebee populations: a modeling approach." In: *Ecotoxicology* ().

[23] J.E. Banks & J.D. Stark. "What is ecotoxicology? An ad-hoc grab bag or an interdisciplinary science?" In: *Integrative Biology* **5** (1998), pp. 1–9.

[24] J.E. Banks, J.D. Stark, R.I. Vargas & A.S. Ackleh. "Deconstructing the surrogate species concept: a life history approach to the protection of ecosystem services." In: *Ecological Applications* **24** (2014), pp. 770–778.

[25] J.E. Banks, J.D. Stark, R.I Vargas & Ackleh A.S. "Parasitoids and ecological risk assessment: Can toxicity data developed for one species be used to protect an entire guild?" In: *Biological Control* **59** (2011), pp. 336–339.

[26] W.F. Barbosa, L. De Meyer, R.N.C. Guedes & G. Smagghe. "Lethal and sublethal effects of azadirachtin on the bumblebee *B*ombus terrestris (Hymenoptera: Apidae)." In: *Ecotoxicology* **24** (2015), pp. 130–142.

[27] I. Bartomeus, J.S. Ascher, J. Gibbs, B.N. Danforth, D.L. Wagner, S.M. Hedtke & R. Winfree. "Historical changes in northeastern US bee pollinators related to shared ecological traits". In: *Proceedings of the National Academy of Sciences* **110**.12 (2013), pp. 4656–4660.

[28] M.A. Becher, V. Grimm, P. Thorbeck, P.J. Horn J.and Kennedy & J.L. Osbourne. “BEEHAVE: a systems model of honeybee colony dynamics and foraging to explore multifactorial causes of colony failure.” In: *Journal of Applied Ecology* **51**.2 (2014), pp. 470–482.

[29] M.A. Becher, G. Twiston-Davies, T.D. Penny, D. Goulson, E.L. Rotheray & J.L. Osborne. “Bumble- BEEHAVE: A systems model for exploring multifactorial causes of bumblebee decline at individual, colony, population and community level.” In: *Journal of Applied Ecology* **55** (2018), pp. 2790–2801.

[30] M. Beekman, R. Lingeman, F.M. Kleijne & M.W. Sabelis. “Optimal timing of the production of sexuals in bumblebee colonies”. In: *Entomologia Experimentalis et Applicata* **88**.2 (1998), pp. 147–154.

[31] M. Beekman, P. Stratum & R. Lingeman. “Diapause survival and post-diapause performance in bumblebee queens (*Bombus* terrestris)”. In: *Entomologia Experimentalis et Applicata* **89**.3 (1998), pp. 207–214.

[32] T. Benton. *Bumblebees: the natural history & identification of the species found in Britain*. Harper Collins, 2006.

[33] J.C. Biesmeijer et al. “Parallel declines in pollinators and insect-pollinated plants in Britain and the Netherlands”. In: *Science* **313**.5785 (2006), pp. 351–354.

[34] A. Biondi & Zappalá. “Do biopesticides affect the demographic traits of a parasitoid wasp and its biocontrol services through sublethal effects?” In: *PLoS ONE* **8**.9 (2013), e76548.

[35] D.L. Bohl & D.C. Brennan. “BK virus nephropathy and kidney transplantation”. In: *CJASN* **2**.Supplement 1) (2007), S36–S46.

[36] R. Bommarco, O. Lundin, H.G. Smith & M. Rundlöf. “Drastic historic shifts in bumble-bee community composition in Sweden”. In: *Proceedings of the Royal Society B* **279**.1727 (2012), pp. 309–315.

[37] J.S. Borrell. “Rapid assessment protocol for pollen settling velocity: implications for habitat fragmentation”. In: *Bioscience Horizons* **5** (2012), hzs002.

[38] C. Brittain & S.G. Potts. “The potential impacts of insecticides on the life-history traits of bees and the consequences for pollination.” In: *Basic and Applied Ecology* **12** (2011), pp. 321–331.

[39] J. Bruminhent, S. Srisala, C. Klinmalai, S. Pinsai, S.P. Watcharananan, S. Kantachuvesiri, S. Hongeng & N. Apiwattanakul. “BK Polyomavirus-specific T cell immune responses in kidney transplant recipients diagnosed with BK Polyomavirus-associated nephropathy”. In: *BMC Infectious Diseases* **19**.1 (2019), pp. 1–8.

[40] J. Bryden, R.J. Gill, R.A.A. Mitton, N.E. Raine & V.A.A. Jansen. “Chronic sublethal stress causes bee colony failure”. In: *Ecology Letters* **16**.12 (2013), pp. 1463–1469.

[41] C. Carvell, A.F.G. Bourke, J.L. Osborne & M.S. Heard. “Effects of an agri-environment scheme on bumblebee reproduction at local and landscape scales”. In: *Basic and Applied Ecology* **16**.6 (2015), pp. 519–530.

[42] J. Choi et al. “Assessment of Tocilizumab (Anti–Interleukin-6 Receptor Monoclonal) as a Potential Treatment for Chronic Antibody-Mediated Rejection and Transplant Glomerulopathy in HLA-Sensitized Renal Allograft Recipients”. In: *American Journal of Transplantation* **17**.9 (2017), pp. 2381–2389.

[43] Mayo Clinic. *Chronic Kidney Disease*. https://www.mayoclinic.org/diseases-conditions/chronic-kidney-disease/symptoms-causes/syc-20354521. Accessed: 2021-07-15.

[44] Mayo Clinic. *Creatinine tests*. https://www.mayoclinic.org/tests-procedures/creatinine-test/about/pac-20384646. Accessed: 2021-07-20.

[45] Department of Surgery Columbia University Irving Medical Center. *Follow-Up visits after kidney transplant surgery*. https://columbiasurgery.org/kidney-transplant/follow-visits-after-kidney-transplant-surgery. Accessed: 2021-07-21.

[46] P. Comoli, H.H. Hirsch & F. Ginevri. “Cellular immune responses to BK virus”. In: *Current Opinion in Organ Transplantation* **13**.6 (2008), pp. 569–574.

[47] C. Cosentino & D. Bates. *Feedback control in systems biology*. CRC Press, 2019.

[48] J.D. Crall, N. Gravish, A.M. Mountcastle & S.A. Combes. “BEEtag: A low cost, image-based tracking system for the study of animal behavior and locomotion.” In: *PLoS ONE* **10** (2015). doi:10.1371/journal.pone.0136487pmid:2633221, e0136487.

[49] J.D. Crall et al. “Neonicotinoid exposure disrupts bumblebee nest behavior, social networks, and thermoregulation.” In: *Science* **362**.6415 (2018), pp. 683–686.

[50] J.E. Cresswell. “A demographic approach to evaluating the impact of stressors on bumble bee colonies.” In: *Ecological Entomology* **42** (2017), pp. 221–29.

[51] E.E. Crone & N.M. Williams. “Bumble bee colony dynamics: quantifying the importance of land use and floral resources for colony growth and queen production”. In: *Ecology Letters* **19**.4 (2016), pp. 460–468.

[52] D.T. Crouse, L.B. Crowder & H. Caswell. “A stage-based population model for loggerhead sea turtles and implications for conservation”. In: *Ecology* **68**.5 (1987), pp. 1412–1423.

[53] J.M. Cushing. *Integrodifferential equations and delay models in population dynamics, Vol. 20*. Springer Science & Business Media, 2013.

[54] A. Dall & S. Hariharan. “BK virus nephritis after renal transplantation”. In: *CJASN* **3**.(Supplement 2) (2008), S68–S75.

[55] J. David, H. Tran & H.T. Banks. “HIV model analysis and estimation implementation under optimal control based treatment strategies”. In: *International Journal of Pure and Applied Mathematics* **57**.3 (2009), pp. 357–392.

[56] J. David, H.T. Tran & H.T. Banks. “HIV model analysis under optimal control based treatment strategies”. In: *International Journal of Pure and Applied Mathematics* **57** (2009), pp. 357–392.

[57] J. David, H.T. Tran & H.T. Banks. “Receding horizon control of HIV”. In: *Optimal Control Applications and Methods* **32**.6 (2011), pp. 681–699.

[58] C. Davis. *Creatinine (Low, High, Blood Test Results Explained).* https://www.medicinenet.com/creatinine_blood_test/article.htm: Accessed: 2021-07-09.

[59] N. Desneux, A. Decourtye & J.M. Delpuech. “The sublethal effects of pesticides on beneficial arthropods.” In: *Annual Review of Entomology* **52** (2007), pp. 81–106.

[60] National Institute of Diabetes, Digestive & Kidney Diseases. *Your Kidneys & How They Work*. https://www.niddk.nih.gov/health-information/kidney-disease/kidneys-how-they-work. Accessed: 2021-07-20.

[61] Centers for Disease Control & Prevention. *Chronic Kidney Disease in the United States, 2021*. US Department of Health, Human Services, Centers for Disease Control, and Prevention https://www.cdc.gov/kidneydisease/publications-resources/ckd-national-facts.html. Accessed: 2021-07-20, 2021.

[62] M.J. Duchateau. “Agonistic behaviours in colonies of the bumblebee *Bombus* terrestris”. In: *Journal of Ethology* **7**.2 (1989), pp. 141–151.

[63] M.J. Duchateau & H.H.W. Velthuis. “Development and reproductive strategies in *Bombus* terrestris colonies”. In: *Behaviour* **107**.3 (1988), pp. 186–207.

[64] M.J. Duchateau, H.H.W. Velthuis & J.J. Boomsma. “Sex ratio variation in the bumblebee *Bombus* terrestris”. In: *Behavioral Ecology* **15**.1 (2004), pp. 71–82.

[65] N. Elfadawy, S. M. Flechner, X. Liu & J. Schold. “The impact of surveillance and rapid reduction in immunosuppression to control BK virus-related graft injury in kidney transplantation”. In: *Transplant International* (2013).

[66] G. Evernsen. *Data Assimilation: The Ensemble Kalman Filter*. Springer, 2009.

[67] Y. Fan, H. Bai, Y. Qian, Z. Sun & B. Shi. “CD4+ T Cell Immune Response to VP1 and VP3 in BK Virus Infected Recipients of Renal Transplantation”. In: *Surgical Infections* **20**.3 (2019), pp. 236–243.

[68] H. Feltham, K. Park & D. Goulson. “Field realistic doses of pesticide imidacloprid reduce bumblebee pollen foraging efficiency”. In: *Ecotoxicology* **23**.3 (2014), pp. 317–323.

[69] V. Filiopoulos & J.N. Boletis. “Renal transplantation with expanded criteria donors: Which is the optimal immunosuppression?” In: *World Journal of Transplantation* **6**.1 (2016), p. 103.

[70] J.C. Fink, R.A. Burdick, S.J. Kurth, S.A. Blahut, N.C. Armistead, M.S. Turner, L.M. Shickle & P.D. Light. “Significance of serum creatinine values in new end-stage renal disease patients”. In: *American Journal of Kidney Diseases* **34**.4 (1999), pp. 694–701.

[71] C. Fontaine, I. Dajoz, J. Meriguet & M. Loreau. “Functional diversity of plant–pollinator interaction webs enhances the persistence of plant communities”. In: *PLoS Biol* **4**.1 (2005), e1.

[72] V.E. Forbes et al. “Adding value to ecological risk assessment with population modelling.” In: *Human and Ecological Risk Assessment* **17** (2011), pp. 287–299.

[73] National Kidney Foundation. *About Chronic Kidney Disease.* https://www.kidney.org/atoz/content/about-chronic-kidney-disease. Accessed: 2021-07-11.

[74] National Kidney Foundation. *How to Classify CKD*. https://www.kidney.org/professionals/explore-your-knowledge/how-to-classify-ckd. Accessed: 2021-07-11.

[75] National Kidney Foundation. *New options in maintenance immunosuppression: a clinical update on managing kidney transplant recipients*. https://www.kidney.org/sites/default/files/02-10-7138.pdf. Accessed: 2021-07-21.

[76] G.A. Funk, R. Gosert, P. Comoli, F. Ginervri & H.H. Hirsch. “Polyomavirus BK replication dynamics in vivo and in silico to predict cytopathology and viral clearance in kidney transplants”. In: *American Journal of Transplantation* **8**.11 (2008), pp. 2368–2377.

[77] L.A. Garibaldi, I. Steffan-Dewenter, R. Winfree, M.A. Aizen, R. Bommarco, S.A. Cunningham, C. Kremen, L.G. Carvalheiro, L.D. Harder, O. Afik, et al. “Wild pollinators enhance fruit set of crops regardless of honey bee abundance”. In: *Science* **339**.6127 (2013), pp. 1608–1611.

[78] A. Génissel, P. Aupinel, C. Bressac, J.N. Tasei & C. Chevrier. “Influence of pollen origin on performance of B. terrestris micro-colonies.” In: *Entomologia Experimentalis et Applicata* **104** (2002), pp. 329–336.

[79] R.J. Gill, O. Ramos-Rodriguez & N.E. Raine. “Combined pesticide exposure severely affects individual- and colony-level traits in bees”. In: *Nature* **491**.7422 (2012), pp. 105–108.

[80] R.J. Gill, O. Ramos-Rodriguez & N.E. Raine. “Combined pesticide exposure severely affects individual-and colony-level traits in bees: Supplementary Material”. In: *Nature* **491** (2012).

[81] H.C.J. Godfray, T. Blacquiere, L.M. Field, R.S. Hails, S.G. Potts, N.E. Raine, A.J. Vanbergen & A.R. McLean. “A restatement of recent advances in the natural science evidence base concerning neonicotinoid insecticides and insect pollinators”. In: *Proceeding of the Royal Society B* **282**.1818 (2015), p. 20151821.

[82] A.S. Goldfarb-Rumyantzev, L.Smith, F.S. Shihab, B.C. Baird, A.N. Habib, S.-J. Lin & L.L. Barenbaum. “Role of maintenance immunosuppressive regimen in kidney transplant outcome”. In: *CJASN* **1**.3 (2006), pp. 563–574.

[83] K. Gopalsamy. *Stability and oscillations in delay differential equations of population dynamics. Vol. 74*. Springer Science & Business Media, 2013.

[84] D. Goulson. *Bumblebees: behaviour, ecology, and conservation*. Oxford University Press on Demand, 2010.

[85] D. Goulson. “Review: An overview of the environmental risks posed by neonicotinoid insecticides”. In: *Journal of Applied Ecology* **50**.4 (2013), pp. 977–987.

[86] D. Goulson, E. Nicholls, C. Botías & E.L. Rotheray. “Bee declines driven by combined stress from parasites, pesticides, and lack of flowers.” In: *Science* **347**.6229 (2015), p. 1255957.

[87] D. Goulson, J. Peat, J.C. Stout, J. Tucker, B. Darvill, L.C. Derwent & W.O.H. Hughes. “Can allotheism in workers of the bumblebee, *Bombus* terrestris, be explained in terms of foraging efficiency?” In: *Animal Behavior* **64** (2002), pp. 123–130.

[88] C. Haldeman-Englert, L. Cunningham & Jr. R. Turley. *Creatinine (Blood)*. University of Rochester Medical Center. https://www.urmc.rochester.edu/encyclopedia/content.aspx?ContentTypeID=167&ContentID=creatinine_serum. Accessed: 2021-07-20.

[89] S. Hariharan, M.A. Mcbride, W.S. Cherikh, C.B. Tolleris, B.A. Bresnahan & C.P. Johnson. “Post-transplant renal function in the first year predicts long-term kidney transplant survival”. In: *Kidney International* **62**.1 (2002), pp. 311–318.

[90] F. Hartung, T. Krisztin, H. Walther & J. Wu. “Chapter 5 Functional Differential Equations with State-Dependent Delays: Theory and Applications”. In: vol. 3. Handbook of Differential Equations: Ordinary Differential Equations. North-Holland, 2006, pp. 435–545.

[91] J. Häussler, U. Sahlin, C. Baey, H.G. Smith & Y. Clough. “Pollinator population size and pollination ecosystem service responses to enhancing floral and nesting resources”. In: *Ecology and Evolution* **7** (1017), pp. 1898–1908.

[92] Indiana University Health. *BK Virus QN PCR BKQN*. https://www.testmenu.com/iuhealthlab/Tests/1007659. Accessed: 2021-07-21.

[93] R. Hellemans, J.L. Bosmans & D. Abramowicz. “Induction Therapy for Kidney Transplant Recipients: Do We Still Need Anti-IL2 Receptor Monoclonal Antibodies?” In: *American Journal of Transplantation* **17**.1 (2017), pp. 22–27.

[94] J.T. Herbeck, J.E. Mittler, G.S. Gottlieb & J.I. Mullins. “An HIV epidemic model based on viral load dynamics: value in assessing empirical trends in HIV virulence and community viral load”. In: *PloS Computational Biology* **10** (2014), e1003673.

[95] E. Herrero-Martinez, C.A. Sabin, J.G. Evans, A. Griffioen, C.A. Lee & V.C. Emery. “The prognostic value of a single hepatitis C virus RNA load measurement taken early after human immunodeficiency virus seroconversion”. In: *Journal of Infectious Diseases* **186** (2002), pp. 470–476.

[96] H.H. Hirsch. “Polyomavirus BK nephropathy: a (re-) emerging complication in renal transplantation”. In: *American Journal of Transplantation* **2**.1 (2002), pp. 25–30.

[97] J.G. Holland, F.S. Guidat & A.F.G. Bourke. “Queen control of a key life-history event in a eusocial insect”. In: *Biology Letters* **9**.3 (2013), p. 20130056.

[98] C. Hopkins, J. Li & M.H. Little. “Stem cell options for kidney disease”. In: *Journal of Pathology* **217**.2 (2009), pp. 265–281.

[99] C. Hopkins, J. Li, F. Rae & M.H. Little. “Stem cell options for kidney disease”. In: *The Journal of Pathology: A Journal of the Pathological Society of Great Britain and Ireland* **217**.2 (2009), pp. 265–281.

[100] G.E. Hutchinson. “Circular causal systems in ecology”. In: *Annals of the New York Academy of Sciences* **50**.4 (1948), pp. 221–246.

[101] The MathWorks Inc. “MathWorks announces release 2018a of the MATLAB and simulink product families”. In: ().

[102] A. Kadala, M. Charreton & P. Charnet. “Voltage-gated sodium channels from the bees *A*pis mellifera and *B*ombus terrestris are differentially modulated by pyrethroid insecticides.” In: *Scientific Reports* **9**.1078 (2019). doi:10.1038/s41598-018-37278-z.

[103] H.V. Kalluri & K.L. Hardinger. “Current state of renal transplant immunosuppression: present and future”. In: *World Journal of Transplantation* **2**.4 (2012), pp. 51–68.

[104] F. Kappel. “Spline approximation for autonomous nonlinear functional differential equations”. In: *Nonlinear Analysis: Theory, Methods & Applications* **10**.5 (1986), pp. 503–513.

[105] F. Kappel & W. Schappacher. “Autonomous nonlinear functional differential equations and averaging approximations”. In: *Nonlinear Analysis: Theory, Methods & Applications* **2**.4 (1978), pp. 391–422.

[106] M. Katzfuss, J.R. Stroud & C.K. Wikle. “Understanding the ensemble kalman filter”. In: *The American Statistician* **70**.4 (2016), pp. 350–357.

[107] N.Z. Kerr, R.L. Malfi, N.M. Wiliams & E.E. Crone. “Larger workers outperform smaller workers across resource environments: an evaluation of demographic data using functional linear models”. In: *Ecology and Evolution* **11**.6 (2021), pp. 2814–2827.

[108] D.S. Khoury, A.B. Barron & M.R. Myerscough. “Modelling food and population dynamics in honey bee colonies”. In: *PloS one* **8**.5 (2013), e59084.

[109] D. Kleijn, R. Winfree, I. Bartomeus, L.G. Carvalheiro, M. Henry, R. Isaacs, A. Klein, C. Kremen, L.K. M’gonigle, R. Rader, et al. “Delivery of crop pollination services is an insufficient argument for wild pollinator conservation”. In: *Nature Communications 6* (2015).

[110] A. Klein, B.E. Vaissiere, J.H. Cane, I. Steffan-Dewenter, S.A. Cunningham, C. Kremen & T. Tscharntke. “Importance of pollinators in changing landscapes for world crops”. In: *Proceedings of the Royal Society of London B: Biological Sciences* **274**.1608 (2007), pp. 303–313.

[111] S. Klein, A. Cabirol, J.M. Devaud, A.B. Barron & M. Lihoreau. “Why bees are so vulnerable to environmental stressors.” In: *Trends in Ecology & Evolution* **32**.4 (2017), pp. 268–278.

[112] M. Kot. *Elements of mathematical ecology*. Cambridge University Press, 2001.

[113] P. Labert, D. Collett, A. Kimber & R. Johnson. “Parametric accelerated failure time models with random effects and an application to kidney transplant survival”. In: *Statistics in Medicine* **23**.20 (2004), pp. 3177–3192.

[114] Mayo Clinic Laboratories. *BK Virus, Molecular Detection, Quantitative, PCR, Plasma*. https://www.mayocliniclabs.com/test-catalog/Clinical+and+Interpretive/83187. Accessed: 2021-07-21.

[115] J. Lämsä, E. Kuusela, J. Tuomi, S. Juntunen & P.C. Watts. “Low dose of neonicotinoid insecticide reduces foraging motivation of bumblebees.” In: *Procedings of the Royal Society B* **285**.1883 (2018).

[116] J. Le, C.M. Durand, I. Agha & D.C. Brennan. “Epstein–Barr virus and renal transplantation”. In: *Transplantation Reviews* **31**.1 (2017), pp. 55–60.

[117] F.L. Lewis. *Optimal Estimation: With an introduction to stochastic control theory*. John Wiley & Sons, 1986.

[118] F.L. Lewis, D.L. Vrabie & V.L. Syrmos. *Optimal Control*. Hoboken, New Jersey: John Wiley & Sons, 2012.

[119] C. Lopez-Vaamonde, N.E. Raine, J.W. Koning, R.M. Brown, J.J.M. Pereboom, T.C. Ings, O. Ramos-Rodriguez, W.C. Jordan & A.F.G. Bourke. “Lifetime reproductive success and longevity of queens in an annual social insect”. In: *Journal of Evolutionary Biology* **22**.5 (2009), pp. 983–996.

[120] O. Lundin, M. Rundlöf, H.G. Smith, I. Fries & R. Bommarco. “Neonicotinoid insecticides and their impacts on bees: a systematic review of research approaches and identification of knowledge gaps”. In: *PloS One* **10**.8 (2015), e0136928.

[121] S. Macevicz & G. Oster. “Modeling social insect populations II: optimal reproductive strategies in annual eusocial insect colonies”. In: *Behavioral Ecology and Sociobiology* **1**.3 (1976), pp. 265–282.

[122] P.S. Macklin, P.J. Morris & S.R. Knight. “A systematic review of the use of rituximab for the treatment of antibody-mediated renal transplant rejection”. In: *Transplantation Reviews* **31**.2 (2017), pp. 87–95.

[123] H.S. Mahato, C. Ahlstrom, R. Jansson-Löfmark, U. Johansson, G. Helminger & K.M. Hallow. “Mathematical model of hemodynamic mechanisms and consequences of glomerular hypertension in diabetic mice”. In: *npj Systems Biology and Applications* **4** (2018), p. 41.

[124] R.L. Malfi, E. Crone & N. Williams. “Demographic benefits of early season resources for bumble bee (*B. vosnesenskii*) colonies”. In: *Oecologia* **191** (2019), pp. 377–388.

[125] C. Manjon et al. “Unravelling the molecular determinants of bee sensitivity to neonicotinoid insecticides.” In: *Current Biology* **28**.7 (2018), pp. 1137–1143.

[126] MATLAB. *9.0 (2016a)*. The Mathworks, Inc. Natick, Massachusetts, 2016.

[127] MATLAB. *9.5 (R2018a)*. The Mathworks Inc. Natick, Massachusetts, 2018.

[128] P. Maybeck. *Stochastic models, estimation, and control Vol. 1*. Academic Press, 1979.

[129] J.T. McCarthy. "A practical approach to the management of patients with chronic renal failure." In: *Mayo Clinic Proceedings* **74** (1999), pp. 269–273.

[130] M. Meskin, H. Nounou, M. Nounou & A. Datta. "Parameter estimation of biological phenomena: an unscented Kalman filter approach". In: *IEEE/ACM transactions on computational biology and bioinformatics* **10**.2 (2013), pp. 537–543.

[131] V. Mommaerts, S. Reynders, J. Boulet, L. Besard, G. Sterk & G. Smagghe. "Risk assessment for side-effects of neonicotinoids against bumblebees with and without impairing foraging behaviour". In: *Ecotoxicology* **19**.1 (2010), pp. 207–215.

[132] M. Morigi, A. Benigni, G. Remuzzi & B. Imberti. "The regenerative potential of stem cells in acute renal failure." In: *Cell Transplantation* **15**.1 (2006), pp. 111–117.

[133] W.F. Morris & D.F. Doak. *Quantitative conservation biology: theory and practice of population viability analysis*. Sinauer Associates, 2002.

[134] C.B. Müller, J.A. Shykoff & G.H. Sutcliffe. "Life history patterns and opportunities for queen-worker conflict in bumblebees (Hymenoptera: Apidae)". In: *Oikos* **65**.2 (1992), pp. 242–248.

[135] N. Murad. "Quantitative Modeling and Optimal Control of Immunosuppressant Treatment Dynamics in Renal Transplant Recipients". PhD thesis. North Carolina State University, 2018.

[136] N. Murad, H.T. Tran & H.T. Banks. "Optimal control of immunosuppressants in renal transplant recipients susceptible to BKV infection". In: *Optimal Control Applications and Methods* **40**.2 (2018), pp. 292–309.

[137] W.W. Murdoch, R.M. Nisbet, S.P. Blythe, W.S. Gurney & J.T. Reeve. "An invulnerable age class and stability in delay-differential parasitoid-host models." In: *American Naturalist* **129**.2 (1987), pp. 263–282.

[138] S. Nakanishi, R. Kageyama & D. Watanabe, eds. *Systems Biology: The Challenge of Complexity*. Springer Science & Business Media, 2009.

[139] H. Neuwirt, M. Rudnicki, P. Schratzberger, M. Pirklbauer, A. Kronbichler & G. Mayer. "Immunosuppression after renal transplantation." In: *Magazine of European Medical Oncology* **12** (2019), pp. 216–221.

[140] J. Ollerton, R. Winfree & S. Tarrant. "How many flowering plants are pollinated by animals?" In: *Oikos* **120**.3 (2011), pp. 321–326.

[141] O. Olsson, A. Bolin, H.G. Smith & E.V. Lonsdorf. "Modeling pollinating bee visitation rates in heterogeneous landscapes from foraging theory." In: *Ecological Modelling* **316** (2015), pp. 133–143.

[142] *Organ Procurement and Transplantation Network*. http://optn.transplant.hrsa.gov/.Accessed: 2021-07-11.

[143] G. Oster. “Modeling social insect populations. I. Ergonomics of foraging and population growth in bumblebees”. In: *American Naturalist* **110**.972 (1976), pp. 215–245.

[144] M. Ostermann & M. Joannidis. “Acute kidney injury 2016: diagnosis and diagnostic workup”. In: *Critical care (London, England)* **20**.1 (2016), p. 299.

[145] K.N. Ouma, S.V. Basavaraju, J.A. Okonji, J. Williamson, T.K. Thomas, L.A. Mills, J.N. Nkengasong & C. Zeh. “Evaluation of quantification of HIV-1 RNA viral load in plasma and dried blood spots by use of the Semiautomated Cobas Amplicor assay and the fully automated Cobas Ampliprep/TaqMan assay, version 2.0, in Kisumu, Kenya”. In: *Journal of Clinical Microbiology* **51** (2013), pp. 1208–1218.

[146] J. Peat & D. Goulson. “Effects of experience and weather on foraging rate and pollen versus nectar collection in the bumblebee, *Bombus* terrestris”. In: *Behavioral Ecology and Sociobiology* **58**.2 (2005), pp. 152–156.

[147] J.J.M. Pereboom. “The composition of larval food and the significance of exocrine secretions in the bumblebee *Bombus* terrestris”. In: *Insectes Sociaux* **47**.1 (2000), pp. 11–20.

[148] J.J.M. Pereboom, H.H.W. Velthuis & M.J. Duchateau. “The organisation of larval feeding in bumblebees (Hymenoptera: Apidae) and its significance to caste differentiation”. In: *Insectes Sociaux* **50**.2 (2003), pp. 127–133.

[149] C.J. Perry, E. Søvik, M.R. Myerscough & A.B. Barron. “Rapid behavioral maturation accelerates failure of stressed honey bee colonies.” In: *Procedings of the National Academy of Sciences* **112**.11 (2015), pp. 3427–3432.

[150] J.D. Phelps, C.G. Strang, M. Gbylik-Sikorska, T. Sniegocki, A. Posyniak & D.F. Sherry. “Imidacloprid slows the development of preference for rewarding food sources in bumblebees (*B*ombus impatiens)”. In: *Ecotoxicology* **27**.2 (2018), pp. 175–187.

[151] N.A. Pilch, L.J. Bowman & D.J. Taber. “Immunosuppression trends in solid organ transplantation: the future of individualization, monitoring, and management”. In: *Pharmacotherapy: The Journal of Human Pharmacology and Drug Therapy* **41**.1 (2021), pp. 119–131.

[152] K. Poitrineau, O. Mitesser & H.J. Poethke. “Workers, sexuals, or both? Optimal allocation of resources to reproduction and growth in annual insect colonies”. In: *Insectes Sociaux* **56**.2 (2009), pp. 119–129.

[153] E. Polak. *Computational Methods in Optimization: A Unified Approach. Vol. 77*. Academic Press, 1971.

[154] N. Pomeroy. “Brood bionomics of *B*ombus ruderatus in New Zealand.” In: *The Canadian Entomologist* **111**.8 (1979), pp. 865–874.

[155] A.A. Pottebaum, K. Venkatachalam, C. Liu, D.C. Brennan, H. Murad, A.F. Malone & T. Alhamad. "Efficacy and Safety of Tocilizumab in the Treatment of Acute Active Antibody-mediated Rejection in Kidney Transplant Recipients". In: *Transplantation Direct* **6**.4 (2020), e543.

[156] S.G. Potts, J.C. Biesmeijer, C. Kremen, P. Neumann, O. Schweiger & W.E. Kunin. "Global pollinator declines: trends, impacts and drivers". In: *Trends in Ecology & Evolution* **25**.6 (2010), pp. 345–353.

[157] F. Requier, K.K. Jownowitsch, K. Kallnik & I. Steffan-Dewenter. "Limitation of complementary resources affects colony growth, foraging behavior, and reproduction in bumble bees". In: *Ecology* **101**.3 (2020), e02946.

[158] M.F. Ribeiro. "Growth in bumble bee larvae: relation between development time, mass, and amount of pollen ingested". In: *Canadian Journal of Zoology* **72**.11 (1994), pp. 1978–1985.

[159] M.F. Ribeiro, H.H.W. Velthuis, M.J. Duchateau & I. Van der Tweel. "Feeding frequency and caste differentiation in *Bombus* terrestris larvae". In: *Insectes Sociaux* **46**.4 (1999), pp. 306–314.

[160] N. Roger, D. Michez, R. Wattiez, C. Sheridan & M. Vanderplanck. "Diet effects on bumblebee health." In: *Journal of Insect Physiology* **96** (2017), pp. 128–133.

[161] P. Röseler. "Unterschiede in der kastendetermination zwischen den hummelarten *Bombus* hypnorum und *Bombus* terrestris (Differences in the caste determination between the bumblebee species *Bombus* hypnorum and *Bombus* terrestris". In: *Zeitschrift für Naturforschung B* **25**.5 (1970), pp. 543–548.

[162] M. Rundlöf, A.S. Persson, H.G. Smith & R. Bommarco. "Late-season mass-flowering red clover increases bumble bee queen and male densities". In: *Biological Conservation* **172** (2014), pp. 138–145.

[163] M. Rundlöf et al. "Seed coating with a neonicotinoid insecticide negatively affects wild bees." In: *Nature* **521** (2015), pp. 77–80.

[164] G. Satyanarayana, F. M. Marty & C.S. Tan. "The polyomavirus puzzle: is host immune response beneficial in controlling BK virus after adult hematopoietic cell transplantion?" In: *Transplant Infectious Disease* **16**.4 (2014), pp. 521–531.

[165] R. Schmitz, Z.W. Fitch, P.M. Schroder, A.Y. Choi, A.M. Jackson, S.J. Knechtle & J. Kwun. "B cells in transplant tolerance and rejection: friends or foes?" In: *Transplant International* **33**.1 (2020), pp. 30–40.

[166] J. Sellares, D. De Freitas, M. Mengel, J. Reeve, G. Einecke, B. Sis, L. Hidalgo, K. Famulski, A. Matas & P. Halloran. "Understanding the causes of kidney transplant failure: The dominant role of antibody-mediated rejection and nonadherence". In: *American Journal of Transplantation* **12**.2 (2012), pp. 388–399.

[167] S. Sharma & G.P. Samanta. "Analysis of the Dynamics of a Tumor–Immune System with Chemotherapy and Immunotherapy and Quadratic Optimal Control". In: *Differential Equations and Dynamical Systems* **24** (2016), pp. 149–171.

[168] H. Smith. *An introduction to delay differential equations with applications to the life sciences*. Springer, 2011.

[169] D.A. Stanley, A.L. Russell, S.J. Morrison, C. Rogers & N.E. Raine. "Investigating the impacts of field- realistic exposure to a neonicotinoid pesticide on bumblebee foraging, hosming ability and colony growth." In: *Journal of Applied Ecology* **53**.5 (2016), pp. 1440–1449.

[170] J.D. Stark & J.E. Banks. "Population-level effects of pesticides and other toxicants on arthropods." In: *Annual Review of Entomolgy* **48** (2003), pp. 505–519.

[171] J.D. Stark, J.E. Banks & R.I. Vargas. "How risky is risk assessment? The role that life history strategies play in susceptibility of species to pesticides and other toxicants." In: *Proceding of the National Academy of Science* **101** (2004), pp. 732–736.

[172] J.D. Stark, R. I. Vargas & J.E. Banks. "Incorporating ecologically relevant measures of pesticide effect for estimating the compatibility of pesticides and biocontrol agents." In: *Journal of Economic Entomology* **100** (2007), pp. 1027–1032.

[173] J.D. Stark, R.I. Vargas & J.E. Banks. "Incorporating variability in point estimates in risk assessment: bridging the gap between LC50 and population endpoints." In: *Environmental Toxicology and Chemistry* **34**.7 (2015), pp. 1683–1688.

[174] G.H. Sutcliffe & R.C. Plowright. "The effects of pollen availability on development time in the bumble bee *Bombus* terricola K.(Hymenoptera: Apidae)". In: *Canadian Journal of Zoology* **68**.6 (1990), pp. 1120–1123.

[175] C.M. Switzer & S.A. Combes. "The neonicotinoid pesticide, imidacloprid, affects *B*ombus impatiens (bumblebee) sonication behavior when consumed at doses below the LD50." In: *Ecotoxicology* **25**.6 (2016), pp. 1150–1159.

[176] United States Renal Data System. *2015 USRDS annual data report: Epidemiology of Kidney Disease in the United States*. National Institutes of Health, Diabetes, Digestive, and Kidney Diseases.

[177] S. Tajiri, S. Ymanaka an T. Fujimoto, K. Matsumoto, A. Taguchi, R. Nishinakamura, H.J. Okano & T. Yokoo. "Regenerative potential of induced pluripotent stem cells derived from patients undergoing haemodialysis in kidney regeneration". In: *Scientific Reports* **8**.1 (2018), pp. 1–12.

[178] K. Tan, W. Chen, S. Dong, X. Liu, Y. Wang & J.C. Nieh. "A neonicotinoid impairs olfactory learning in Asian honey bees (Apis cerana) exposed as larvae or as adults." In: *Scientific Reports* **5** (2015), p. 10989.

[179] S.K. Tan, S. Milligan, M.K. Sahoo, N. Taylor & B.A. Pinsky. "Calibration of BK virus nucleic acid amplification testing to the 1st WHO international standard for BK virus". In: *Journal of Clinical Microbiology* **55**.3 (2017), pp. 923–930.

[180] J.N. Tasei & P. Aupinel. "Nutritive value of 15 single pollens and pollen mixes tested on larvae produced by bumblebee workers." In: *Apidologie* **39** (2008), pp. 397–409.

[181] J.N. Tasei, J. Lerin & G. Ripault. “Sub-lethal effects of imidacloprid on bumblebees, *B.* terrestris (Hymenoptera: Apidae), during a laboratory feeding test.” In: *Pest Management Science* **56** (2000), pp. 784–788.

[182] P. Thorbek, Campbell P.J. & H.M. Thompson. “Colony impact of pesticide-induced sublethal effects on honeybee workers: A simulation study using BEEHAVE.” In: *Environmental Toxicology and Chemistry* **36**.6 (2017), pp. 831–840.

[183] K. Topuz, F.D. Zengul, A. Dag, A. Almehmi & M. Yildirim. “Predicting graft survival among kidney transplant recipients: A Bayesian decision support model”. In: *Decision Support Systems* **106** (2018), pp. 97–109.

[184] A.A. Justiz Vaillant, S. Misra & B.M. Fitzgerald. “Acute transplantation rejection”. In: *StatPearls [Internet]* (2021), https://europepmc.org/article/nbk/nbk535410. Accessed: 2021–07–25.

[185] J. Vanichanan, S. Udomkarnjananum, Y. Avihingsanon & K. Jutivorakool. “Common viral infections in kidney transplant recipients”. In: *Kidney Research and Clinical Practice* **37**.4 (2018), pp. 323–337.

[186] M. Verma, S. Erwin, V. Abedi, R. Hontecillas, S. Hoops, A. Leber, J. Bassaganya-Riera & S.M. Ciupe. “Modeling the Mechanisms by Which HIV-Associated Immunosuppression Influences HPV Persistence at the Oral Mucosa”. In: *PloS one* **12**.1 (2017), e0168133.

[187] M. Walser. “Assessing renal function from creatinine measurements in adults with chronic renal failure.” In: *American Journal of Kidney Disease* **32**.1 (1998), pp. 23–31.

[188] B.J.D. Weist, P. Wehler, L. El Ahmad, M. Schmueck-Henneresse, J.M. Millward, M. Nienen, A.U. Neumann, P. Reinke & N. Babel. “A revised strategy for monitoring BKV-specific cellular immunity in kidney transplant patients”. In: *Kidney International* **88**.6 (2015), pp. 1293–1303.

[189] R.R. West, D.L. Crosby & J.H. Jones. “A mathematical model of an integrated haemodialysis and renal transplantation programme”. In: *British Journal* **28**.3 (1974), pp. 149–155.

[190] N.M. Williams, J. Regetz & C. Kremen. “Landscape-scale resources promote colony growth but not reproductive performance of bumble bees”. In: *Ecology* **93**.5 (2012), pp. 1049–1058.

[191] N.M. Williams, J. Regetz & C. Kremen. “Landscape-scale resources promote colony growth but not reproductive performance of bumble bees.” In: *Ecology* **93**.5 (2012), pp. 1049–1058.

[192] R. Winfree, R. Aguilar, D.P. Vázquez, G. LeBuhn & M.A. Aizen. “A meta- analysis of bees’ responses to anthropogenic disturbance.” In: *Ecology* **90**.8 (2009), pp. 2068–2076.

[193] R. Winfree, I. Bartomeus & D.P. Cariveau. “Native pollinators in anthropogenic habitats”. In: *Annual Review of Ecology, Evolution, and Systematics* **42**.1 (2011), p. 1.

[194] T.J. Wood, J.M. Holland, W.O.H. Hughes & D. Goulson. “Targeted agri-environment schemes significantly improve the population size of common farmland bumblebee species”. In: *Molecular Ecology* **24**.8 (2015), pp. 1668–1680.

[195] S.D. Wratten, M. Gillespie, E. Decourtye A. andMader & N. Desneux. “Pollinator habitat enhancement: benefits to other ecosystem services.” In: *Agriculture, Ecosystems & Environment* **159** (2012), pp. 112–122.

[196] Y.M. Yoon, J.H. Lee, K.-H. Song, H. Noh & S.H. Lee. “Melatonin-stimulated exosomes enhance the regenerative potential of chronic kidney disease-derived mesenchymal stem/stromal cells via cellular prion proteins”. In: *Journal of Pineal Research* **68** (2020), e12632.

[197] Y. Zhang, D. Briggs, D. Lowe, D. Mitchell, S. Daga, N. Krishnan, R. Higgins & N. Khovanova. “A new data-driven model for post-transplant antibody dynamics in high risk kidney transplantation”. In: *Mathematical Biosciences* **284** (2017), pp. 3–11.